MASS SPECTROMETRY AND NATURAL VARIATIONS OF IRON ISOTOPES

Nicolas Dauphas[1]* and Olivier Rouxel[2]

[1]*Origins Laboratory, Department of the Geophysical Sciences, Enrico Fermi Institute, and Chicago Center for Cosmochemistry, The University of Chicago, 5734 South Ellis Avenue, Chicago, Illinois 60637*
[2]*Woods Hole Oceanographic Institution, Marine Chemistry and Geochemistry Department, MS#8, Woods Hole, Massachusetts 02543*

Although the processes that govern iron isotope variations in nature are just beginning to be understood, multiple studies attest of the virtue of this system to solve important problems in geosciences and biology. In this article, we review recent advances in the geochemistry, cosmochemistry, and biochemistry of iron isotopes. In Section 2, we briefly address the question of the nucleosynthesis of Fe isotopes. In Section 3, we describe the different methods for purifying Fe and analyzing its isotopic composition. The methods of SIMS, RIMS, and TIMS are presented but more weight is given to measurements by MC-ICPMS. In Section 4, the isotope anomalies measured in extraterrestrial material are briefly discussed. In Section 5, we show how high temperature processes like evaporation, condensation, diffusion, reduction, and phase partitioning can affect Fe isotopic composition. In Section 6, the various low temperature processes causing Fe isotopic fractionation are presented. These involve aqueous and biologic systems. © 2006 Wiley Periodicals, Inc., Mass Spec Rev 25:515–550, 2006

Keywords: *isotopes; ICPMS; mass spectrometry; geochemistry; cosmochemistry; biochemistry*

I. INTRODUCTION

Until recently, the science of describing, understanding, and using stable isotope abundance variations was restricted to light elements, primarily H, C, N, O, and S. This stemmed from analytical difficulties in the mass spectrometry. Early attempts to measure the stable isotopic composition of Fe relied on thermal ionization mass spectrometers (TIMS, Völkening & Papanastassiou, 1989; Beard et al., 1999; Herzog et al., 1999; Johnson & Beard, 1999; Brantley, Liermann, & Bullen, 2001; Bullen et al., 2001). These instruments have variable instrumental mass fractionation and, unless one can control these variations, Fe isotopic spikes must be used. The precision that is attainable with this method is at best 0.15 ‰/amu (Johnson & Beard, 1999). *In situ* techniques such as secondary ionization mass spectrometry

(SIMS, Davis et al., 1991; Davis & Brownlee, 1993; Wang et al., 1994; Alexander & Wang, 2001; Alexander et al., 2002; Alexander & Hewins, 2004; Marhas, Hoppe, & Besmehn, 2004), resonant ionization mass spectrometry (RIMS, Tripa et al., 2002), and laser-ablation multi-collection inductively coupled plasma mass spectrometry (LA-MC-ICPMS, Hirata & Ohno, 2001) have also been used but their application is limited to samples that show large isotopic variations and do not require high precision. The recent advent of multi-collection inductively coupled plasma mass spectrometers (MC-ICPMS) has solved many of the problems associated with other techniques (ion yields and stability of the instrumental mass bias) and the isotopic composition of Fe can now be analyzed routinely in the laboratory (Belshaw et al., 2000; Hirata & Ohno, 2001; Sharma, Polizzotto, & Anbar, 2001; Walczyk & von Blanckenburg, 2002; Beard et al., 2003a; Kehm et al., 2003; Mullane et al., 2003; Roe, Anbar, & Barling, 2003; Rouxel et al., 2003; Weyer & Schwieters, 2003; Arnold, Weyer, & Anbar, 2004a; Dauphas et al., 2004a). In this article, we review recent advances in the geochemistry, cosmochemistry, and biochemistry of iron isotopes (also see Beard et al., 2003a; Anbar, 2004; Beard & Johnson, 2004; Johnson et al., 2004 for complementary efforts).

II. STELLAR NUCLEOSYNTHESIS

Primordial nucleosynthesis formed H, He, and some Li. Heavier elements, which are also denoted as metals in astrophysics, were synthesized in stars (Pagel, 1997; Truran & Heger, 2004). Iron was produced in massive stars that end up their lives as very energetic explosions, called supernovae (Woosley, Heger, & Weaver, 2002). Two types of supernovae are distinguished based on the presence (II) or absence (I) of hydrogen lines in their spectra.

Type II supernovae (SNII) are the end product of stars more massive than 8 M⊙. Such stars burn through successive stages, whereby the product of a nuclear reaction becomes the fuel of another that operates deeper in the star, at higher temperature and pressure. When the fuel of a nuclear reaction in the core is exhausted, the star collapses onto itself, compressing and heating up ashes at its center until a new reaction occurs that uses ashes of the previous stage as fuel. At the stage of pre-supernova, the star has an onion shell structure with a Fe-Ni rich core and successive layers of Si, O, Ne, C, He, and H that burn hydrostatically. Because any fusion reaction on Fe is endothermic, the Fe core is

TABLE 1. Origins and cosmic abundances of Fe isotopes

Isotopes	^{54}Fe	^{56}Fe	^{57}Fe	^{58}Fe
Origin	Ia,*x*Si	*x*Si, Ia	*x*Si, Ia	He(s), nse-IaMCh
Cosmic abundances	48,980	768,900	17,760	2,360
Atom percent	5.845	91.754	2.119	0.282

Ia corresponds to nucleosynthesis by type Ia supernovae, xSi denotes explosive silicon burning, He(s) refers to slow neutron capture during hydrostatic helium burning in the pre-supernova, and nse-IaMCh stands for nuclear statistical equilibrium in accreting white dwarfs that ignite carbon deflagration near the Chandrasekhar mass (from Woosley et al. 2002 and references therein). Cosmic abundances are given on a scale where Si=10^6 (Lodders, 2003). Atom percent abundances are for IRMM-014 (Taylor, Maeck, & De Bièvre, 1992).

unstable and collapses. The inner layers of the star collapse on this incompressible core and bounce back in a shock wave that propagates outward. This explosion modifies the abundances of elements inherited from the pre-supernova stage and ejects the newly synthesized material into the interstellar medium.

The other group of stars that can produce iron isotopes is type Ia supernovae (SNIa). These stars are part of a binary system, whereby a white dwarf left over from an earlier generation of stars accretes hydrogen and helium from a companion star. This mass transfer eventually leads to the explosion of the accreting star. The nucleosynthesis occurring in SNIa is in many respects similar to that occurring in SNII. Because of this similarity, it is impossible to infer from solar system abundances how much of Fe that is present on Earth owes its existence to SNII and SNIa. Fortunately, astronomical observations and the theory of galactic chemical evolution allow us to answer this question (Truran & Heger, 2004). It is estimated that approximately 30% of the total Fe was produced in SNIa while the rest was synthesized by SNII. The proportion applies to ^{56}Fe as it is the dominant isotope of Fe and it is therefore the isotope that is measured in stellar spectra. The exact mechanisms responsible for the nucleosynthesis of the various isotopes of Fe are compiled in Table 1 (Woosley, Heger, & Weaver, 2002).

III. MASS SPECTROMETRY OF STABLE ISOTOPES

Iron possesses four stable isotopes, ^{54}Fe, ^{56}Fe, ^{57}Fe, and ^{58}Fe, which represent 5.845, 91.754, 2.1191, and 0.2819 atom % of the total (Taylor, Maeck, & De Bièvre, 1992, Fig. 1). For two
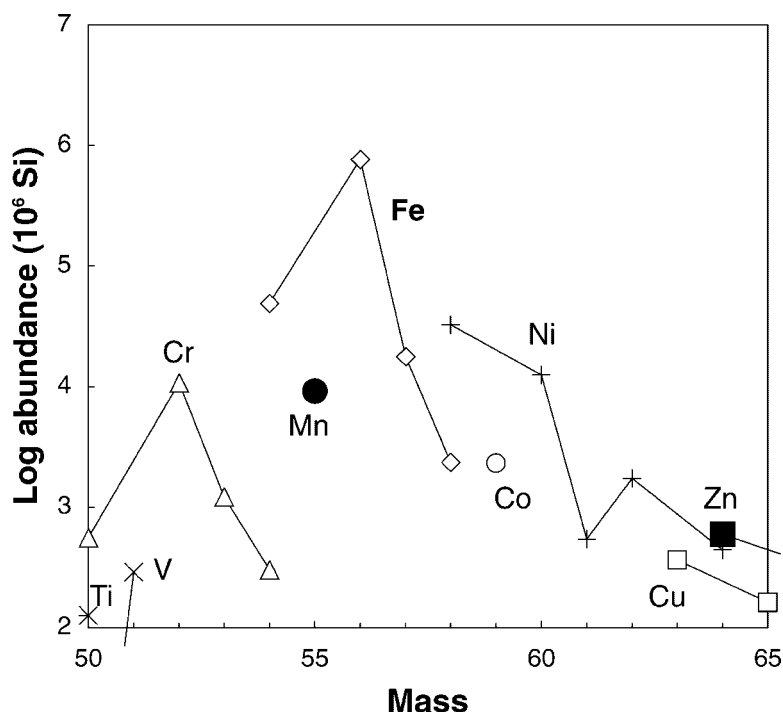
FIGURE 1. Solar atom abundances of the nuclides in the Fe mass region normalized to Si = 10^6 (Lodders, 2003, Table 1). The commonly encountered interferences in ICPMS during Fe isotope measurements are ArN$^+$ and Cr$^+$ on 54, ArO$^+$ on 56, ArOH$^+$ and CaOH$^+$ on 57, and Ni$^+$ on 58.

arbitrary isotopes of Fe, i and j, it is convenient to introduce the widely used δ notation

$$\delta_j^i\text{Fe} = \left[\left(\frac{^i\text{Fe}}{^j\text{Fe}} \right)_{\text{sample}} \middle/ \left(\frac{^i\text{Fe}}{^j\text{Fe}} \right)_{\text{standard}} - 1 \right] \times 10^3 \qquad (1)$$

This value is quantified in *permil* (‰) deviation relative to the isotopic composition of a reference sample or reservoir. Twelve different δ values can be calculated for the 12 possible isotopic ratios and another notation is sometimes used, which gives identical values if the isotope variations result from mass-dependent phenomena and the law describing the mass fractionation does not depart very much from linearity (Wombacher et al., 2003).

$$F_{\text{Fe}} = \left[\left(\frac{^i\text{Fe}}{^j\text{Fe}} \right)_{\text{sample}} \middle/ \left(\frac{^i\text{Fe}}{^j\text{Fe}} \right)_{\text{standard}} - 1 \right] \times \frac{10^3}{i - j} \qquad (2)$$

This value is quantified in units of permil per atomic mass unit (‰/amu) deviation relative to the isotopic composition of a reference sample or reservoir. The main virtue of this last notation is that in first approximation, it does not depend on the pair of isotopes that is used, the choice of which is often dictated by analytical constraints and differs from one laboratory to another. Its main drawback is that in details, when the law describing the mass fractionation is non-linear and the samples show large fractionation, the F_{Fe} values actually depend on the pair of isotopes that is used. As a rule, even though F_{Fe} can be calculated to facilitate inter-laboratory comparisons, one should always report all the isotopic ratios that have been measured because the form of the mass fractionation relationship can potentially shed some light on the process at hand (Young, Galy, & Nagahara, 2002). In the following, care is taken to state which notation is used when isotopic compositions are given.

In some instances, isotopic variations are not smooth functions of the masses of the isotopes (Völkening & Papanastassiou, 1989; Davis et al., 2002; Tripa et al., 2002; Dauphas et al., 2004a; Marhas, Hoppe, & Besmehn, 2004). Such isotopic effects are extremely rare in nature and arise primarily from nuclear reactions and photo-chemistry. In order to investigate these variations, the isotopic ratios are often corrected for mass fractionation by internal normalization (Völkening & Papanastassiou, 1989; Dauphas et al., 2004a). The resulting ratios, noted with a star hereafter, would be constant in nature if it were for the non-mass-dependent component of the variations. These variations are in most cases of smaller magnitude than the mass-dependent variations. We therefore use a different notation

$$\varepsilon_j^i\text{Fe} = \left[\left(\frac{^i\text{Fe}}{^j\text{Fe}} \right)_{\text{sample}}^* \middle/ \left(\frac{^i\text{Fe}}{^j\text{Fe}} \right)_{\text{standard}}^* - 1 \right] \times 10^4 \qquad (3)$$

In that case, the variations are quantified in parts *per* 10,000 and a ratio must be arbitrarily fixed to a given value to correct the raw ratios for the mass-dependent component of the isotopic variations.

Four mass spectrometric methods have been used to measure the stable isotopic composition of Fe. On the one hand, secondary ionization (SIMS), resonant ionization (RIMS), and laser ablation inductively coupled plasma mass spectrometers (LA-MC-ICPMS) allow one to measure Fe isotopic composition at high spatial resolution but with comparatively low precision. On the other hand, thermal ionization mass spectrometers (TIMS) and multiple collector inductively coupled plasma mass spectrometers (MC-ICPMS) allow one to measure bulk samples with high precision. The choice of an instrument is ultimately dictated by the samples that are analyzed and by the isotope variations that are expected. MC-ICPMS is the most versatile technique and coupled with lased ablation or microsampling apparatus, it can compete with more specialized *in situ* techniques. For this reason, more emphasis will be given to this category of instruments.

A. *In Situ* Measurements

In situ measurements are useful when the isotopic variations are large and the required precision is not high. There are three methods for analyzing Fe isotopic composition at the nm-mm scale: SIMS (Davis et al., 1991; Davis & Brownlee, 1993; Wang et al., 1994; Alexander & Wang, 2001; Alexander et al., 2002; Alexander & Hewins, 2004; Marhas, Hoppe, & Besmehn, 2004; Taylor et al., 2005), RIMS (Tripa et al., 2002), and LA-ICPMS (Hirata & Ohno, 2001; Ohno et al., 2004; Graham et al., 2004; Kosler et al., 2005; Steinhoefel et al., 2005). Much development remains to be done, notably for LA-ICPMS. In Fe isotope analyses with SIMS, a primary ion beam of O^- is directed towards the sample. The secondary Fe ions thus generated are accelerated and separated in mass in a magnetic sector. Difficulties arise due to the presence of a $^{56}\text{Fe}^1\text{H}$ interference on ^{57}Fe but this can be circumvented by working either at high mass resolution ($M/\Delta M = 8,000$, Alexander & Wang, 2001) or by bracketing with standards ran in the same conditions as the sample (Davis et al., 1991; Davis & Brownlee, 1993). The main virtue of SIMS is the spatial resolution, which can reach 50 nm in the latest generation Cameca NanoSIMS 50. The main drawback is the presence of possible isobaric interferences from ^{54}Cr and ^{58}Ni on Fe isotopes when the concentrations of Cr and Ni are high.

This problem is not present when using time of flight resonant ionization mass spectrometers (RIMS) such as CHARISMA (Savina et al., 2003). The CHARISMA instrument operates as follows. A pulsed laser ablates the sample in high vacuum with a high repetition rate. At each pulse, a cloud of neutrals and secondary ions is generated. Imposing a high extraction voltage eliminates the ions generated at this stage. What is left are neutral atoms and molecules. Laser beams are then shot to the cloud. The wavelengths of the lasers are adjusted to selectively photoionize the element of interest through resonant electronic transitions. The element selectivity of the photoionization scheme depends on the number of lasers that are used. For Fe, Tripa et al. (2002) used two lasers tuned at 226.021 and 460.694 nm. Note that resonant ionization can potentially induce isotope specific effects. The selectively ionized Fe atoms are then accelerated and separated according to their travel times in a flight tube. They are finally detected with microchannel plates. The sequence that has just been described is repeated a large number of times with a typical repetition rate of 1 kHz. This technique has limited precision but is first in class regarding ion

yields and selectivity. For instance, Tripa et al. (2002) measured the composition of all Fe isotopes (including ^{58}Fe) with precisions of 50–100 ‰, in 2–4 μm SiC grains which contain Fe present at trace levels (200 ppm, Kashiv et al., 2001).

Laser ablation ICPMS has also been successfully applied to the determination of Fe stable isotope variations. In that case, the sample is continuously ablated with a Laser (193 nm ArF excimer or 266 nm Nd:YAG, Günther & Heinrich, 1999a) and the resulting aerosols are carried to the torch by a carrier gas, He, Ar, or both (Günther & Heinrich, 1999b). The rest of the instrument is a standard MC-ICPMS. This method does not separate Fe from direct isobaric elements but with most MC-ICPMS, there is sufficient provision of Faraday collectors to monitor other isotopes, such as ^{53}Cr and ^{60}Ni, which can be used to subtract the contributions of Cr and Ni on Fe isotopes. The spatial resolution of this technique can be as low as 4 μm and the precision can be better than 0.1–0.2 ‰/amu (Hirata & Ohno, 2001; Hirata, Hayano, & Ohno, 2003). To date, few natural samples have been measured with this promising technique (Hirata & Ohno, 2001; Graham et al., 2004; Kosler et al., 2005; Steinhoefel et al., 2005).

B. Bulk Measurements

Both P-TIMS (P stands for positive ions) and MC-ICPMS can be used to measure Fe isotopic composition at a bulk sample scale. However, in regard of precision and ease of use, P-TIMS has largely been superseded by MC-ICPMS in laboratories around the world. For this reason, only the latter category of instruments will be described hereafter. Analytical methods that have been developed to measure natural variations of Fe isotopes by P-TIMS are described in detail in Beard & Johnson (1999), Bullen et al. (2001), and Fantle & DePaolo (2004).

1. Separation of Iron

Before isotopic analysis, Fe must be separated from (i) isobaric elements that can potentially interfere with Fe isotopes and (ii) matrix elements that can affect the mass bias on the mass spectrometer and can form complex compounds that can also interfere with Fe. Commonly encountered interferences in MC-ICPMS are ^{54}Cr, ^{58}Ni, ^{40}Ar^{14}N, ^{40}Ar^{16}O, ^{40}Ar^{16}O^{1}H, and ^{40}Ca^{16}O^{1}H. The most versatile chemistry used for separating Fe from other elements is based on anion exchange chromatography in HCl medium. The sorption of Fe(III) on anion exchange resin increases with HCl molarity while Cr, Ni, and several other elements are not quantitatively retained. Iron is therefore fixed on the column at high HCl molarity and is then eluted at low HCl molarity (Strelow, 1980). Several groups have developed different chemical separation procedures based on the same idea (Beard et al., 2003a; Kehm et al., 2003; Rouxel et al., 2003; Dauphas et al., 2004a; Poitrasson et al., 2004). The protocol described in Dauphas et al. (2004a) is presented hereafter. It is well suited for solid samples weighing less than ~10 mg. After dissolution of the samples in suitable acids, repeated evaporations in *aqua regia* and HNO$_3$-HCl-HClO$_4$ are performed to eliminate insoluble fluorides (if HF was used to dissolve silicates) and to ensure that any reduced Fe present in the sample is fully oxidized to Fe(III). The sample is then taken up in solution in 6M HCl. Note that in some studies (Kehm et al., 2003), trace H$_2$O$_2$ (0.001 %) is added at this stage to prevent the possible reduction of Fe on the column. The solution is then loaded in 0.2–0.5 mL of acid on disposable Bio-Rad Poly-Prep columns filled with 1 mL (*l*, 2.0 cm; *i.d.*, 0.8 cm) of AG1-X8 200–400 mesh chloride form previously cleaned and conditioned by running 10 mL of H$_2$O, 5 mL of 1M HNO$_3$, 10 mL of H$_2$O, 10 mL of 0.4M HCl, 5 mL of H$_2$O, and 2 mL of 6M HCl through them. Matrix elements, Cr, and Ni are then eluted from the column in 8 mL of 6M HCl, while Fe, with a partition coefficient of more than 10^3 in favor of the resin, stays fixed. Iron is then eluted from the column in 9 mL of 0.4M HCl. The total sequence of chromatography is repeated a second time. The yield is close to 100%. Anion exchange resins are known to fractionate Fe isotopes (Anbar et al., 2000; Roe, Anbar, & Barling, 2003). It is therefore crucial to ensure that no fractionation is present, which is the case within 0.02 ‰/amu (Dauphas et al., 2004a). After elution, the solution can be dried down and is then ready for isotope analysis by MC-ICPMS.

2. MC-ICPMS Analysis

a. Interference Corrections. Polyatomic interferences at masses 54, 56, and 57 from ArN$^+$, ArO$^+$, and ArOH$^+$ and atomic interferences at masses 54 and 58 from Cr$^+$ and Ni$^+$ present a major challenge for high precision measurements of Fe isotopes by MC-ICPMS. These interferences arise from the Ar gas used to generate the plasma and from N and O present in the atmosphere and in the solution. Several solutions to this problem have been developed in the past and include (i) desolvation, (ii) cold plasma, (iii) collision cell, and (iv) high resolution techniques.

(i) Sample desolvation

Early attempts at measuring Fe isotopic compositions used a desolvating nebulizer and large quantities of Fe (5–10 μg) to minimize argide interferences. Commercially available desolvating nebulizers (Cetac Aridus, MCN6000, Apex, Elemental Scientific, Inc.) can be operated with Ar flow alone (optional N$_2$ gas is not used in order to minimize the formation of ArN$^+$ species). Because of the stability of the residual Ar-based interferences when using the same acid solution for diluting standard and sample solutions, a correction is possible with an uncertainty of less than 0.1‰ (Anbar et al., 2000; Belshaw et al., 2000). The uncertainty can be further reduced by matching exactly the sample and standard concentrations and by subtracting the background signal from both the standard and sample ion intensities ("on peak zeros"). The external precision obtained with a Plasma 54 (VG Elemental, Winsford, UK) is about 0.3 ‰ for δ^{56}Fe values (Anbar et al., 2000; Roe, Anbar, & Barling, 2003). The Plasma 54 is the first generation of double-focusing multiple collector ICPMS. It is equipped with four moveable Faraday collectors on each side of the central axial collector (Walder & Freedman, 1992; Halliday et al., 1995). Better precision is obtained on more recent double focusing instruments such as the Nu
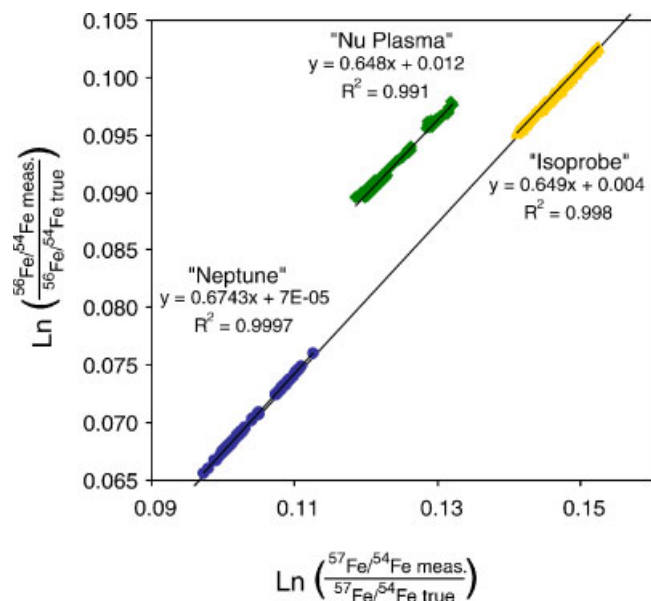
FIGURE 2. Three-isotope representation of the natural logarithm of the measured Fe isotope ratios of IRMM-014 normalized to the true ratios as reported in Taylor, Maeck, and De Bièvre (1992). In this graph, the theoretical relationships between the instrumental mass-dependent fractionation for the $^{56}Fe/^{54}Fe$ and $^{57}Fe/^{54}Fe$ ratios are straight lines. The solid line corresponds to the evolution of the $^{56}Fe/^{54}Fe$ and $^{57}Fe/^{54}Fe$ ratios of 0.672 following theoretical mass fractionation (Maréchal, Télouk, & Albarède, 1999). [Color figure can be viewed in the online issue, which is available at www.interscience.wiley.com.]

Plasma (Nu Instruments, Wrexham, Wales). This mass spectrometer is equipped with variable dispersion ion optics and a fixed array for 12 Faraday collectors (Belshaw et al., 1998). In order to minimize $ArN^+/^{54}Fe$, $ArO^+/^{56}Fe^+$, and $ArOH^+/^{57}Fe^+$ ratios, high concentrations of Fe (up to 10 ppm) and a desolvating nebulizer are used. An external precision of better than 0.1 ‰ for $\delta^{57}Fe$ values can be obtained with this setting (Belshaw et al., 2000). In this case, the large $^{56}Fe^+$ beam signal is measured on a Faraday cup equipped with a high resistor (10^{10} Ω resistor compared to conventional 10^{11} Ω resistor), allowing measurements at higher ion intensities without saturation of the amplifiers. Examples of $^{56}Fe/^{54}Fe$ and $^{57}Fe/^{54}Fe$ analyses of IRMM-014 using the Nu plasma Instrument at the University of Cambridge are presented in Figure 2. The relationship between $^{56}Fe/^{54}Fe$ and $^{57}Fe/^{54}Fe$ ratios is offset relative to theoretical mass fractionation due to the contribution of a residual interference from ArO^+. Because of the good stability of these residual interferences and of the instrumental mass bias (~4.4% per mass unit), precise measurement of Fe isotopes is possible.

(ii) Cold plasma

Only a few studies have reported high precision Fe isotope measurements by cold plasma MC-ICPMS (Kehm et al., 2003; Walczyk & von Blanckenburg, 2002). The Axiom MC-ICPMS introduced by VG Instrument is now off market. Operating this instrument at low plasma power (600

W instead of 1,300 W in normal conditions) allows one to reduce Ar-based polyatomic interferences. In cold plasma operation, ArO^+ and ArN^+ ion intensities are significantly reduced relative to the Fe signal. However, the reduction of the power of the plasma decreases significantly the ionization efficiency and it does not allow removal of hydroxide interferences, which makes it difficult to measure $^{57}Fe/^{54}Fe$ ratios.

(iii) Collision cell

Iron isotope ratios can be determined without argide interferences (ArO and ArN and to a lesser extent ArOH) using the Isoprobe MC-ICPMS. This instrument was initially produced by Micromass and is now marketed by GV Instruments. The Isoprobe is equipped with a standard ICP source and a magnetic mass analyzer that incorporates a RF-only hexapole collision cell (Turner et al., 1998). By addition of minute amounts of gas in the collision cell (such as Ar, at a typical flow rate of 1.8 mL/min), interactions of ions from the plasma with the collision gas reduce the energy spread of the incoming ions from 20 to 30 eV to less than 1 eV. It has been shown that this ''collisional focusing'' (Douglas and French, 1992) in a RF-only hexapole device also induces a series of ion-molecule reactions between the gas and the ion beam allowing the removal of certain molecular ion interferences. The addition of a mixture of H_2 and Ar as reactive collision gases eliminates or greatly reduces Ar-based interferences, in particular Ar_2^+ (Rouxel et al., 2002), ArO^+, and ArN^+ (Beard et al., 2003a; Rouxel et al., 2003). The most difficult interference to handle is $ArOH^+$, which may or may not be reduced by the addition of H_2 as a collision gas (Beard et al., 2003a; Rouxel et al., 2003). In order to measure accurately $^{57}Fe/^{54}Fe$ ratios together with $^{56}Fe/^{54}Fe$ ratios, ^{56}Fe can be measured on a Faraday collector using a 10^{10} Ω resistor to avoid saturation of the amplifier, all other masses being measured using a 10^{11} Ω resistor (Beard et al., 2003a). The samples are introduced into the MC-ICP-MS *via* either a PFA nebulizer with a cyclonic spray chamber or a desolvating nebulizer at a concentration as low as 300 ppb. Examples of $^{56}Fe/^{54}Fe$ and $^{57}Fe/^{54}Fe$ analysis of IRMM-014 using the Isoprobe operated at the Field Museum (Chicago), are presented in Figure 2. The relationship between $^{56}Fe/^{54}Fe$ and $^{57}Fe/^{54}Fe$ ratios is very close to the theoretical mass fractionation, suggesting that residual Ar-based interferences have only a minor effect. However, the instrumental mass bias, around 5.3% per amu, is larger than other instruments. Using collision cell technology, Dauphas et al. (2004a) could measure accurately the least abundant isotope of iron, ^{58}Fe, with a precision that was one order of magnitude better than earlier studies (Fig. 3).

(iv) High resolution

High mass resolution through optical peak separation is the most robust way to eliminate spectral interferences and the ThermoFinnigan Neptune MC-ICPMS was the first instrument designed specifically for high mass resolution. More recently, the Nu-1700 from Nu Instruments, with its large geometry, has been designed for isotope ratio measurements
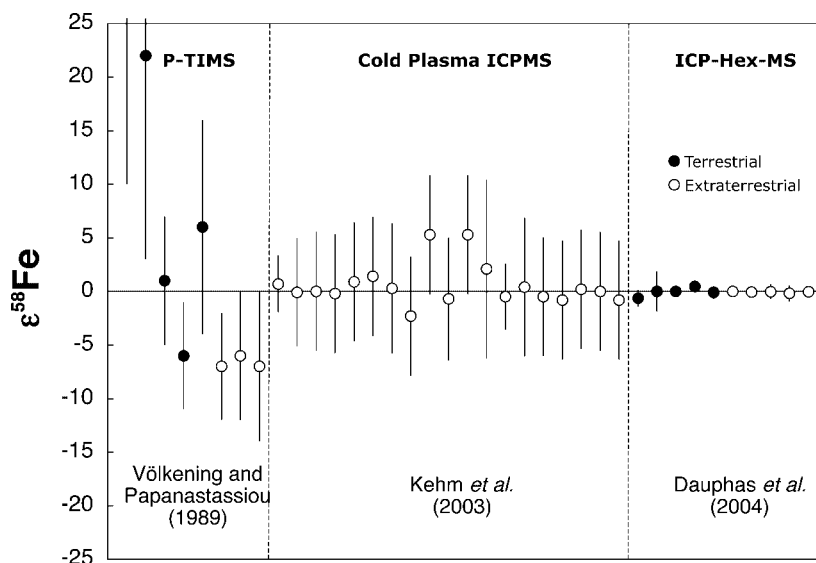
FIGURE 3. Comparison between studies reporting ^{58}Fe isotopic compositions using positive thermal ionization mass spectrometry (Völkening & Papanastassiou, 1989), cold plasma inductively coupled plasma mass spectrometry (Kehm et al., 2003), and ICPMS incorporating hexapole collision cell technology (Dauphas et al., 2004a). Only the mass-independent component of the variations is shown (all terrestrial samples should plot at zero in this diagram). As shown, ^{58}Fe can be measured accurately with a precision of 0.5 ε at 2σ.

at high mass resolution with high transmission (Williams et al., 2005). High mass resolution that preserves flat-topped peaks is realized by adjusting the source slit to generate an interference-free space between ion beams in the focal plane of the mass spectrometer. The slits at the detector are set wider than the beam profiles in the focal plane. The Finnigan Neptune is capable to reach a resolving power ($M/\Delta M$) of about 9,500 for medium and 12,500 for high resolution modes, which are sufficient to safely separate molecular interferences from Fe isotopes with flat top peak sections (Weyer & Schwieters, 2003). At these mass resolutions, the sensitivity for Fe is reduced by factors of approximately 6 (medium) and 12 (high) relative to full transmission in low mass resolution mode. Iron isotope analyses with the Neptune MC-ICPMS are not conducted at conditions that achieve full resolution of the Fe isotope peaks from the interfering molecular ions. Rather, the peaks are only partially resolved and the detector is positioned on a peak shoulder for data collection. In contrast, the Nu 1700 is tuned to achieve a full baseline separation of the Fe and ArN/O peaks. The samples are introduced into the Neptune *via* either a PFA nebulizer with a cyclonic spray chamber or a desolvating nebulizer at concentrations as low as 100 ppb. Under these conditions, the typical precision is less than 0.1‰ for ^{56}Fe/^{54}Fe and ^{57}Fe/^{54}Fe ratios (Arnold, Weyer, & Anbar, 2004a; Rouxel, Bekker, & Edwards, 2005; Schoenberg & von Blanckenburg, 2005). Examples of ^{56}Fe/^{54}Fe and ^{57}Fe/^{54}Fe analyses of IRMM-014 using the Neptune operating at WHOI are presented in Figure 2. The relationship between ^{56}Fe/^{54}Fe and ^{57}Fe/^{54}Fe ratios is undistinguishable from the theoretical mass fractionation,

suggesting that Ar-based interferences are quantitatively separated. Another advantage of this instrument is the small instrumental mass bias compared to other MC-ICPMS, around 3.6% *per* amu.

b. Instrumental Mass Bias. Despite the large instrumental mass bias in MC-ICPMS (between 3.5% and 5.5% per amu) and its variability with time, instrumental set-up, and sample matrices, a variety of methods have been developed to measure natural Fe isotope compositions with a precision often better than 0.1‰/amu. Most commonly used is the standard-sample bracketing method in which measurements of standards of known Fe isotope compositions are alternated with sample measurements (Belshaw et al., 2000; Beard et al., 2003a; Rouxel et al., 2003; Dauphas et al., 2004a; Schoenberg & von Blanckenburg, 2005). The isotopic composition of an unknown sample is derived by interpolating the instrumental mass bias between two measurements of a standard of known isotopic composition. A second approach derives the instrumental mass bias by measuring an internal standard, such as Cu (Anbar et al., 2000; Kehm et al., 2003; Arnold, Weyer, & Anbar, 2004a) or Ni (Malinovsky et al., 2003; Rouxel, Bekker, & Edwards, 2005) of known isotopic composition. A more detailed description of measurement schemes for both methods can be found in Albarède and Beard (2004) and Dauphas et al. (2004a). The double spike methodology has also been successfully applied to mass bias correction in MC-ICPMS measurements (Dideriksen, Baker, & Stipp, 2005). The precision that is obtained in this case (0.025 ‰/amu, 2σ) is comparable to that obtained using element addition or standard bracketing. The main virtue of double spike methodology is that it is not affected by mass fractionation during

column chromatography or matrix effects during MC-ICPMS analysis.

c. The IRMM-014 Reference Material. In the field of stable isotopes, it is common to normalize the isotopic ratios to a widely distributed, homogeneous, isotopic standard. In the case of Fe, the standard that is most commonly used is a batch of iron metal distributed by the Institute for Reference Materials and Measurements of the European Commission, IRMM-014. The isotope abundances of this material are in percent, 5.845 ± 0.023 (2σ) for ^{54}Fe, 91.754 ± 0.024 for ^{56}Fe, 2.1192 ± 0.0065 for ^{57}Fe, and 0.2818 ± 0.0027 for ^{58}Fe (Taylor, Maeck, & De Bièvre, 1992). Although the organizations that promote the use of such standards claim that these are isotopically homogeneous and can therefore be used to normalize to a common baseline measurements obtained in different laboratories, it has been shown that the magnesium standard SRM980 actually had a heterogeneous isotopic composition (Galy et al., 2003). In the case of IRMM-014, a comparison made between two solutions prepared in different laboratories from different batches showed that IRMM-014 has homogeneous isotopic composition, within 0.024 ‰/amu (Dauphas et al., 2004a). Note that the Orgueil meteorite, which is a CI chondrite and has the composition that matches the best the composition of the sun (Lodders, 2003), has indistinguishable Fe isotopic composition relative to IRMM-014, -0.013 ± 0.018 ‰/amu, excluding the measurement of Zhu et al. (2001) which may reflect small scale isotope heterogeneity or analytical artifacts (Table 2). More work is required to ascertain this statement but all chondrite measurements done so far (Zhu et al., 2001; Kehm et al., 2003; Poitrasson et al., 2004; Dauphas et al., 2004a, in prep) indicate that IRMM-014 is a good proxy for the cosmic composition (the average of 26 published and unpublished bulk chondrite measurements yields an average of -0.001 ± 0.019 ‰/amu relative to IRMM-014, Fig. 4). The cosmic composition may actually not reflect the composition of the Sun but it provides a good baseline for bulk planetary compositions.

For the isotopic composition of light elements, it is common to use a geochemical reservoir as a standard. Hydrogen is normalized to ocean water, carbon is normalized to pee-dee belemnites, nitrogen is normalized to air, oxygen is normalized to ocean water, sulfur is normalized to Canyon Diablo troilite (or equivalent homogeneous standard materials like V-PDB, V-SMOW, or V-CDT). Following these lines, some laboratories report the Fe isotopic composition relative to igneous rocks from the Earth–Moon system (Mandernack et al., 1999; Beard et al., 2003a; Kehm et al., 2003; Fantle & DePaolo, 2004). It was found that most of these rocks have homogeneous compositions and are enriched in the heavy isotopes of Fe relative to IRMM-014 by 0.039 ± 0.008 ‰/amu (Beard et al., 2003a, Fig. 4). However, more detailed studies have shown that the Fe isotopic composition of the Moon is different from that of the Earth (Poitrasson et al., 2004) and that variations are present in bulk igneous rocks (Williams et al., 2004a; Poitrasson & Freydier, 2005, Fig. 4). Because there is no large homogenized powdered material that is agreed upon to define the silicate Earth (different laboratories use different igneous baselines) and because the composition of IRMM-014 is very close to the cosmic (chondritic) composition,

we propose that Fe isotope compositions be normalized to IRMM-014.

d. Geostandards. A variety of geotandards (AC-E, AGV-1, AGV-2, BCR-1, BCR-2, BE-N, BHVO-1, BIR-1, BR, DT-N, DTS-1, DTS-2, G-2, GA, GSP-1, GSR-1, IF-G, JP-1, OU-2, PCC-1, RGM-1, STM-1, and WITS-1) have already been characterized for their Fe isotopic compositions. A compilation of working values is given in Table 2. Surprisingly, all the standards analyzed so far, except IF-G (iron formation from Isua, Greenland), have igneous affinities. Given that most applications of Fe isotope geochemistry are related to aqueous surface environments, more work is required to characterize geostandards from a wider variety of sources. Bulk carbonaceous chondrites such as Allende (3,000 kg total mass), which define a narrow range of Fe isotopic composition (average -0.012 ± 0.010 ‰/amu relative to IRMM-014, Table 2), could also be used as standard material when analyzing extraterrestrial samples.

IV. ISOTOPE ANOMALIES

Theory predicts that for any single element, the isotopic variations should be smooth functions of the mass, with differences in isotopic ratios being approximately proportional to the difference in mass of the isotopes involved. All the variations that depart from this rule are referred to as isotope anomalies. An important aspect to note is that in most cases, the variations are too small to be measured without very precise and reproducible correction of the instrumental mass fractionation. This is often done by the method of internal normalization, which consists in arbitrarily fixing the ratio of a given pair of isotopes to a fixed value in order to calculate a mass bias and then apply this value to other ratios. The most versatile phenomenological fractionation law that can be used is the generalized power law (Maréchal, Télouk, & Albarède, 1999). A special case of the generalized power law that is commonly encountered in mass spectrometry is the exponential law

$$r = R(1 + \Delta M/M)^{\beta} \tag{4}$$

where r is the measured ratio of the nuclides i and j, R is the true ratio, and $\Delta M/M$ is the relative mass difference $(i-j)/j$. The way internal normalization works is described hereafter (Fig. 5). For an arbitrary pair of isotopes, a value for the true ratio R is assumed and is used with the measured ratio r to calculate β. This value is then applied to other isotope pairs to calculate their true ratios. The normalized values are then compared with a standard to calculate departure from normal composition, often in ε units (Eq. 3). In some cases, when other considerations allow prediction of which isotope is likely to vary in a non-mass-dependent way, then the choice of the ratio used for normalization does not change anything to the result. Otherwise, the measured spectrum depends on the normalization scheme.

A. Circumstellar Grains

Presolar grains are solids that condensed around stars that died before the formation of the solar system (Anders & Zinner, 1993).

TABLE 2. Compilation of Fe isotopic compositions for geostandards and carbonaceous chondrites

Sample	Description	Reference	#	[Fe] wt%	δ^{56}Fe ‰	± 2σ	δ^{57}Fe ‰	± 2σ	F_{Fe} ‰/amu	± 2σ
AC-E	Granite, Ailsa Craig Island, Scotland (IWG-GIT)	Dauphas et al. (in prep)	1	1.77	0.295	0.067	0.414	0.180	0.148	0.034
AGV-1	Andesite, Oregon, USA (USGS)	Beard et al. (2003)	2		0.130	0.102	0.140	0.152	0.065	0.051
		Poitrasson et al. (2004)	3				0.139	0.064	0.046	0.021
		Average AGV-1		4.73	0.130	0.102	0.139	0.059	0.049	0.020
AGV-2	Andesite, Oregon, USA (USGS)	Dauphas et al. (2004)	1	4.68	0.112	0.081	0.165	0.275	0.056	0.041
BCR-1	Basalt, Oregon, USA (USGS)	Beard et al. (2003)	3		0.090	0.128	0.120	0.146	0.045	0.064
		Fantle & DePaolo (2004)	1		0.240	0.128			0.120	0.064
		Poitrasson et al. (2004)	6				0.109	0.055	0.036	0.018
		Rouxel et al. (2003)	4				0.080	0.100	0.027	0.033
		Butler et al. (2005)	18		0.117	0.017	0.206	0.026	0.059	0.009
		Average BCR-1		9.37	0.119	0.017	0.180	0.023	0.054	0.007
BCR-2	Basalt, Oregon, USA (USGS)	Dauphas et al. (2004, in prep)	2	9.66	0.039	0.055	0.116	0.131	0.019	0.028
BE-N	Basalt, Essey-la-Cote, France (IWG-GIT)	Rouxel et al. (2003)	2	8.99			0.180	0.060	0.060	0.020
BHVO-1	Basalt, Hawaii, USA (USGS)	Poitrasson et al. (2004)	5				0.164	0.032	0.055	0.011
		Rouxel et al. (2003)	3				0.220	0.130	0.073	0.043
		Rouxel et al. (2005)	20		0.106	0.108	0.149	0.133		
		Average BHVO-1		8.55	0.106	0.108	0.166	0.031	0.056	0.010
BIR-1	Basalt, Reykjavik, Iceland (USGS)	Poitrasson et al. (2004)	46				0.102	0.015	0.034	0.005
		Rouxel et al. (2003)	1				0.060		0.020	
		Williams et al. (2005)	6				0.090	0.130	0.030	0.043
		Average BIR-1		7.90			0.102	0.015	0.034	0.005
BR	Basalt, Essey-la-Cote, France (CRPG)	Rouxel et al. (2003)	12	9.02			0.120	0.190	0.040	0.063
DR-N	Diorite, Neuntelsein, France (ANRT)	Poitrasson et al. (2004)	3	6.78			0.054	0.053	0.018	0.018
DTS-1	Dunite, Washington, USA (USGS)	Poitrasson et al. (2004)	3				0.159	0.044	0.053	0.015
		Rouxel et al. (2005)	3		0.056	0.101	0.082	0.154	0.028	0.051
		Average DTS-1		6.08	0.056	0.101	0.153	0.042	0.051	0.014
DTS-2	Dunite, Washington, USA (USGS)	Dauphas et al. (2004)	1	5.43	0.022	0.041	-0.058	0.072	0.011	0.021
G-2	Granite, Rhode Island, USA (USGS)	Beard et al. (2003)	1	1.86	0.070	0.172	0.130	0.161	0.035	0.086
GA	Granite, Vosges Mountains, France (CRPG)	Poitrasson & Freydler (2005)	9	1.98			0.137	0.027	0.046	0.009
GSP-1	Granodiorite, Colorado, USA (USGS)	Beard et al. (2003)	1	3.00	0.110	0.128	0.080	0.152	0.055	0.064
GSR-1	Granite, Binzhou, China (IGGE)	Poitrasson & Freydier (2005)	9	1.50			0.243	0.049	0.081	0.016
IF-G	Iron formation, Isua, Greenland (IWG-GIT)	Dauphas et al. (2004, in prep)	14		0.630	0.021	0.942	0.047	0.315	0.010
		Rouxel et al. (2003)	4		0.639	0.058	0.957	0.087	0.320	0.029
		Average IF-G		39.10	0.631	0.019	0.945	0.041	0.316	0.010
JP-1	Dunite, Horoman, Japan (GSJ)	Poitrasson et al. (2004)	8	5.85			0.006	0.034	0.002	0.011
OU-2	Dolerite, Belford, UK (IAG)	Poitrasson et al. (2004)	3	9.30			0.132	0.071	0.044	0.024
PCC-1	Peridotite, California, USA (USGS)	Beard et al. (2003)	3		0.030	0.156	0.020	0.184	0.015	0.078
	Peridotite, California, USA (USGS)	Poitrasson et al. (2004)	6				0.034	0.038	0.011	0.013
		Average PCC-1		5.78	0.030	0.156	0.033	0.037	0.011	0.013
RGM-1	Rhyolite, California, USA (USGS)	Beard et al. (2003)	1	1.30	0.180	0.242	0.290	0.172	0.090	0.121
STM-1	Syenite, Oregon, USA (USGS)	Beard et al. (2003)	1	3.65	0.040	0.471	0.060	0.539	0.020	0.235
WITS-1	Komatiite, Barberton, South Adrica	Poitrasson et al. (2004)	5	8.34			0.057	0.024	0.019	0.008
Orgueil	CI1	Dauphas et al. (2004)	1	18.30	-0.030	0.065	-0.066	0.111	-0.015	0.033
Orgueil	CI1	Kehm et al. (2002)	1	18.30	0.050	0.156			0.025	0.078
Orgueil	CI1	Poitrasson et al. (2004)	5	18.30			-0.043	0.066	-0.014	0.022
Orgueil	CI1	Zhu et al. (2001)	1	18.30	0.380	0.060	0.600	0.060	0.200	0.020
	Average CI1				-0.018	0.060	-0.066	0.111	-0.013	0.018
Murchison	CM2	Kehm et al. (2002)	1	20.90	-0.030	0.156			-0.015	0.078
Murchison	CM2	Poitrasson et al. (2005)	3	20.90			-0.037	0.108	-0.012	0.036
Murchison	CM2	Zhu et al. (2001)	1	20.90	0.000	0.060	-0.010	0.060	-0.003	0.020
	Average CM2				-0.004	0.056	-0.016	0.052	-0.006	0.017
Lance	CO3	Dauphas et al. (in prep)	1	24.80	0.030	0.157	0.191	0.135	0.015	0.079
Ornans	CO3	Dauphas et al. (in prep)	1	24.70	-0.097	0.082	-0.224	0.212	-0.049	0.041
	Average CO3				-0.070	0.073	0.071	0.114	-0.035	0.036
Allende	CV3	Kehm et al. (2002)	1	23.70	0.030	0.102			0.015	0.051
Allende	CV3	Poitrasson et al. (2005)	4	23.70			-0.105	0.066	-0.035	0.022
Allende	CV3	Zhu et al. (2001)	1	23.70	-0.040	0.060	-0.050	0.060	-0.017	0.020
Leoville	CV3	Kehm et al. (2002)	1	23.87	-0.040	0.156			-0.020	0.078
Vigarano	CV3	Dauphas et al. (in prep)	1	23.10	0.034	0.110	-0.060	0.587	0.017	0.055
	Average CV3				-0.025	0.050	-0.050	0.060	-0.013	0.018
	Average carbonaceous chondrites				-0.025	0.029	-0.025	0.035	-0.012	0.010

All the measurements reported relative to igneous rocks have been renormalized to IRMM-014 using the relationship given by Beard et al. (2003a), δ^{56}Fe$_{IRMM-014}$ = δ^{56}Fe$_{Igneous}$ + 0.09 ± 0.10 (2σ) and δ^{57}Fe$_{IRMM-014}$ = δ^{57}Fe$_{Igneous}$ + 0.11 ± 0.14 (2σ), where δ^{56}Fe is for the ^{56}Fe/^{54}Fe ratio and δ^{57}Fe is for the ^{57}Fe/^{54}Fe ratio. When δ^{56}Fe was available, F_{Fe} was calculated as δ^{56}Fe/2. When only δ^{57}Fe was available, F_{Fe} was calculated as δ^{57}Fe/3. The averages are weighted by $1/\sigma^2$ and their uncertainties are calculated accordingly. Uncertainties are reported as 2σ.

Among all the types of grains that have been recovered, silicon carbide grains are the most extensively studied. This is probably due to their high abundance in primitive meteorites (10 ppm, Huss & Lewis, 1995), the fact that they are chemically resistant and can easily be isolated by dissolving the rest of the meteorite (Amari, Lewis, & Anders, 1994), and the fact that they sample many different kinds of stars, including asymptotic giant branch-AGB stars and supernovae (Anders & Zinner, 1993). For most

elements, the isotopic compositions measured in SiC are clearly distinct from average solar system material. Tripa et al. (2002) and Davis et al. (2002) reported large isotopic anomalies for Fe in pre-solar SiC using TOF-RIMS, up to several hundreds of permil relative to the terrestrial composition. The signatures measured in SiC coming from AGB stars are difficult to interpret in terms of nuclear processes operating in these stars (Davis et al., 2002). Clayton et al. (2002) argued that the ^{58}Fe richness measured in
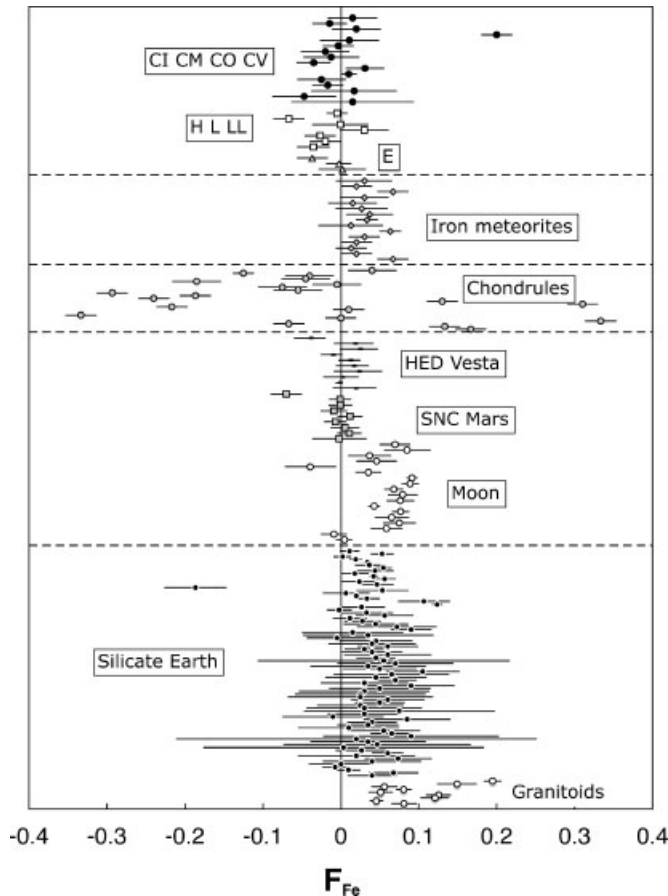
FIGURE 4. Iron isotopic compositions in ‰/amu (F_{Fe} notation, Eq. 2) of planetary and meteoritic reservoirs. As shown, chondrites have Fe isotopic compositions that are very close to IRMM-014, which is the standard used for normalization (Table 2). The Earth and the Moon are slightly enriched in the heavy isotopes of Fe relative to IRMM-014. Data from Sharma, Polizzotto, and Anbar (2001), Zhu et al. (2001, 2002), Beard et al. (2003a), Kehm et al. (2003), Mullane et al. (2003), Rouxel et al. (2003), Dauphas et al. (2004a,c, in prep), Poitrasson et al. (2004), Poitrasson and Freydier (2005), Poitrasson, Levasseur, and Teutsch (2005), Williams et al. (2004a, 2005).

SiC coming from supernovae (Davis et al., 2002) results from implantation of ^{58}Fe-rich gas in the ejecta. However, using NanoSIMS, Marhas, Hoppe, and Besmehn (2004) were unable to replicate some of the earlier findings. They measured the isotope abundances of ^{54}Fe, ^{56}Fe, and ^{57}Fe (not ^{58}Fe) in SiC grains and found that they had terrestrial isotopic compositions within the error bars of approximately 100 ‰. Possible reasons for the discrepancy are analytical artifacts from unsuppressed isobaric interferences in Tripa et al. (2002) and Davis et al. (2002), or contamination by terrestrial Fe in Marhas, Hoppe, and Besmehn (2004).

B. Refractory Inclusions in Meteorites

Refractory inclusions are solids now found in meteorites that are thought to have formed in the solar nebula as it cooled. They are used to define time zero and their age is taken to represent that of
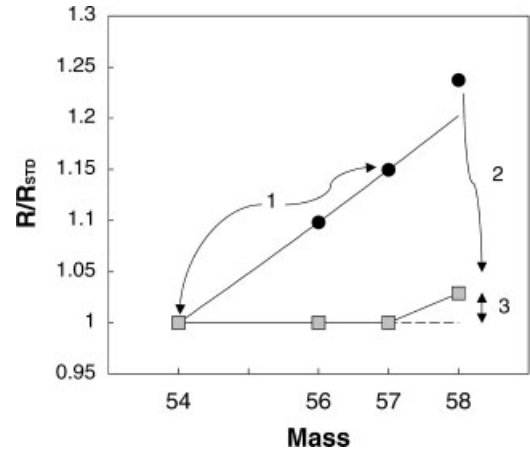

FIGURE 5. Correction of Fe isotopic fractionation by internal normalization for the search of isotopic anomalies. The analyzed sample is isotopically fractionated (from both natural and instrumental sources) (1). An arbitrarily fixed ratio (here ^{57}Fe/^{54}Fe) is assigned a fixed value, allowing the calculation of the mass bias (β in Eq. 4). Given a mass fractionation law, the other isotopic ratios (^{56}Fe/^{54}Fe and ^{58}Fe/^{54}Fe) are corrected for this mass bias (2). The corrected ratios are then normalized to a standard analyzed in the same conditions. Any residual departure between the sample and standard compositions can be taken to be an isotopic anomaly (3).

the solar system (4.5672 ± 0.0003 Gy, Pb-Pb age, Amelin et al., 2002). Some calcium-aluminum rich inclusions called FUN (Fractionated and Unknown Nuclear effects, Clayton & Mayeda, 1977; Wasserburg, Lee, & Papanastassiou, 1977) show isotope anomalies for a variety of elements (O, Mg, Ca, Ti, Cr, Fe, Zn, Sr, Ba, Nd, and Sm, Birck, 2004). Most of these anomalies correspond to excesses or deficits in the neutron-rich isotopes. Iron itself shows excesses in its least abundant neutron-rich isotope, ^{58}Fe, up to 300 ‰ in the inclusion EK-1-4-1 (Völkening & Papanastassiou, 1989, Fig. 6). What these inclusions exactly represent and why they do show large nucleosynthetic anomalies remains unexplained at present. They are some of the most enigmatic objects in the solar system.

C. The Planetary Scale Isotope Homogeneity of the Solar System

The solar system contains a variety of objects that have anomalous isotopic compositions, including refractory inclusions and pre-solar grains. For many elements, isotopic anomalies that had been characterized at a local scale have subsequently been found, although of a much smaller magnitude, in planetary scale objects. For instance, molybdenum and ruthenium show isotopic anomalies at the scale of µm-sized pre-solar SiC grains (Nicolussi et al., 1998; Savina et al., 2004) and such effects are also found in differentiated planetary objects (Dauphas, Marty, & Reisberg, 2002a; Chen et al., 2004; Dauphas et al., 2004b; Papanastassiou, Chen, & Wasserburg, 2004). If any, the presence of Fe isotope anomalies at a planetary scale would be a tremendous discovery, as it would allow tracing of genetic relationships between various objects in the solar system. Zhu et al. (2001) addressed this issue
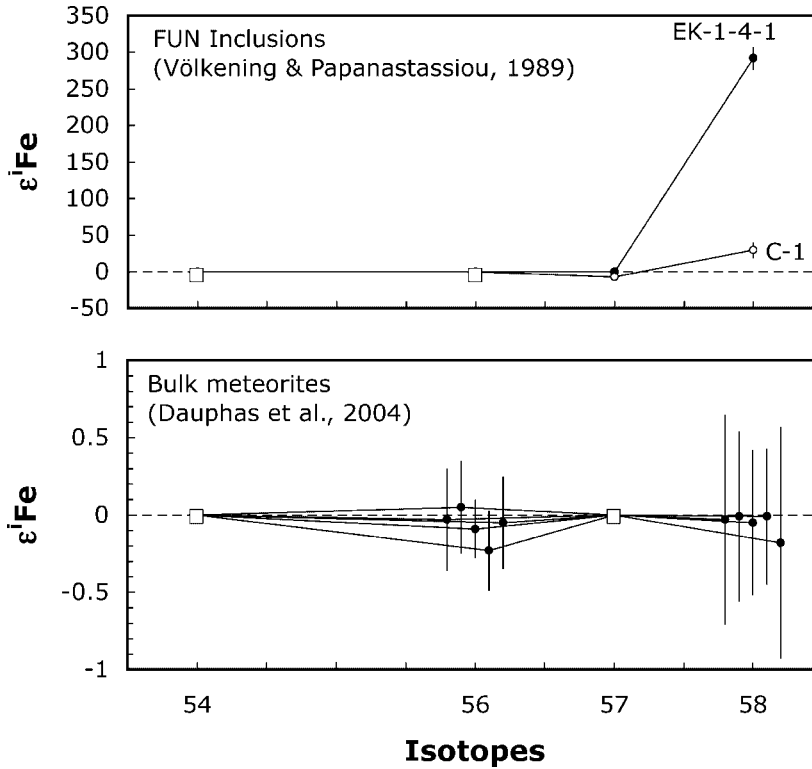
FIGURE 6. Comparison between Fe isotopic anomalies measured in Allende FUN inclusions EK-1-4-1 and C-1 (Völkening & Papanastassiou, 1989, **top panel**) and the bulk meteorites Orgueil, Allende, Eagle Station, Brenham, and Old Woman (Dauphas et al., 2004a, **bottom panel**). In Völkening and Papanastassiou (1989), the values are for the ^{i}Fe/^{56}Fe ratios normalized to ^{54}Fe/^{56}Fe $= 0.062669$ for mass bias correction. In Dauphas et al. (2004a), the values are for the ^{i}Fe/^{54}Fe ratios normalized to ^{57}Fe/^{54}Fe $= 0.36255$ for mass bias correction (note that the second column entry of Table 5 in Dauphas et al., 2004a is erroneously labeled ε^{57}Fe while it should be ε^{56}Fe). All uncertainties are 2σ. See Equations 3 and 4 for the definition of the ε notation.

by analyzing the Fe isotopic composition of various meteorites. They did not find any departure from mass-dependent fractionation and concluded that the solar system had been well homogenized for Fe. Unfortunately, their study did not provide the final word on this question because they did not analyze the least abundant isotope of iron (^{58}Fe), which is also the most likely to vary (Völkening & Papanastassiou, 1989). There are actually few studies where the abundance of this isotope is reported (Völkening & Papanastassiou, 1989; Kehm et al., 2003; Dauphas et al., 2004a). The reason is that there is a huge dynamic contrast between the most and the least abundant isotopes of iron (^{56}Fe/^{58}Fe=325.6), which causes tremendous technical challenges. Völkening and Papanastassiou (1989) and Kehm et al. (2003) measured ^{58}Fe with precisions of approximately 5 ε. Very recently, Dauphas et al. (2004a) used larger ion beams and reported accurate measurements of ^{58}Fe with an improvement by a factor of 10 in terms of precision compared to earlier work (Fig. 3). This quantum leap in precision allowed reinvestigation of the question of the homogeneity of the solar system for Fe isotopes. No anomaly was detected in the measured samples (Fig. 6). Among the major rock-forming elements, oxygen lays as an outlier with the large non-mass-dependent isotope heterogeneity that it shows at a planetary scale (Clayton, 1993).

V. HIGH TEMPERATURE MASS FRACTIONATION

At least three processes are capable of creating isotopic fractionation at high temperature in natural systems. These are diffusion in liquids, solids, or gases, evaporation, condensation, and phase partitioning.

A. Theory and Experiments

1. Evaporation and Condensation

Evaporation and condensation are phase exchange processes that can give rise to kinetic mass fractionation. Some equilibrium mass fractionation may be present but it is always negligible compared to kinetic effects. The kinetic theory of gases allows prediction of the isotopic fractionation resulting from evaporation and condensation (Tsuchiyama, Tachibana, & Takahashi, 1999; Humayun & Cassen, 2000; Richter et al., 2002; Davis & Richter, 2004; Richter, 2004). For an ideal gas with velocities distributed following a Maxwellian distribution, the one-sided flux per unit time per unit surface is given by

$$J_i = \frac{P}{\sqrt{2\pi m_i \mathrm{R}T}} \qquad (5)$$

where P is the pressure, m_i is the molecular weight of i, R is the gas constant, and T is the temperature. At equilibrium between the liquid and gas, the pressure in the gas phase is the saturation vapor pressure of i. Only a fraction γ of the impinging atoms is adsorbed. This value is called the sticking coefficient, which must be equal to the evaporation coefficient at equilibrium. The flux of atoms that are incorporated in the liquid is therefore

$$J_i^{\text{sat}} = \frac{\gamma_i P_{i,\text{sat}}}{\sqrt{2\pi m_i \text{R}T}} \qquad (6)$$

This is known as the Hertz–Knudsen equation. Let us now consider a liquid or a solid that is evaporated in partial vacuum. In that case, the flux from the liquid into the gas is not balanced by a flux from the gas into the liquid and the net evaporation flux is simply given by

$$J_i = \frac{\gamma_i (P_{i,\text{sat}} - P)}{\sqrt{2\pi m_i \text{R}T}} \qquad (7)$$

When $P_i < P_{i,\text{sat}}$, the flux is positive and this corresponds to a net evaporation. When $P_i > P_{i,\text{sat}}$, the flux is negative and this corresponds to net condensation. If the pressure in the gas is very small compared to the saturation vapor pressure, a situation known as free evaporation, then the ratio of the fluxes of two isotopes 1 and 2 is

$$\frac{J_1^e}{J_2^e} = \frac{P_{1,\text{sat}}}{P_{2,\text{sat}}} \frac{\gamma_1}{\gamma_2} \sqrt{\frac{m_2}{m_1}} \qquad (8)$$

This is also true in the case of condensation with no return from the condensate to the gas, with P_i in place of $P_{i,\text{sat}}$

$$\frac{J_1^c}{J_2^c} = \frac{P_1}{P_2} \frac{\gamma_1}{\gamma_2} \sqrt{\frac{m_2}{m_1}} \qquad (9)$$

It is assumed that the ratio $P_{1,\text{sat}}/P_{2,\text{sat}}$ is equal to the isotopic ratio in the liquid during evaporation and that P_1/P_2 is equal to the isotopic ratio in the gas during condensation. We thus obtain a fractionation factor α between the starting reservoir and the flux from one reservoir to the other $\alpha = (N_1/N_2)/(J_1/J_2)$

$$\alpha = \frac{\gamma_2}{\gamma_1} \sqrt{\frac{m_1}{m_2}} \qquad (10)$$

Condensation does fractionate isotopes as much as evaporation. The only difference is that during condensation, the reservoir effect is less important in the condensate than it is in the solid or liquid residue during evaporation. During condensation, the solid or liquid is enriched in the light isotopes while during evaporation; it is enriched in the heavy isotopes relative to the gas. When one component of the pressure is not negligible compared to the other (P relative to P_{sat}) and there is return from one reservoir to the other, the fractionation factor is actually smaller than what has been derived here. Complete and detailed treatment of this question can be found in Richter et al. (2002). During evaporation in a medium of non-negligible pressure (Eq. 7), the ratio of the evaporative fluxes of two species is

$$\frac{J_1}{J_2} = \frac{\gamma_1}{\gamma_2} \sqrt{\frac{m_2}{m_1}} \left(\frac{P_{1,\text{sat}} - P_1}{P_{2,\text{sat}} - P_2} \right) \qquad (11)$$

This can be rewritten as

$$\frac{J_1}{J_2} = \frac{1}{\alpha} \frac{P_{1,\text{sat}}}{P_{2,\text{sat}}} \left(\frac{1 - P_1/P_{1,\text{sat}}}{1 - P_2/P_{2,\text{sat}}} \right) \qquad (12)$$

where α is the fractionation factor previously derived for free evaporation or condensation (Eq. 10). If we assume that the liquid or solid residues only see the gas that has just been evaporated, we can also write $P_1/P_2 = J_1/J_2$ and $P_{1,\text{sat}}/P_{2,\text{sat}} = N_1/N_2$. Let us denote $\alpha_e' = (N_1/N_2)/(J_1/J_2)$, then it is easy to rearrange the previous equation and solve it for α_e'

$$\alpha_e' = \alpha - \frac{P}{P_{\text{sat}}} (\alpha - 1) \qquad (13)$$

with α given by Equation 10. During net condensation, the same analysis can be made except that in this case, it is assumed that the gas only sees the last condensate and the prescriptions are $P_{1,\text{sat}}/P_{2,\text{sat}} = J_1/J_2$ and $P_1/P_2 = N_1/N_2$

$$\alpha_c' = \alpha - \frac{P_{\text{sat}}}{P} (\alpha - 1) \qquad (14)$$

When the pressure in the medium is equal to the saturation vapor pressure ($P/P_{\text{sat}} = 1$), then no kinetic isotope fractionation occurs as there is balance between the evaporation and condensation fluxes and the gas and the solid or liquid are in equilibrium. The formalism given to this point can be used to estimate the fractionation factor between the source reservoir and the flux, as a function of the partial pressure in the gas (Eqs. 13 and 14). What is also required is a formalism to describe the time-integrated evolution of the isotopic compositions of the different reservoirs. In most cases, the fractionation can be modeled as a Rayleigh distillation whereby the initial reservoir is depleted without replenishment

$$dN_1 = -J_1 A \, dt \qquad (15)$$

$$dN_2 = -J_2 A dt \qquad (16)$$

where A is the surface area. These two equations can be rewritten as

$$d\ln N_1 = -J_1 A dt / N_1 \qquad (17)$$

$$d\ln N_2 = -J_2 A dt / N_2 \qquad (18)$$

We also have, $\alpha' = (N_1/N_2)(J_1/J_2)$. The previous two equations can therefore be combined to give

$$d\ln(N_1/N_2) = (1 - 1/\alpha') d\ln(N_2) \qquad (19)$$

If R_A is the ratio N_1/N_2 in the starting reservoir, R_0 is the initial ratio, and f is the fraction of the denominator isotope remaining ($f = N_1/N_2$), we have

$$R_A = R_0 f^{1/\alpha' - 1} \qquad (20)$$

The ratio in the other reservoir can be obtained by mass balance

$$R_B = R_0 \frac{1 - f^{1/\alpha'}}{1 - f} \qquad (21)$$

These values are easily converted in δ notation, $\delta = (R/R_0 - 1) \times 10^3$.

Experimentally, it is easier to study evaporation than condensation. The evaporation experiments consist of a solid or a liquid evaporated at high temperature in a vacuum furnace (Hashimoto, 1990; Wang et al., 1999). It is crucial to design the experiment so that no pressure builds up near the sample, which would otherwise lower the observed fractionation factor by allowing recondensation to occur. Various tests have shown that in the experimental apparatus described in Hashimoto (1990) and Wang et al. (1999), no recondensation occurs. The equation describing Rayleigh distillation can also be rewritten as, $\ln(R_A/R_0) = (1 - 1/\alpha')(-\ln f)$. By plotting the logarithm of the ratios as a function of the logarithm of the fraction of ^{54}Fe remaining, we obtain a line with a slope equal to $1 - 1/\alpha'$ for such a distillation.

Dauphas et al. (2004a) measured the Fe isotopic composition in free evaporation experiments for two compositions, one is a molten mixture of oxides in close to solar proportions (24.3 wt % MgO, 2.8% Al_2O_3, 34.1% SiO_2, 1.9% CaO, and 36.8% FeO) and the other is a liquid of pure wüstite composition (FeO). During evaporation of the simple component FeO at 1,823 K, the residue evolves along a Rayleigh distillation with a fractionation factor that is very close to the square root of the masses of the considered isotopes (Wang et al., 1994; Dauphas et al., 2004a). For the pair ^{56}Fe/^{54}Fe, a fractionation factor of 1.01877 ± 0.00047 (2σ) has been measured while theory with $\gamma_{56} = \gamma_{54}$ predicts a value of $(56/54)^{0.5} = 1.01835$. During evaporation of solar composition at 1,923 K, the experimental results depart from theory and the measured fractionation factor is lower than the square root of the masses, 1.01322 ± 0.00067 (2σ) (Dauphas et al., 2004a). This departure can be explained in two ways. It can be due to the fact that the evaporation coefficients of ^{54}Fe and ^{56}Fe are not equal and that for a melt of this composition, $\gamma_{56} > \gamma_{54}$. Another possibility is that the surface of the liquid or the solid is corrugated at a very fine scale so that part of the gas equilibrates with the liquid or the solid before it is lost. As an extreme case, bubbles could form that would be fully equilibrated with the residue before being released to the surface (Wombacher, Rehkðmper, & Mezger, 2004). More work is required to investigate isotope fractionation during evaporation, notably by coupling in the same experiments elements having different chemical affinities. As a rule, when evaporation experiments are available, one should use the fractionation factor that has been measured rather than assume its value based on theoretical considerations.

2. Diffusion

High temperature diffusion experiments have been done for various elements (Richter, Liang, & Davis, 1999; Richter et al., 2003). These consist in putting together two contrasted compositions, like molten basalt and rhyolite. The activity gradient induces a net flow of the elements. Because the lower mass isotopes diffuse faster than the heavier ones, this leads to isotopic fractionation. Molecular dynamics calculations are required to adequately describe the mass fractionation (Bearman & Jolly, 1981; Tsuchiyama et al., 1994) but, from a phenomenological point of view, it can be parameterized as follows

$$\frac{D_1}{D_2} = \left(\frac{m_2}{m_1}\right)^{\beta} \tag{22}$$

No measurements have been made in silicate-oxide systems for Fe but Richter et al. (2003) suggested that it might follow calcium, which has a β of approximately 0.075. The extent of the fractionation will depend on the specific case that is being studied. Isotopic fractionation due to diffusion at high temperature in a natural system has only been documented for Li (Beck et al., 2005; Lundstrom et al., 2005). For Fe, places to look for such effects are solids or liquids that have been evaporated in a diffusion-limited regime (Wang et al., 1999; Richter, 2004) or silicate material left after iron reduction and sequestering of the metal (Cohen et al., 2005; Roskosz, Luais, & Toplis, 2005a; Roskosz et al., 2005b). In a reduction experiment, Roskosz et al. (2005b) documented large isotopic fractionation during diffusion of Fe in the platinum wire that was used to scavenge metallic Fe from the silicate (corresponding to $\beta \approx 0.27$). Clearly, more work is required to document Fe isotopic fractionation by diffusion at high temperature, which may be relevant to volatile loss by evaporation in the protosolar nebula and reduction during metal/silicate differentiation in planets and asteroids.

3. Phase Partitioning

Theory predicts that there may be measurable equilibrium isotope fractionation between coexisting minerals at high temperature in planetary bodies (Polyakov & Mineev, 2000). Cohen et al. (2005) and Roskosz, Luais, & Toplis (2005a), Roskosz et al. (2005b) measured the isotopic fractionation associated with iron reduction at high temperature. The isotopic fractionation that they observed more likely reflects kinetic isotope fractionation associated with diffusive transport and/or the reduction reaction. In a time-resolved reduction experiment, Roskosz et al. (2005b) estimated that the fractionation between Pt-Fe alloy and a proxy composition for the silicate Earth at 1,500°C and log(fO_2) = −5 was small (<0.2 ‰/amu). Natural systems provide some clues on what the equilibrium isotope fractionation between high temperature phases might be (Zhu et al., 2002; Beard & Johnson, 2004; Poitrasson, Levasseur, & Teutsch, 2005) but more work remains to be done to document these effects under laboratory controlled pressure-temperature-composition conditions.

B. Selected Natural Variations

1. Planets and Planetesimals

It was recognized early on that the silicate Earth had approximately homogeneous isotopic composition (Beard & Johnson, 1999), being enriched by 0.039 ± 0.008 ‰/amu in the heavy isotopes of Fe relative to IRMM-014 or chondrites (Fig. 4). This conclusion was ascertained by subsequent studies (Beard et al., 2003a; Rouxel et al., 2003; Dauphas et al., 2004a,c;

Poitrasson et al., 2004; Williams et al., 2004a). Other planetary bodies, such as the Moon, Mars (sampled by SNC meteorites), or Vesta (sampled by Howardite-Eucrite-Diogenite HED meteorites) also have remarkable homogeneous compositions. However, the compositions seem to vary from one planet or asteroid to another (Poitrasson et al., 2004). Vesta ($F_{Fe} = 0.010 \pm 0.010$ ‰/amu) and Mars ($F_{Fe} = 0.001 \pm 0.006$ ‰/amu) have approximately the same isotopic composition as IRMM-014 or chondrites, but the moon is markedly enriched in the heavy isotopes relative to both the silicate Earth and the chondritic reservoir ($F_{Fe} = 0.069 \pm 0.010$ ‰/amu). Note that iron meteorites of all groups seem to be enriched in heavy Fe relative to IRMM-014, by 0.032 ± 0.010 ‰/amu (Zhu et al., 2001; Kehm et al., 2003; Poitrasson, Levasseur, & Teutsch, 2005). The reasons for these variations at a planetary scale are poorly understood. Poitrasson et al. (2004) suggested that the enrichment in heavy Fe of the Moon and the Earth compared to other planetary bodies (and chondrites) was the result of evaporative loss of Fe during the Moon-forming impact, which would have left the residue depleted in volatiles and isotopically fractionated. In order to reconcile this interpretation with K isotope data, which shows no isotopic fractionation between the Earth and the Moon (Humayun & Clayton, 1995), they further argued that Fe had been primarily lost from the metal cores of the proto-Earth and the impactor. If true, then other metals like nickel should show the same effect and the hypothesis that they propose should be testable.

2. Inter-Mineral Variations

Zhu et al. (2002) and Poitrasson, Levasseur, and Teutsch (2005) documented the Fe isotopic compositions of mineral separates of differentiated meteorites. These two groups measured the compositions of coexisting metal, olivine, troilite, and schreibersite in pallasite meteorites. Pallasites are meteorites consisting primarily of metal and olivine, which are thought to be samples from the core-mantle boundaries of small-differentiated planetesimals. These studies showed that the metal is systematically enriched in the heavy isotopes of Fe compared to the olivine by 0.02–0.09 ‰/amu. The lower end of the range may reflect equilibrium isotope fractionation as the calculations of Polyakov and Mineev (2000) predict an equilibrium fractionation of approximately 0.03 ‰/amu between metal and olivine at 1,000°C but the larger values remain unexplained. Poitrasson, Levasseur, and Teutsch (2005) also found that the isotopic composition of taenite (metallic Fe with more than 25% Ni in solid solution) in iron meteorites is enriched in the heavy isotopes of Fe by approximately 0.05–0.10 ‰/amu relative to kamacite (metallic Fe with less than 7.5% Ni in solid solution). This may reflect a kinetic isotope effect associated with diffusion. Indeed, during formation of the Widmanstätten patterns, kamacite grows at the expense of taenite and Fe must diffuse from taenite to kamacite. If the light isotopes of Fe diffuse faster, one would therefore expect kamacite to be light relative to taenite. Another possibility is that it reflects equilibrium fractionation between taenite and kamacite during kamacite crystal growth. Detailed analysis of Fe and Ni isotopic compositions along diffusion profiles in Widmanstätten patterns

may help to test which of the two scenarios is correct. Williams et al. (2004b) reported Fe isotope fractionation between coexisting metal and sulfide phases in iron meteorites, which most likely reflect equilibrium fractionation.

Isotopic variations are also observed among coexisting mantle minerals and in bulk mantle rocks (Zhu et al., 2002; Beard & Johnson, 2004; Williams et al., 2004a; Poitrasson, Levasseur, & Teutsch, 2005; Poitrasson & Freydier, 2005; Williams et al., 2005). This heterogeneity is to a very large extent erased during melting as, except for granitoids which show a spread in isotopic compositions from 0.05 to 0.20 ‰/amu relative to IRMM-014 (Poitrasson & Freydier, 2005), rocks that are derived from magmas show no resolvable Fe isotopic fractionation from one to another (Beard & Johnson, 2004). Mid-ocean ridge basalts may actually differ in their Fe isotopic compositions relative to ocean island basalts by +0.02 ‰/amu (Williams et al., 2004a). It is not clear at present what can be ascribed in the variations measured in igneous rocks, to kinetic or equilibrium fractionation, or modification through metasomatism.

3. Cosmic Spherules

Cosmic spherules are the result of the ablation and subsequent melting of meteorites during their travel across the atmosphere to reach the Earth's surface. These spherules are usually collected in deep-sea clays, where the sedimentation rate is low and the extraterrestrial contribution per unit mass of sediment is therefore high. The cosmic spherules are systematically enriched in the heavy isotopes of Fe relative to bulk chondrites, by as much as 25 ‰/amu (Davis et al., 1991; Davis & Brownlee, 1993; Herzog et al., 1999; Alexander et al., 2002; Taylor et al., 2005). There is no doubt that these enrichments result from evaporative loss of Fe during travel across the terrestrial atmosphere.

4. Lunar Soils

A study by Wiesli et al. (2003) showed that lunar soils are enriched in the heavy isotopes of Fe relative to bulk planetary material. This is reminiscent of what has been observed for other elements in similar samples. The enrichment in heavy Fe compared to indigenous lunar Fe correlates with the ratio np-Fe^0/FeO, where np-Fe^0 stands for nanophase Fe metal grains. The Fe isotopic composition of this phase is inferred to be around 0.4 ‰/amu relative to IRMM-014. Various scenarios have been proposed to explain the presence of these metal grains and include (i) reduction by implanted solar wind H_2 and (ii) solar sputtering-impact evaporation and subsequent vapor deposition of the metal. The observed enrichment in heavy Fe is consistent with the second scenario, although more work is needed to estimate the effect of reduction on the isotopic composition of Fe (Cohen et al., 2005; Roskosz, Luais, & Toplis, 2005a; Roskosz et al., 2005b).

5. Chondrules

Chondrules are submillimeter spheres that formed by solidification of a melt under low gravity conditions, early in the solar system history (Zanda, 2004). They represent a large fraction of

the most represented group of meteorites on Earth, chondrites. Despite decades of effort, the exact mechanism of their formation is poorly understood. Experiments aimed at reproducing the textures observed in chondrules indicate that they must have been heated near liquidus peak temperatures (1,700–2,100 K) and must have subsequently cooled at rates of 10–1,000 K/hr. For a submillimiter object heated to such temperatures, a significant loss of the most volatile elements by evaporation is expected. Iron is depleted in some chondrules compared to others, notably between type I and type II chondrules. This depletion may have resulted from evaporation, Fe reduction, and physical separation of the metal and silicate, or may simply have been inherited from the precursors from which the chondrules formed. Depending on the partial pressure of Fe in the gas phase, evaporation may or may not induce isotopic fractionation (Eq. 13). Alexander and Wang (2001) measured the isotopic compositions of some chondrules by SIMS but they had limited precision and were unable to detect any variation relative to the terrestrial standard. More recently, measurements have been performed by MC-ICPMS, which show that the Fe isotopic composition of chondrules is variable (Zhu et al., 2001; Kehm et al., 2003; Mullane et al., 2003, Fig. 4). However, the size of these fluctuations is small, typically <0.5 ‰/amu, and does not correspond to a systematic enrichment in the heavy isotopes of Fe relative to bulk meteorites. Approximately half (14/22) of all the chondrules measured so far have negative F_{Fe} values. This is contrary to the expectation if Fe had been lost from the system by evaporation. These observations can be explained in multiple ways. Chondrules may have formed from precursors that contained light Fe, they may have acquired Fe by condensation from a gas of normal composition, or diffusion/reduction processes might have been involved. Whatever the mechanism is, it must account for the fact that the Fe isotopic composition of chondrules is symmetrically distributed around the bulk chondrite value. To understand the origin of the observed Fe isotope variations in chondrules, more experimental work is required. The kinetic and equilibrium effects associated with Fe reduction must be documented and the microdistribution of Fe isotopes in well-preserved chondrules must be analyzed.

6. Metal Condensates

Some chondritic meteorites, specifically CH and CB, contain zoned metal grains with nickel and refractory platinum group element compositions which indicate that they were probably formed by condensation from a gas phase (Newsom & Drake, 1979; Meibom et al., 1999; Campbell et al., 2001). As discussed previously (Eqs. 10 and 14), condensation theory predicts that there should be a kinetic isotope effect that enriches the condensate in the light isotopes of Fe relative to the gas phase. If the square root of the masses is adopted for α, the first solid that condenses must be enriched in the light isotopes by approximately 9 ‰/amu relative to the starting gas. Alexander and Hewins (2004) recently measured the Ni and Fe isotopic compositions of zoned metal grains and found them to be enriched in the light isotopes by approximately the right value (Fig. 7). They also observed a zoning in the grains, with the center being lighter than the rim. Nickel shows exactly the same systematic as what is observed for Fe. These observations
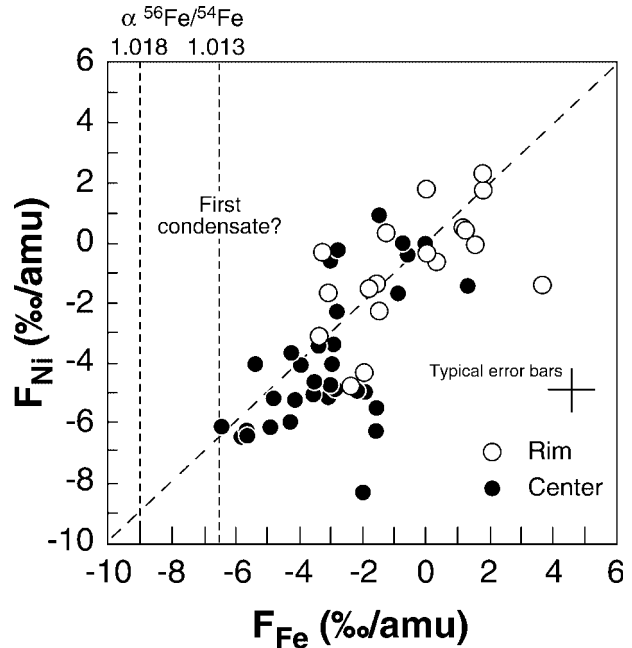
FIGURE 7. Iron and nickel isotopic compositions in meteoritic metal grains thought to have formed by condensation from gas (Alexander & Hewins, 2004). If metal in the center represents the first condensate, then one would expect it to have light isotopic composition relative to the gas (Eq. 14), which is observed here. As light Fe and Ni is being subtracted from the system during condensation, the remaining gas gets enriched in the heavy isotopes and the late condensates that form the rim must have heavier isotopic compositions compared to the center, which is also observed. If the center represents the first condensate and if the initial gas had solar composition, then the composition measured at the center can be used to retrieve the value of the fractionation factor, $\alpha = 1.013$ (1.018 for the square root of the masses of ^{56}Fe and ^{54}Fe).

make perfect sense with the suggestion that the grains formed by condensation. This is the first natural evidence for isotopic fractionation during condensation. The relationship does not extend all the way down to -9 ‰/amu but assumes an end-member at around -6.5 ‰/amu for both Fe and Ni. If this really represents the first condensate, it may imply that during condensation, the fractionation factor departs from ideal behavior, as has already been documented for evaporation (Dauphas et al., 2004a). Alternatively, it may indicate that Fe in the gas was not largely oversaturated and that there was exchange between the gas and the solid phases, which reduced the apparent fractionation factor. This is a very interesting result that deserves further attention, notably taking advantage of LA-MC-ICPMS.

VI. LOW TEMPERATURE MASS FRACTIONATION

Initially, the possibility that Fe isotopes might be used to trace life in past and present terrestrial and extraterrestrial environments represented a strong driving force for people to analyze Fe isotopic compositions (Beard et al., 1999). Subsequent studies questioned this idea and showed that Fe isotopes could be fractionated in aqueous systems under conditions that do not

involve life (Anbar et al., 2000; Bullen et al., 2001; Skulan, Beard, & Johnson, 2002; Roe, Anbar, & Barling, 2003; Welch et al., 2003; Anbar, 2004; Brantley et al., 2004; Rodushkin et al., 2004). Iron isotopes can therefore not be taken as a biosignature but can potentially be used to trace its transport in aqueous systems. Molecular vibration theory predicts that Fe isotopes vary at equilibrium between two phases in which Fe forms bounds of different strengths (Polyakov, 1997; Polyakov & Mineev, 2000; Schauble, Rossman, & Taylor, 2001; Schauble, 2004; Jarzecki, Anbar, & Spiro, 2004; Anbar, Jarzecki, & Spiro, 2005). It may also vary due to kinetic isotope effects associated with unidirectional chemical reactions and transport. In most instances, it is difficult to disentangle what arises from equilibrium and kinetic effects. Many aspects of the Fe isotope chemistry in solution have been tested in the past few years (Table 3). In this section, only some of these aspects that are directly applicable to natural systems are discussed.

A. Abiotic Aqueous Processes

1. Redox

Bullen et al. (2001) showed that abiotic oxidation of ferrous iron into ferric iron in nature can cause isotopic fractionation of Fe. They analyzed precipitated ferrihydrite and found it to be enriched in the heavy isotopes of Fe by approximately 0.45 ‰/amu relative to the source material. The authors argued that this probably reflected equilibrium fractionation between Fe(II)aq and Fe(III)aq. However, interpretation of the results was complicated by the fact that Fe precipitation can cause kinetic isotope fractionation, which enriches the precipitate in the light isotopes relative to the fluid (Skulan, Beard, & Johnson, 2002).

Johnson et al. (2002) and Welch et al. (2003) explored in more details some of the issues associated with the experimental determination of the equilibrium isotope fractionation between Fe(II)aq and Fe(III)aq (also see Bullen, White, & Childs, 2003; Johnson et al., 2003a). They investigated the kinetics of isotope exchange between Fe(II)aq and Fe(III)aq by mixing solutions of dissolved ferrous and ferric iron labeled with isotopic spikes. They showed that the two pools are equilibrated isotopically in HCl at room temperature in approximately 150–300 sec (Fig. 8A). In regard of geological timescales, this is almost instantaneous and in most cases, it is reasonable to assume that dissolved Fe(II)aq and Fe(III)aq remain in isotopic equilibrium. There are many caveats in the estimation of the Fe(III)aq-Fe(II)aq isotopic fractionation, as the two species must be separated before being analyzed with mass spectrometers, and kinetic isotope fractionation or partial re-equilibration of the Fe(III)aq-Fe(II)aq pools during precipitation would lead to erroneous results. Welch et al. (2003) achieved Fe(III)aq separation by $BaCO_3$ co-precipitation, which scavenges the solution of ferric iron on timescales that are shorter than 1 sec. The study of the kinetics of isotope exchange between Fe(II)aq and Fe(III)aq was used to correct for partial re-equilibration during precipitation. The issues of kinetic isotope fractionation during precipitation and diffusion in solution are more difficult to handle but both processes would tend to enrich the precipitate in the light isotopes, which is opposite to what is observed. The inferred equilibrium fractionation factor between Fe(III)aq and Fe(II)aq does not depend on the Cl^- concentration but depends on the temperature

$$10^3 \ln \alpha_{Fe(III)-Fe(II)} = \frac{0.334 \pm 0.032 \times 10^6}{T^2} - 0.88 \pm 0.38$$

(23)

TABLE 3. Summary of Fe isotope fractionation factors between Fe species in abiotic and biological systems

Species	Reactions	δ^{56}Fe	References
Aqueous species fractionation factor			
Fe(II)aq - Fe(III)aq	Abiotic oxidation 22C (equilibrium)	-2.9 +/- 0.2	Welch et al. (2003)
Fe(II)aq - Fe(II)>Fe(III)-oxides	Abiotic adsorption	-0.8	Teutsch et al. (2005)
Fe(II)aq - Fe(II)>Fe(III)-oxides	Abiotic adsorption	-2.1 (calculated)	Icopini et al. (2004)
Fe(II)aq - Fe(II)>Fe(III)-oxides	Adsorption in DIR experiment	-0.9 to -0.4	Crosby et al. (2005)
Fe(III)aq - ([FeII(bipy)3]2+)	Ligand dissociation (kinetic)	-1.7 to -11.7	Matthews et al. (2001)
Fluid-mineral fractionation factor during mineral precipitation			
Fe(II)aq - Fe(III)-oxides	Abiotic precipitation (kinetic)	-0.9 +/- 0.2	Bullen et al. (2001)
Fe(II)aq - Fe_3O_4 (magnetite)	Dissimilatory Fe reduction (kinetic)	-1.3 +/- 0.1	Johnson et al. (2005)
Fe(II)aq - $FeCO_3$ (siderite)	Abiotic precipitation (equilibrium)	0.4 to 0.6	Wiesli et al. (2004)
Fe(II)aq - $FeCO_3$ (siderite)	Dissimilatory Fe reduction (kinetic)	0.0 +/- 0.1	Johnson et al. (2005)
Fe(II)aq - FeS (gregite)	Abiotic precipitation (kinetic)	0.9 to 0.2	Butler et al. (2005)
Fe(III)aq - Fe_2O_3 (hematite)	Abiotic precipitation (equilibrium)	0.1 +/- 0.2	Skulan et al. (2002)
Fe(III)aq - Fe_2O_3 (hematite)	Abiotic precipitation (kinetic)	Up to 0.8	Skulan et al. (2002)
Fluid-mineral fractionation factor during Fe(III) reduction			
Fe(II)aq - Fe(III)-oxides	Dissimilatory Fe reduction (kinetic)	-2.6 to -1.3	Beard et al. (1999, 2003); Johnson et al. (2005)
Fluid-mineral fractionation factor during Fe(II) oxidation			
Fe(II)aq - Fe(III)-oxides	Photosynthetic Fe oxidation	-1.5 +/- 0.2	Croal et al. (2004)
Fe(II)aq - Fe(III)-oxides	Abiotic Fe oxidation	-0.9 +/- 0.2	Bullen et al. (2001)
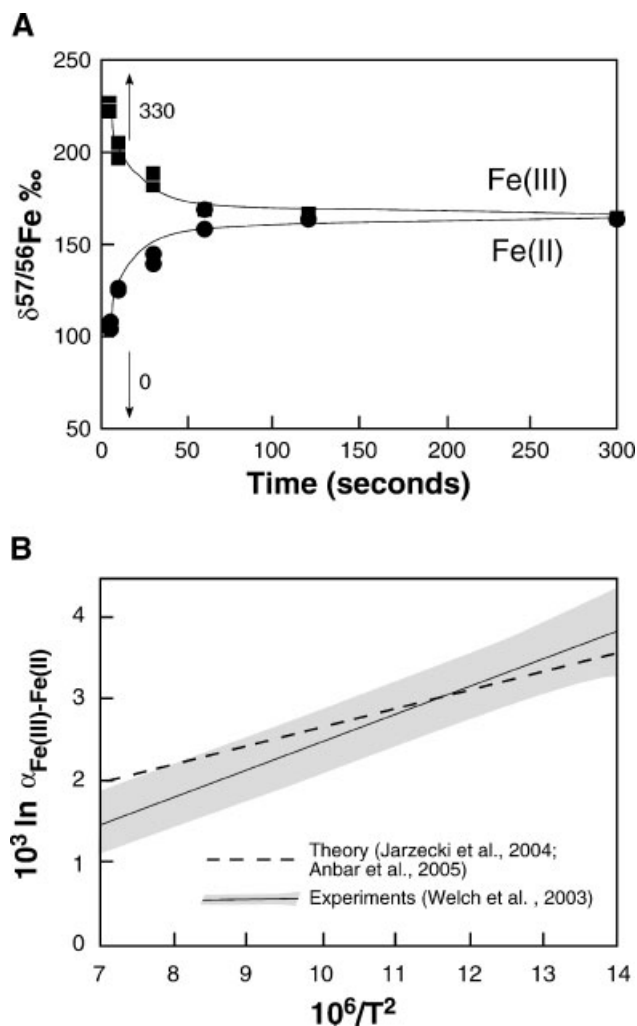
FIGURE 8. Fe(II)aq-Fe(III)aq equilibrium isotope fractionation. **A:** Determination of Fe(II)-Fe(III) isotope exchange kinetics by mixing Fe(II)aq and Fe(III)aq solutions labeled with a spike of ^{57}Fe (Welch et al., 2003). The initial Fe(II)aq and Fe(III)aq solutions had $\delta^{57/56}$Fe = 0 ‰ and $\delta^{57/56}$Fe = 330 ‰, respectively. As shown, the two reservoirs reach isotopic equilibrium within minutes after mixing. **B:** Equilibrium isotope fractionation for the ^{56}Fe/^{54}Fe ratio between Fe(II)aq and Fe(III)aq as a function of temperature based on experiments (Welch et al., 2003; Beard & Johnson, 2004) and theory (Jarzecki, Anbar, & Spiro, 2004; Anbar, 2004). The shaded gray area is the 2σ envelope of the equilibrium isotopic fractionation between Fe(II)aq and Fe(III)aq.

where the temperature is in °C and the fractionation factor $\alpha_{\text{Fe(III)-Fe(II)}}$ is for the couple ^{56}Fe$-^{54}$Fe (Welch et al., 2003, Fig. 8B). At 25°C and under equilibrium conditions, Fe(III)aq is enriched in the heavy isotopes by 1.4 ‰/amu relative to Fe(II)aq. Recent theoretical calculations predict a value that is very close to the one measured experimentally (Jarzecki, Anbar, & Spiro, 2004; Anbar, Jarzecki, & Spiro, 2005). Kavner et al. (2005) found a large isotopic fractionation in an electroplating experiment, which they suggest is due to electron charge transfer. The strong isotopic fractionation associated with Fe oxidation/reduction makes this system a powerful tracer of redox changes in aqueous fluids.

2. Adsorption and Mineral Dissolution

Mineral dissolution tends to enrich the fluid in the light isotopes (Brantley, Liermann, & Bullen, 2001; Brantley et al., 2004). The magnitude of this effect, documented for hornblende crystals, depends on the affinity of Fe with the ligands that are present in the fluid (see section B.4.). Many factors come into play and it is very difficult to disentangle the various mechanisms that are responsible for the net isotopic fractionation that is observed. Skulan, Beard, and Johnson (2002) investigated kinetic isotope fractionation during hematite dissolution in acid medium. On the basis of the results using natural, and presumably, homogeneous hematite, it has been demonstrated that partial dissolution of hematite in concentrated HCl produces no significant isotopic fractionation, within the uncertainty of 0.10‰.

Adsorption of Fe(II) on goethite may induce an isotopic fractionation $\Delta_{\text{Fe(II)ad-Fe(II)aq}}$ of 1.5 ‰/amu (Icopini et al., 2004). In an experiment of microbial dissimilatory iron oxide reduction, Crosby et al. (2005) measured the Fe isotopic compositions of Fe(II) adsorbed on the ferric oxide substrate and Fe(II) dissolved in the fluid. The inferred fractionations $\Delta_{\text{Fe(II)ad-Fe(II)aq}}$ between these two reservoirs are 0.19 ± 0.05 and 0.43 ± 0.09 ‰/amu for hematite and goethite substrates, respectively.

In an *in situ* field experiment, Teutsch et al. (2005) injected oxygenated water at a test well into an aquifer containing dissolved Fe(II). They then extracted water from this well and measured the isotopic composition and concentration of Fe(II)aq. They found that the isotopic composition of Fe(II) in the extracted water was enriched in the light isotopes relative to the source groundwater and interpreted their results as follows:

(i) When oxygenated water is injected, it moves the groundwater out of the injection zone. The fraction of Fe(II) that is adsorbed on the particles is oxidized into Fe(III) and forms a reactive surface.

(ii) During extraction, the groundwater that contains Fe(II), moves in this reactive zone and part of Fe(II) is adsorbed on Fe-oxyhydroxide. The authors argue that the adsorption of Fe(II) on Fe(III)-oxyhydroxides is associated with an equilibrium isotopic fractionation that enriches dissolved Fe(II) in the light isotopes relative to Fe(II) adsorbed on the substrate.

(iii) When steady-state is reached, what comes in the reactive zone must be equal to what goes out and there is no isotopic fractionation of extracted Fe(II)aq relative to Fe(II)aq in the initial groundwater.
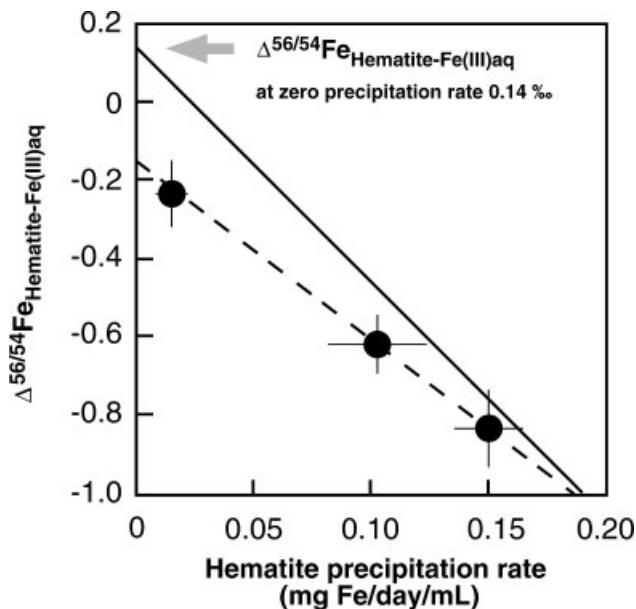
From this field experiment, they estimate a fractionation $\Delta_{\text{Fe(II)ad-Fe(II)aq}}$ of 0.3 ‰/amu, which is close to the value estimated by Crosby et al. (2005). As discussed by Teutsch et al. (2005), partial oxidation of dissolved Fe(II)aq by oxygenated waters and precipitation of heavy Fe(III)s could also explain these results. However, the authors argue that dispersive mixing between Fe(II)aq- and O_2-bearing waters is inefficient and that at pH 7 the kinetics of Fe(II)aq-oxidation are slow.

3. Precipitation

It is difficult to probe equilibrium fractionation between aqueous liquids and minerals because the exchange kinetics are very slow at low temperature. For this reason, one has to rely on precipitation experiments done at low precipitation rates to infer the equilibrium fractionation factor. Experiments of hematite (Fe_2O_3) precipitation from Fe(III)aq show that there is a correlation between the isotopic fractionation and the rate of precipitation (Skulan, Beard, & Johnson, 2002, Fig. 9). This is interpreted to result from kinetic isotope fractionation, which tends to enrich the precipitate in the light isotopes of Fe relative to the fluid. The degree of kinetic isotope fractionation during precipitation increases with the rate of precipitation. If this correlation is extrapolated to zero precipitation rate, then the inferred fractionation $\Delta_{Hematite-Fe(III)aq} = 0.075$ ‰/amu (Beard & Johnson, 2004) may be close to the equilibrium value (each increment of Fe precipitated may be in equilibrium with the fluid). These results shed new light on the earlier work of Bullen et al. (2001). The fractionation that these authors had found between Fe(II)aq in solution and precipitated ferrihydrite may represent the superposition of two processes that act against each other from an isotopic point of view. Oxidation from Fe(II)aq to Fe(III)aq enriches ferric iron in the heavy isotopes but precipitation of Fe(III)aq into ferrihydrite enriches the precipitate in the light isotopes due to kinetic isotope fractionation.

Similar precipitation experiments have been performed for formation of siderite ($FeCO_3$) from Fe(II)aq (Wiesli, Beard, & Johnson, 2004). The documented fractionation at a low precipitation rate is $\Delta_{Siderite-Fe(II)aq} = -0.24$ ‰/amu. Interest-ingly, theory, laboratory experiments, and observations of natural samples seem to indicate that the isotopic fractionation between Fe-carbonates and Fe(II)aq depends on the degree of Ca (or other cation) substitutions (Polyakov & Mineev, 2000; Schauble, Rossman, & Taylor, 2001; Johnson et al., 2003a, 2005). The precipitated carbonates should become more negative relative to the fluid as the mol fraction of Fe decreases. This needs to be confirmed in well-controlled abiotic carbonate precipitation experiments.

Butler et al. (2005) explored the isotopic fractionation of Fe during FeS precipitation from Fe(II)aq solutions. They found that the zero-age precipitate has systematically light isotopic composition relative to the fluid, by approximately -0.4 ‰/ amu. During aging, the precipitate and the fluid tend to converge towards the same isotopic composition. The minimum difference that is observed after 170 hr is -0.15 ‰/amu, but this may still not represent the isotope fractionation at equilibrium. The initial enrichment in the light isotopes of the precipitate relative to the fluid is interpreted to reflect a kinetic isotope effect associated with ligand exchange between hexaqua Fe(II) and aqueous sulfide complexes. This fractionation may be relevant to the formation of pyrite, which is an important repository of Fe in sediments.

4. Diffusion

Strong concentration contrasts may develop in natural systems, notably when precipitation occurs. As discussed previously, during diffusion, the light atoms tend to move faster than the heavy ones and the region from which the atoms diffuse out gets enriched in the heavy isotopes compared to the region where the atoms diffuse in. One recent study documented the isotopic fractionation of transition metals during diffusion in water (Rodushkin et al., 2004). The diffusion profile in the diffusion cell is not perfect for Fe but it seems to be similar to that observed for Zn, which is better defined. If the same parameterization is adopted as before for the fractionation factor as a function of the mass, $D_1/D_2 = (m_2/m_1)\beta$ (Eq. 22), the experiments of Rodushkin et al. (2004) indicate that the exponent β must be around $0.0015-0.0025$, for both Zn and Fe. This is small compared to what is observed in silicate melts for other elements. This may be due to charge interactions because diffusion of anions or charge transfer must occur to maintain electroneutrality as Fe diffuses away.

FIGURE 9. Isotope fractionation during hematite precipitation (Skulan, Beard, & Johnson, 2002). At high precipitation rate, kinetic isotope effects enrich the precipitate in the light isotopes relative to Fe(III)aq. At zero precipitation rate, the isotopic fractionation between the precipitate and the fluid may approximate equilibrium conditions (see Skulan, Beard, & Johnson, 2002, for the corrections that have been applied to the raw data to derive the continuous heavy line).

5. Modeling Fractionation by Oxidation-Precipitation in a Closed System

In terrestrial aqueous systems, ferric iron is very insoluble at neutral pH and rapidly precipitates to form oxyhydroxides. The precipitation of Fe oxyhydroxides from the oxidation of aqueous Fe(II) can be explored by using a two-stage model already used in the same context by Anbar (2004), Beard and Johnson (2004), and Johnson et al. (2004). It assumes that Fe(II)aq is first oxidized (by O_2 or Fe(II)-oxidizers) into Fe(III)aq, and that Fe(III)aq then precipitates into Fe(III)s

$$Fe(II)_{aq} \Leftrightarrow Fe(III)_{aq} \Rightarrow Fe(III)_s \qquad (24)$$
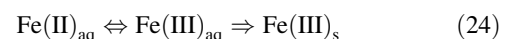
As discussed previously, the exchange isotope kinetics between Fe(II)aq and Fe(III)aq are very rapid (Welch et al., 2003) and it will be assumed here that the pools of the dissolved species remain in equilibrium, with a fractionation factor

$$\alpha_{\text{IIaq}}^{\text{IIIaq}} = \frac{R_{\text{IIIaq}}}{R_{\text{IIaq}}} \qquad (25)$$

which corresponds to a shift of approximately $+1.4$ ‰/amu at 25°C. For the second stage, we assume that there is no return from the precipitated reservoir to the pool of Fe(III)aq and a Rayleigh condition can be imposed whereby the fractionation factor is the ratio of the fluxes of the two isotopes divided by the ratio of the initial pool

$$\alpha_{\text{IIIaq}}^{\text{IIIaq}\rightarrow s} = \frac{R_{\text{IIIaq}\rightarrow s}}{R_{\text{IIIaq}}} \qquad (26)$$

We follow Beard and Johnson (2004) and Johnson et al. (2004), and use a first order kinetic model (also see Anbar (2004))

$$\begin{aligned}
\frac{d\text{Fe}_{\text{aq}}^{\text{II}}}{dt} &= -k_1 \text{Fe}_{\text{aq}}^{\text{II}} \\
\frac{d\text{Fe}_{\text{aq}}^{\text{III}}}{dt} &= k_1 \text{Fe}_{\text{aq}}^{\text{II}} - k_2 \text{Fe}_{\text{aq}}^{\text{III}} \\
\frac{d\text{Fe}_{\text{s}}^{\text{III}}}{dt} &= k_2 \text{Fe}_{\text{aq}}^{\text{III}}
\end{aligned} \qquad (27)$$

If we fix $\text{Fe}_{\text{aq}}^{\text{II}} + \text{Fe}_{\text{aq}}^{\text{III}} + \text{Fe}_{\text{s}}^{\text{III}} = \text{Fe}_{\text{aq},0}^{\text{II}} = 1$, these equations can be solved and yield

$$\begin{aligned}
\text{Fe}_{\text{aq}}^{\text{II}} &= e^{-k_1 t} \\
\text{Fe}_{\text{aq}}^{\text{III}} &= \frac{k_1}{k_2 - k_1}(e^{-k_1 t} - e^{-k_2 t}) \\
\text{Fe}_{\text{s}}^{\text{III}} &= 1 - \text{Fe}_{\text{aq}}^{\text{II}} - \text{Fe}_{\text{aq}}^{\text{III}}
\end{aligned} \qquad (28)$$

The following mathematical treatment regarding isotopic compositions in the 2-stage distillation model is a new and original contribution of this review (Beard & Johnson, 2004, and Johnson et al., 2004 did not derive the analytical solution but relied on numerical integration). For isotopic ratios, the system is entirely described by the following prescriptions

$$\begin{aligned}
R_{\text{aq},0}^{\text{II}} &= 1 \\
\frac{d\ln R_{\text{aq}}^{\text{II}}}{dt} &= \frac{(\alpha_{\text{IIIaq}}^{\text{IIIaq}\rightarrow s}-1)\frac{d\text{Fe}_{\text{aq}}^{\text{III}}}{dt} + (\alpha_{\text{IIIaq}}^{\text{IIIaq}\rightarrow s}-1/\alpha_{\text{IIaq}}^{\text{IIIaq}})\frac{d\text{Fe}_{\text{aq}}^{\text{II}}}{dt}}{\text{Fe}_{\text{aq}}^{\text{III}}+\text{Fe}_{\text{aq}}^{\text{II}}/\alpha_{\text{IIaq}}^{\text{IIIaq}}} \\
R_{\text{aq}}^{\text{III}} &= R_{\text{aq}}^{\text{II}}\alpha_{\text{IIaq}}^{\text{IIIaq}} \\
R_{\text{s}}^{\text{III}} &= \frac{1 - \text{Fe}_{\text{aq}}^{\text{II}}R_{\text{aq}}^{\text{II}} - \text{Fe}_{\text{aq}}^{\text{III}}R_{\text{aq}}^{\text{III}}}{1 - \text{Fe}_{\text{aq}}^{\text{II}} - \text{Fe}_{\text{aq}}^{\text{III}}}
\end{aligned} \qquad (29)$$

These equations are valid regardless of the model that is used for the exchange kinetics between the reservoirs. The values of $\text{Fe}_{\text{aq}}^{\text{II}}$, $\text{Fe}_{\text{aq}}^{\text{III}}$, and their derivatives are given above for the first order kinetic model. Using this model, it is straightforward to solve the equation describing the evolution of the isotopic ratio of ferrous iron in solution

$$\ln R_{\text{aq}}^{\text{II}} = \frac{a}{c}\ln X + \left(b - \frac{a}{c}\right)\ln\left(\frac{X+c}{1+c}\right) \qquad (30)$$

where the parameters a, b, and c are

$$\begin{aligned}
a &= \left(\alpha_{\text{IIIaq}}^{\text{IIIaq}\rightarrow s} - 1\right)\left(1 - \frac{\mu}{\mu-1}\right) + \left(1/\alpha_{\text{IIaq}}^{\text{IIIaq}} - \alpha_{\text{IIIaq}}^{\text{IIIaq}\rightarrow s}\right) \\
b &= \left(\alpha_{\text{IIIaq}}^{\text{IIIaq}\rightarrow s} - 1\right)\frac{\mu}{\mu-1} \\
c &= \frac{1-\mu}{\alpha_{\text{IIaq}}^{\text{IIIaq}}} - 1
\end{aligned} \qquad (31)$$

and

$$\begin{aligned}
\mu &= k_2/k_1 \\
X &= e^{(k_1-k_2)t}
\end{aligned} \qquad (32)$$

In the case of isotopic ratios, simplifications can be brought to this equation and the solution in δ notation takes the form

$$\begin{aligned}
\delta_{\text{aq}}^{\text{II}} &= \left(\frac{\Delta_{\text{IIIaq}}^{\text{IIIaq}\rightarrow s}}{\mu-1} + \frac{\Delta_{\text{IIaq}}^{\text{IIIaq}}}{\mu}\right)\ln X + \left(\Delta_{\text{IIIaq}}^{\text{IIIaq}\rightarrow s} - \frac{\Delta_{\text{IIaq}}^{\text{IIIaq}}}{\mu}\right)\ln\left(\frac{X-\mu}{1-\mu}\right) \\
\delta_{\text{aq}}^{\text{III}} &= \delta_{\text{aq}}^{\text{II}} + \Delta_{\text{IIaq}}^{\text{IIIaq}} \\
\delta_{\text{s}}^{\text{III}} &= \frac{\text{Fe}_{\text{aq}}^{\text{II}}\delta_{\text{aq}}^{\text{II}} + \text{Fe}_{\text{aq}}^{\text{III}}\delta_{\text{aq}}^{\text{III}}}{\text{Fe}_{\text{aq}}^{\text{II}} + \text{Fe}_{\text{aq}}^{\text{III}} - 1}
\end{aligned} \qquad (33)$$

where $\Delta_{\text{IIIaq}}^{\text{IIIaq}\rightarrow s} = (\alpha_{\text{IIIaq}}^{\text{IIIaq}\rightarrow s} - 1) \times 10^3$ and $\Delta_{\text{IIaq}}^{\text{IIIaq}} = (\alpha_{\text{IIaq}}^{\text{IIIaq}} - 1)\times 10^3$. If the initial isotopic composition is different from zero, this simply shifts all the calculated isotopic compositions by the same amount, $\delta_{\text{aq},0}^{\text{II}}$. Note that it is easy to follow the composition of the instantaneous fraction of ferric iron precipitated as we have

$$\delta_{\text{aq}\rightarrow s}^{\text{III}} = \delta_{\text{aq}}^{\text{III}} + \Delta_{\text{IIIaq}}^{\text{IIIaq}\rightarrow s} \qquad (34)$$

(Eq. 33 gives the composition of the bulk precipitate $\delta_{\text{s}}^{\text{III}}$.) For illustration, Figure 10 shows the calculated isotopic compositions of the different reservoirs as a function of the fraction of Fe precipitated for $\Delta_{\text{IIaq}}^{\text{IIIaq}} = 1.4$ ‰/amu, $\Delta_{\text{IIIaq}}^{\text{IIIaq}\rightarrow s} = -0.5$ ‰/amu, and $k_2/k_1 = 10$. This formalism could be applied in the context of banded-iron-formation precipitation in the Archaean.

6. Modeling Fractionation by Diffusion-Precipitation during Crystal and Concretion Growth

Diffusion can be the limiting process in the supply of Fe during crystal and concretion growth (Frank, 1950; Berner, 1968). This can affect the isotopic composition of the growing phase in two ways:

(i) Crystal or concretion growth takes up some Fe and creates a concentration gradient between the surface and the surrounding medium. The different isotopes of Fe have slightly different diffusion coefficients. Therefore, they can be supplied at different rates to the surface of the growing phase.

(ii) If there is any equilibrium or kinetic isotope fractionation at the interface between the two phases, diffusion will control whether this fractionation is expressed in the fluid or in the solid.

These two processes are explored theoretically hereafter. Frank (1950) and Berner (1968) evaluated the influence of supersaturation at infinity on the rate of crystal and concretion growth in a diffusion-limited regime, but to our knowledge this is the first time that isotopic fractionation associated with such a process is studied. The precipitate (Fe volume concentration C_p) grows at the expense of Fe in the fluid (volume concentration at the
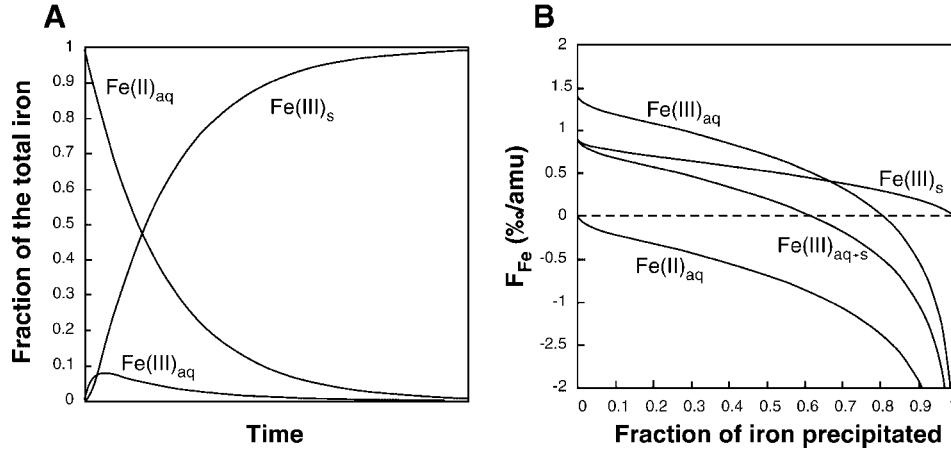
FIGURE 10. Evolution of a closed system for the two-stage distillation model discussed in the text ($FeII_{aq} \Leftrightarrow FeIII_{aq} \Rightarrow FeIII_s$, where $FeII_{aq}$ denotes the reservoir of ferrous iron in solution, $FeIII_{aq}$ denotes ferric iron in solution, $FeIII_s$ denotes ferric iron in the form of a precipitated solid, and $FeIII_{aq \rightarrow s}$ denotes the flux from $FeIII_{aq}$ to $FeIII_s$). A first order kinetic model is assumed for the rates of disappearance of the different species of Fe (Eq. 27). The curves are calculated for a ratio between the rate constants of ferrous iron oxidation (k_1) and ferric iron precipitation (k_2) of $k_2/k_1 = 10$. The **left panel** (**A**) shows the abundances of the various chemical species of Fe as a function of time (Eq. 28). The **right panel** (**B**) shows the isotopic composition of Fe in the various reservoirs as a function of the fraction of Fe precipitated. Equilibrium is assumed between $FeII_{aq}$ and $FeIII_{aq}$. A Rayleigh condition is prescribed for the precipitation stage (see text for the detailed mathematical treatment of this process, Eq. 33).

surface C_S). We write D_k the diffusion coefficient of the isotope k of Fe (e.g., see Eq. 22 with $\beta = 0.0025$ for the ratio of the diffusion coefficients of ^{54}Fe and ^{56}Fe in water, Rodushkin et al., 2004) and α_i^k the fractionation factor at the interface between the two phases

$$\alpha_i^k = (^kC/^iC)_p/(^kC/^iC)_S \quad (35)$$

We first consider the growth of an infinite plate. The differential equation that controls the evolution of the concentration away from the boundary is

$$\frac{\partial C}{\partial t} = D\frac{\partial^2 C}{\partial r^2} \quad (36)$$

where D is the diffusion coefficient and r is the distance from the origin (position of the boundary at time zero). At the boundary ($r = R$), the increase in concentration from C_S to C_p due to growth of the precipitate is balanced by diffusion of Fe to the surface

$$(C_A - C_S)\frac{\partial R}{\partial t} = D\left(\frac{\partial C}{\partial r}\right)_{r=R} \quad (37)$$

For solving these equations, it is convenient to use adimensional coordinates,

$$\sigma = \frac{r}{\sqrt{Dt}} \quad (38)$$

In this system of coordinates, Equation 36 takes the form

$$\frac{\partial^2 C}{\partial \sigma^2} + \frac{\sigma}{2}\frac{\partial C}{\partial \sigma} = 0 \quad (39)$$

If one writes $p = \partial C/\partial\sigma$, then the solution for p is

$$p = Ae^{-\sigma^2/4} \quad (40)$$

where A is an integration constant that does not depend on σ. The concentration of Fe in the fluid is the integral of this equation

$$C_\sigma = C_\infty - A\int_\sigma^\infty e^{-z^2/4}dz \quad (41)$$

where C_∞ is the concentration at infinity. This is equal to,

$$C_\sigma = C_\infty - A\sqrt{\pi}[1 - \text{erf}(\sigma/2)] \quad (42)$$

The integration constant A can be calculated using the boundary condition (Eq. 37). We write S the position of the boundary in σ coordinates. Introducing the expression previously derived for $\partial C/\partial\sigma$ (Eq. 40) in (Eq. 37) one gets

$$(C_p - C_S)\left[\sqrt{Dt}\left(\frac{\partial\sigma}{\partial t}\right)_{\sigma=S} + \frac{S}{2}\sqrt{\frac{D}{t}}\right] = \sqrt{\frac{D}{t}}Ae^{-S^2/4} \quad (43)$$

At this point, we assume for dimensional reasons that the interface moves as $\sqrt{t}$ (quasi-stationary solution). We therefore have S constant and

$$(C_p - C_S)\frac{S}{2} = Ae^{-S^2/4} \quad (44)$$

From this we can derive A and inject it in Equation 42 and can derive the general expression for the concentration

$$C_\sigma = C_\infty + (C_S - C_p)\frac{\sqrt{\pi}}{2}Se^{S^2/4}[1 - \text{erf}(\sigma/2)] \quad (45)$$

For a boundary moving as $\sqrt{t}$, the concentration must remain constant in σ coordinates. This is also true for the surface concentration, which must remain constant at the saturation

concentration for the phase that is precipitating. Using the condition $C_S = C_{sat}$ at the boundary in (Eq. 45), one can calculate $S = R/\sqrt{Dt}$. This constant gives the position of the boundary in σ coordinates. In the following, we normalize all concentrations to C_∞ and note them with an asterisk ($C^* = C/C_\infty$). We also note

$$g(S) = \frac{\sqrt{\pi}}{2} S e^{S^2/4}[1 - \mathrm{erf}(S/2)] \qquad (46)$$

In the case of precipitation of a phase containing Fe as a major constituent, the concentration in the precipitate is much higher than the concentration at infinity ($C_p^* >> 1 \geq C_{sat}^*$, with C_p^* fixed by the stoichiomerty of the precipitating phase and C_{sat}^* fixed by thermodynamics at the interface) and we have from Equations 38 and 45 taken at $\sigma = S$

$$R \approx \frac{2}{\sqrt{\pi}} \frac{1 - C_{sat}^*}{C_p^*} \sqrt{Dt} \qquad (47)$$

The degree of supersaturation at infinity relative to the surface can be used in this equation to determine the rate of plate growth in a diffusion-limited regime (the formalism used up to this point is similar to that used by Frank, 1950 and Berner, 1968). Let us consider an element that has n stable isotopes. The equations that can be written are

$$
\begin{aligned}
C_{sat}^* &= \sum_{k=1}^{n} C_S^{k*} \\
C_p^* &= \sum_{k=1}^{n} C_p^{k*} \\
C_S^{k*} &= 1 + (C_S^{k*} - C_p^{k*})g(S_k), \quad 1 \leq k \leq n \\
(C^{k*}/C^{i*})_p/(C^{k*}/C^{i*})_S &= \alpha_i^k, \quad i \neq k \\
S_k\sqrt{D_k} &= S_i\sqrt{D_i}, \quad i \neq k
\end{aligned}
\qquad (48)
$$

where i is a reference isotope. There are $3n$ equations (Eq. 48) in $3n$ unknowns (C_S^{k*}, C_p^{k*}, and S_k, with $1 \leq k \leq n$). The system can thus be solved. However, some of these equations are non-linear and the resolution is non-trivial. Because isotopic variations are small, simplifications can be brought to the system. For the reference isotope, we simply have (Eq. 45),

$$C_S^{i*} = \frac{1 - C_p^{i*}g(S_i)}{1 - g(S_i)} \qquad (49)$$

For any other isotope k, the concentration at the surface takes the form,

$$C_S^{k*} = \frac{1}{1 + g(S_k)\left(\alpha_i^k \frac{C_i^{i*}}{C_S^{i*}} - 1\right)} \qquad (50)$$

The isotopic composition at the surface relative to the isotopic composition at infinity is expressed in δ notation

$$\delta_S^{k/i} = (C_S^{k*}/C_S^{i*} - 1) \times 10^3 \qquad (51)$$

with the two terms in the ratio given by Equations 49 and 50. Because $C_p^* >> 1$, S and $g(S)$ are small and simplifications can be brought to this expression

$$\delta_S^{k/i} \approx [g(S_k) - g(S_i) - \alpha_i^k C_p^{i*} g(S_k) + C_p^{i*} g(S_i)] \times 10^3 \qquad (52)$$

Recognizing that $S_k\sqrt{D_k} = S_i\sqrt{D_i}$, $D_k/D_i \approx 1$, and $C_p^{i*} \approx C_p^*$, Equation 52 can be further simplified

$$\delta_S^{k/i} \approx (1 - C_{sat}^*)\left[\frac{1}{2}\left(\frac{D_k}{D_i} - 1\right) - (\alpha_i^k - 1)\right] \times 10^3 \qquad (53)$$

The isotopic composition of the precipitate is shifted by an increment of $(\alpha_i^k - 1) \times 10^3$ relative to the isotopic composition of the fluid at the interface

$$\delta_p^{k/i} \approx \left[C_{sat}^*(\alpha_i^k - 1) + (1 - C_{sat}^*)\frac{1}{2}\left(\frac{D_k}{D_i} - 1\right)\right] \times 10^3 \qquad (54)$$

Equation 45 can be used to calculate the concentration and isotopic composition of Fe away from the boundary. A numerical example is given in Figure 11 for the precipitation of an infinite plate of hematite. The transient solution for an initial step function is also given (the numerical integration was done using the front-tracking fixed finite-difference grid method with Lagrangian interpolation described by Crank, 1984). The system reaches the quasi-stationary regime very rapidly (on the order of a day) and in most cases, the transient period can be neglected. In this calculation, the saturation concentration at the surface was fixed at $C_{sat}^* = 0.2$. As shown in Figure 11, the fluid near the boundary has negative isotopic composition relative to infinity, while further away from the boundary the fluid has positive isotopic composition. The integral of $C\delta$ (including the growing phase) is zero, which is required by mass conservation.

The most important question that needs to be addressed is whether diffusion could have left its imprint in the isotopic composition of concretions and crystals formed from aqueous fluids in a diffusion-limited regime. This is illustrated in Figure 12 (Eqs. 54 and 57). If the concentration at infinity is similar to the saturation concentration at the surface of the growing phase ($C_{sat}^* \to 1$), then the rate of growth of the plate is small (Eq. 47), the isotopic fractionation due to differences in diffusivities of the isotopes is negligible (Eq. 54, D_k/D_i), but the fractionation due to differences in partitioning of the isotopes at the interface between the two phases is maximal (the isotopic composition of the fluid at the interface is at zero, and the fractionation between the fluid and the solid is expressed in the solid, Eq. 54, α_i^k). On the contrary, when there is a large concentration gradient between infinity and the surface ($C_{sat}^* \to 0$) then the plate can grow rapidly, the fractionation due to differences in diffusivities of the isotopes is maximal, but the fractionation due to differences in partitioning of the isotopes is negligible (the isotopic composition of the solid is at zero and the fractionation at the interface between the fluid and the solid is expressed in the fluid). For the set of parameters used in Figure 12, which is relevant to the growth of an infinite plate of hematite, the isotopic fractionation is small compared to natural variations.

A similar treatment can be applied to the case of the growth of a sphere and the results are

$$C_\sigma^* = 1 + (C_S^* - C_p^*)\frac{S^3}{2}e^{S^2/4}\left[\frac{1}{\sigma}e^{-\sigma^2/4} - \frac{\sqrt{\pi}}{2}\left(1 - \mathrm{erf}\frac{\sigma}{2}\right)\right] \qquad (55)$$

A

B
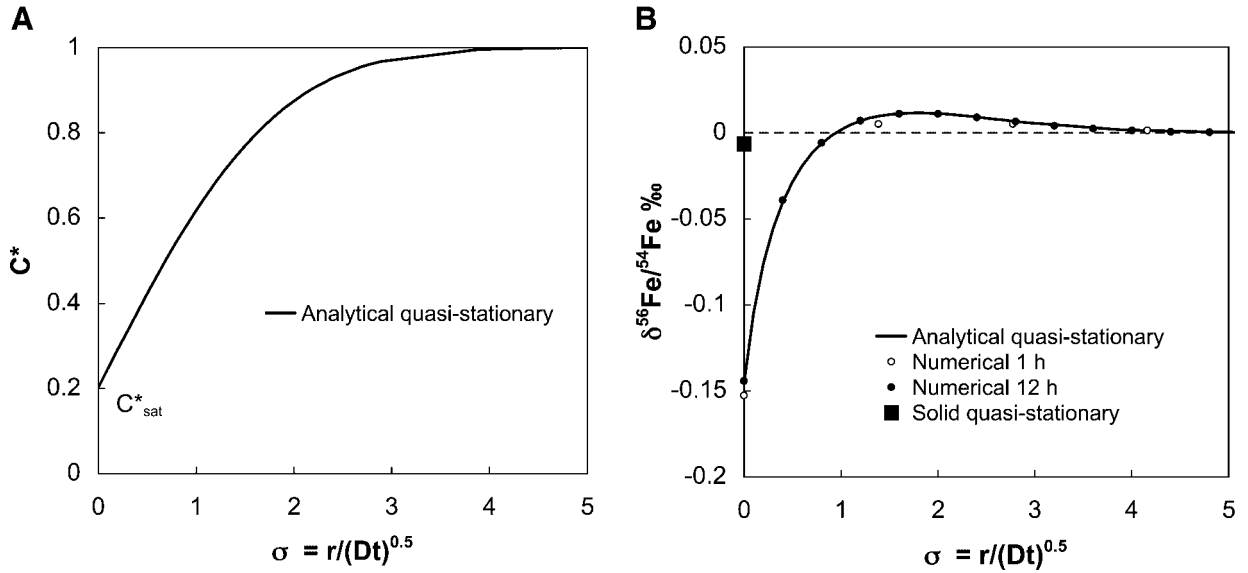
FIGURE 11. Iron concentration (**A**) and isotopic composition (**B**) of the fluid during growth of an infinite plate of hematite in a diffusion-limited regime. The heavy line is the quasi-stationary solution (Eqs. 45, 49, and 50, with $C_p = 3.682 \times 10^6$ mg/L, $C_\infty = 20$ mg/L, $C_{sat} = 4$ mg/L, Parry, Chan, & Beitler, 2004, $D_{56}/D_{54} = 0.999914$, $D_{Fe} = 5.78 \times 10^{-10}$ m²/sec, Rodushkin et al., 2004, and $\alpha_{54}^{56} = 1.00014$, Skulan, Beard, & Johnson, 2002, see text for details). On the **right panel** is also shown the isotopic composition of the precipitate (filled square) and the isotopic composition of the fluid evolving from an initial step function in concentration (transient profile obtained by numerical integration).
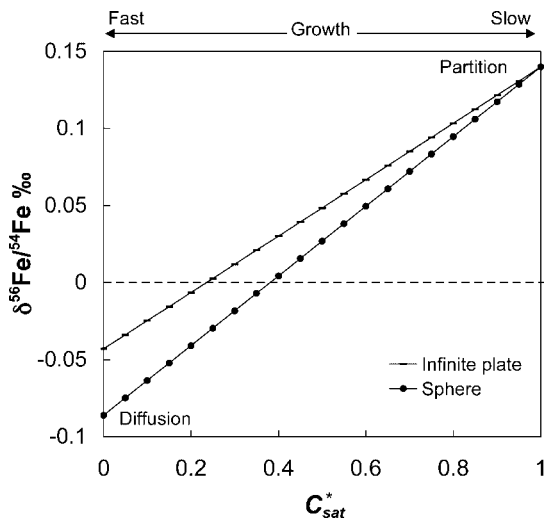
FIGURE 12. Isotopic composition of a hematite precipitate as a function of the degree of supersaturation at infinity relative to the surface. The two lines correspond to growth of a sphere or an infinite plate and were calculated using Equations 54 and 57. When the degree of supersaturation is large, then the phase grows slowly and Fe is fractionated due to differences in diffusivities of Fe isotopes ($D_{56}/D_{54} = 0.999914$, Rodushkin et al., 2004). When the degree of supersaturation is small, then the phase grows slowly and Fe is fractionated due to differences in partitioning of Fe isotopes at the interface between the two phases ($\alpha_{54}^{56} = 1.00014$, Skulan, Beard, & Johnson, 2002).

and

$$R \approx \sqrt{\frac{2(1 - C_{sat}^*)}{C_p^*}}\sqrt{Dt} \qquad (56)$$

(see Frank, 1950 and Berner, 1968 for details). As far as isotopes are concerned, the result for a growing sphere is (Fig. 12)

$$\delta_p^{k/i} \approx \left[C_{sat}^*(\alpha_i^k - 1) + (1 - C_{sat}^*)\left(\frac{D_k}{D_i} - 1\right) \right] \times 10^3 \qquad (57)$$

This formalism can be applied to the formation of spherical hematite concretions in the Navajo sandstone (Busigny & Dauphas, 2005), which may be the best terrestrial analogue for the formation of hematite spherules on Mars (Chan et al., 2004). It may also be relevant to crystallization in magmatic systems and could be applied to different elements and different types of concretions. Experimental determinations of diffusion coefficients of Fe isotopes in various media will provide useful constraints on whether or not diffusion can create isotopic fractionation in natural systems.

B. Biological Processes

1. Dissimilatory Iron Reduction (DIR)

The importance of Fe(III) oxides as electron acceptors for anaerobic respiration in Fe-rich modern sediments is widely recognized (Lovley et al., 1987; Roden, 2004) and may have been

associated with some of the earliest forms of metabolism on Earth (Vargas et al., 1998). Mineralogical products of dissimilatory Fe(III) reduction that may be preserved in the rock record include magnetite, Fe carbonates, and sulfides. In pioneering studies, Bullen and McMahon (1998) and Beard et al. (1999) reported that δ^{56}Fe-value of dissolved Fe(II) produced by dissimilatory Fe-reducing bacteria was fractionated by ~ -1.3 ‰ relative to the ferrihydrite substrate. Subsequent results have been extended to different DIR bacteria, growth conditions, and substrates (Beard et al., 2003a; Icopini et al., 2004; Johnson et al., 2005; Crosby et al., 2005). In particular, at high reduction rates, produced Fe(II) has δ^{56}Fe values that are up to 2.6‰ lower than ferric substrate (Johnson et al., 2005), possibly reflecting the effect of DIR. Icopini et al. (2004) suggested that abiotic adsorption of heavy Fe(II) on hydrous ferric oxide could explain the low δ^{56}Fe of Fe(II)aq measured in DIR experiments. However, Crosby et al. (2005) have shown that Fe(II) adsorbed on the ferric substrate has a δ^{56}Fe that is very close to Fe(II)aq. Significant Fe isotope fractionations have also been reported between dissolved Fe(II) and magnetite, siderite, and Ca-substitute siderite produced by Fe-reducing bacteria grown on ferrihydrite (Johnson et al., 2005; Table 3).

2. Bacterial Fe Oxidation

Although chemical oxidation of ferrous iron is thermodynamically favored during the interaction of reduced fluids with oxygenated waters, bacterial Fe(II) oxidation may prevail in microaerobic or anoxic environments. Microorganisms that oxidize Fe(II) to generate energy for growth include those that couple Fe(II)-oxidation to the reduction of nitrate at neutral pH (Benz, Brune, & Schink, 1998), or to the reduction of oxygen at either low (Edwards et al., 2000), or neutral pH (Emerson and Moyer, 1997), and the anaerobic Fe(II)-oxidizing phototrophs (Widdel et al., 1993).

Croal et al. (2004) investigated Fe isotope fractionation produced by Fe(II)-oxidizing phototrophs under anaerobic conditions. Among key results, the ferrihydrite precipitate has δ^{56}Fe-value that is ~ 1.5‰ higher than the aqueous Fe(II) source. Since the degree of isotopic fractionation is not correlated to the rate of oxidation (controlled by changing the light intensity), it has been suggested that kinetic isotope effects are not of great importance in controlling the fractionation factor. In fact, the enrichment of heavy Fe isotope in the oxidation product is globally consistent with equilibrium effects between Fe(II) and Fe(III) (Welch et al., 2003). The fractionation factor, however, is higher than for abiotic Fe(II) oxidation (Bullen et al., 2001) and lower than for equilibrium fractionation between aqueous Fe(II) and Fe(III) (Welch et al., 2003; Anbar, Jarzecki, & Spiro, 2005; Table 3), possibly reflecting kinetic effects during Fe-oxyhydroxide precipitation.

3. Magnetotactic Bacteria

Magnetotactic bacteria (MB) are prokaryotes participating in the chemical transformation of Fe and S species *via* both redox and mineral precipitation processes. MB precipitates intracellular single domain ferromagnetic iron oxide (magnetite) or iron sulfide (greigite) minerals, causing them to respond to geomagnetic fields. These bacteria are globally distributed in suboxic to anoxic freshwater (Frankel, Blakemore, & Wolfe, 1979; Spring et al., 1993; Sakaguchi, Arakaki, & Matsunaga, 2002) and marine sediments, soils, and stratified marine water columns (Stolz, Chang, & Kirschvink, 1986; Bazylinski et al., 2000; Simmons et al., 2004).

Initial Fe isotope studies of magnetite produced by magnetotactic bacteria (Mandernack et al., 1999) have shown no detectable fractionation when either Fe(II) or Fe(III) source were used in the growth media. These results contrast strongly with recent experimental work of Fe isotope fractionation during magnetite formation coupled to dissimilatory hydrous ferric oxide reduction, which shows large isotopic fractionation between Fe in magnetite and Fe in the fluid (Johnson et al., 2005). However, this does not preclude that there is an isotopic effect produced by MB because only two strains were investigated over a restricted range of laboratory conditions. In particular, Fe isotope fractionation might be dependent on the kinetics of Fe uptake by MB, which may vary with Fe concentration, Fe redox state, and the presence of Fe chelators (Schuler & Baeuerlein, 1996). It is presently unknown if any Fe isotope variability occurs in naturally occurring magnetite produced by MB.

4. Organic Ligands and Biomolecules

Iron is an essential element for the biogeochemical and physiological functioning of terrestrial and oceanic organisms, and in particular phytoplankton, which is responsible for the primary productivity in the world's ocean. Changes in the supply of Fe to the upper ocean may lead to climate change by affecting biological productivity and altering rates of carbon sequestration (e.g., Martin, 1990; Hutchins & Bruland, 1998; Boyd, 2000; Watson et al., 2000). However, due to the low solubility of Fe in oxygenated water, microorganisms are often limited by their inability to incorporate Fe. Dissolved Fe in the oceans is overwhelmingly complexed (>99%) by strong organic ligands (siderophores) that may control the uptake of Fe by microbiota (Hutchins et al., 1999; Macrellis et al., 2001; Wu et al., 2001). Siderophores and low molecular weight organic acids may also be ubiquitous in soil systems (Powell et al., 1980; Neilands, 1982).

Significant Fe isotopic fractionation may be produced during mineral dissolution in the presence of organic ligands such as siderophore produced by soil bacteria (Brantley, Liermann, & Bullen, 2001; Brantley et al., 2004). The magnitude of the Fe isotope fractionation during hornblende dissolution correlates with the binding constant of the chelating agent. Higher binding strength ligands such as siderophores produce larger δ^{56}Fe differences (up to 0.8‰) between the aqueous Fe and Fe remaining in the mineral. The Fe isotope fractionation observed during mineral dissolution with organic ligands is attributed predominantly to the preferential retention of the heavy isotopes in an altered surface layer. Mineral precipitation of isotopically heavy alteration phases may also contribute to the observed fractionation (Brantley et al., 2004).

Matthews, Zhu, and O'Nions (2001) investigated Fe isotope fractionation between Fe(II) complexed with an organic molecule *tris*(2,2′ bipyridine) ([Fe^{II}(bipy)$_3$]$^{2+}$) and Fe(III) chloride complexes. Large isotope variations have been produced between Fe(II) and Fe(III) complexes and ranged from 1.7 to 11.7 ‰ for ^{56}Fe/^{54}Fe ratios. The unusually large Fe isotope fractionation factor of up to 11.7‰ is likely due to the strong covalent bonds between *tris*(2,2′ bipyridine) and Fe(II).

Experimental data of Fe isotope fractionation during Fe complexation by organic ligands confirm that the coordination chemistry of Fe exhibits a profound control on its isotopic behavior and may be of major importance in natural systems.
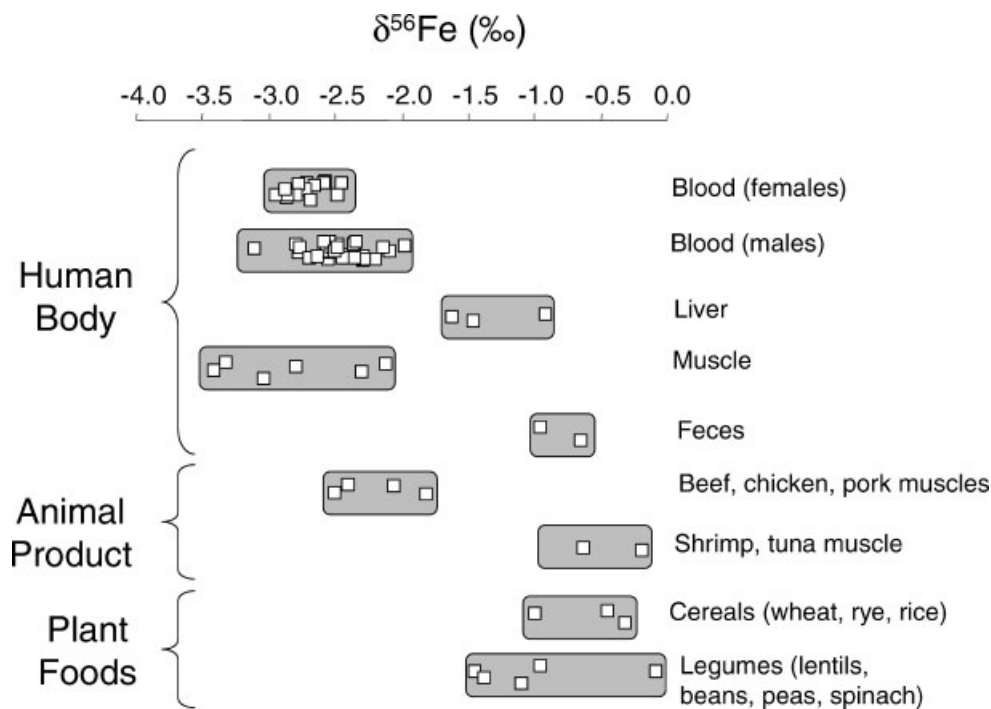
5. Human Body

Iron is essential to the human body for oxygen transport in blood, for oxygen storage in muscle tissue, and as an enzyme co-factor. Recent studies have indicated natural variations of Fe isotope abundances in whole blood, hemoglobin, and tissues by as much as ~3‰ in the ^{56}Fe/^{54}Fe ratios (Walczyk & von Blanckenburg, 2002, 2005; Zhu et al., 2002; Stenberg et al., 2003, 2005; Ohno et al., 2004). In particular, isotopic analysis of human blood, liver, and muscle tissue indicates that each individual bears a long-term Fe isotope signature in the blood. Blood and, tissue have δ^{56}Fe values lower by up to 2.6 ‰ relative to dietary Fe, and the results have been interpreted to reflect Fe isotope fractionation during intestinal Fe absorption (Walczyk & von Blanckenburg, 2002, Fig. 13). Although the exact biochemical pathways of Fe isotope fractionation in the human body are not fully understood, Fe isotopes appear to be useful tracers of long-term dietary Fe

absorption (Walczyk & von Blanckenburg, 2005). Interestingly, animals in general are enriched in lighter Fe isotopes relative to dietary Fe suggesting that Fe isotopes can be used to study trophic level along a food chain (Walczyk & von Blanckenburg, 2002).

C. Modern Aqueous Systems

Iron is a particle reactive trace metal present at extremely low concentrations in the upper oceans ($<$1 nM, Wu et al., 2001) and is now recognized as a limiting nutrient in large regions of world's ocean and in certain coastal waters (Johnson, Gordon, & Coale, 1997; Johnson, Chavez, & Friederich, 1999; Hutchins & Bruland, 1998). The main sources of dissolved Fe into the ocean are wet and dry deposition from the atmosphere, input from rivers, returned sediment and pore water along continental shelves, and hydrothermal vents (Wells, Price, & Bruland, 1995; Elderfield & Schultz, 1996; Johnson, Gordon, & Coale, 1997; de Barr & de Jong, 2001). Because Fe has a very short residence time in seawater, concentrations are highest near its sources, such as coastal waters with high continental input and deep-ocean at ridge axis with high hydrothermally derived Fe. Remineralization from sinking particulate organic matter and vertical mixing may also affect the distribution of dissolved Fe in seawater (Hutchins, DiTullio, & Bruland, 1993).

Despite the great interest in using Fe isotopes as biogeochemical tracers in marine systems, the variability of Fe isotopes in coastal and open seawater remains largely unexplored, mainly due to analytical difficulties. The partition of Fe isotopes among the different Fe-bearing species in seawater, including soluble Fe (Fe-organic complexes and ferrous Fe),

FIGURE 13. Iron isotope variations in the human body and different food samples covering the most relevant dietary Fe sources. Data are from Walczyk and von Blanckenburg (2002).

colloidal, and particulate Fe (detrital or biological) must be documented. Ultimately, Fe isotopes could be used to better constrain the relative contributions of Fe sources in seawater and help improve our understanding of how Fe is mobilized from its source region, transported into the surface ocean, and deposited in the deep sea.

1. Marine Sediments

Modern marine sediments, such as deep-sea clays, terrigenous sediments, turbidite clays, and volcanoclastites, have a restricted range of Fe isotopic compositions clustered around the igneous δ^{56}Fe values (Beard et al., 2003b; Rouxel et al., 2003; Fantle & DePaolo, 2004; Fig. 14). Similarly, δ^{56}Fe values of siliceous and calcareous ooze, and to a lesser extent deep sea cherts are identical to δ^{56}Fe values of pelagic clays (Beard et al., 2003b; Rouxel et al., 2003; Fantle & DePaolo, 2004), with variations of less than 0.3‰. These observations are consistent with the homogeneous Fe-isotope composition of loess and aerosols (Zhu et al., 2000; Beard et al., 2003b) and suggest that the effect of continental weathering, transport, and deposition does not significantly modify Fe isotope composition in the solid phase.

In contrast, marine sediments in which the budget of Fe is controlled by hydrogenous ferromanganese precipitates are characterized by negative δ^{56}Fe values of Fe-Mn crusts down to −0.8‰ (Zhu et al., 2000; Rouxel et al., 2003; Levasseur et al., 2004; Fig. 14). The cause of the observed Fe isotope variability in hydrogeneous Fe-Mn deposits is still poorly constrained. Beard

et al. (2003b) suggested that δ^{56}Fe values are controlled by the relative flux of Fe from aerosol particles (at around 0‰) and mid-oceanic ridge hydrothermal flux (at around −0.5 to −1‰). However, Levasseur et al. (2004) studied global variations in the Fe composition of marine hydrogenetic ferromanganese crusts, and found no significant basin to basin trends, discounting previous hypothesis. Based on these results, it seems likely that δ^{56}Fe values in Fe-Mn crusts are not only controlled by the relative contributions of Fe sources (such as hydrothermal or atmospheric sources) but possibly by local effects such as diagenetic remobilization of Fe from seafloor sediments or kinetic isotope effects during formation of the Fe-Mn crusts. Important questions remain concerning the Fe isotope composition of deep water masses to fully realize the paleoceanographic potential of Fe isotope records in Fe-Mn crusts.

In suboxic and anoxic marine environments, dissimilatory sulfate and Fe(III) reduction are the dominant pathways for organic matter oxidation (Berner, 1984; Canfield, 1989). Hence, significant Fe isotope variability is expected in organic-rich sediments. For example, diagenetic fluids with isotopically light Fe(II) (down to −2‰) have been found in anoxic and suboxic marine sediments (Severmann et al., 2004a) and are likely related to bacterial reduction of lithogenic Fe(III) oxides. Pyrite formation in modern organic-rich marine sediments is mediated by sulfate-reducing bacteria and proceeds through the dissolution and reduction of lithogenic Fe oxides and silicates to Fe(II), either below the sediment-water interface or in stratified euxinic bottom waters (Canfield, 1989; Wijsman et al., 2001; Anderson
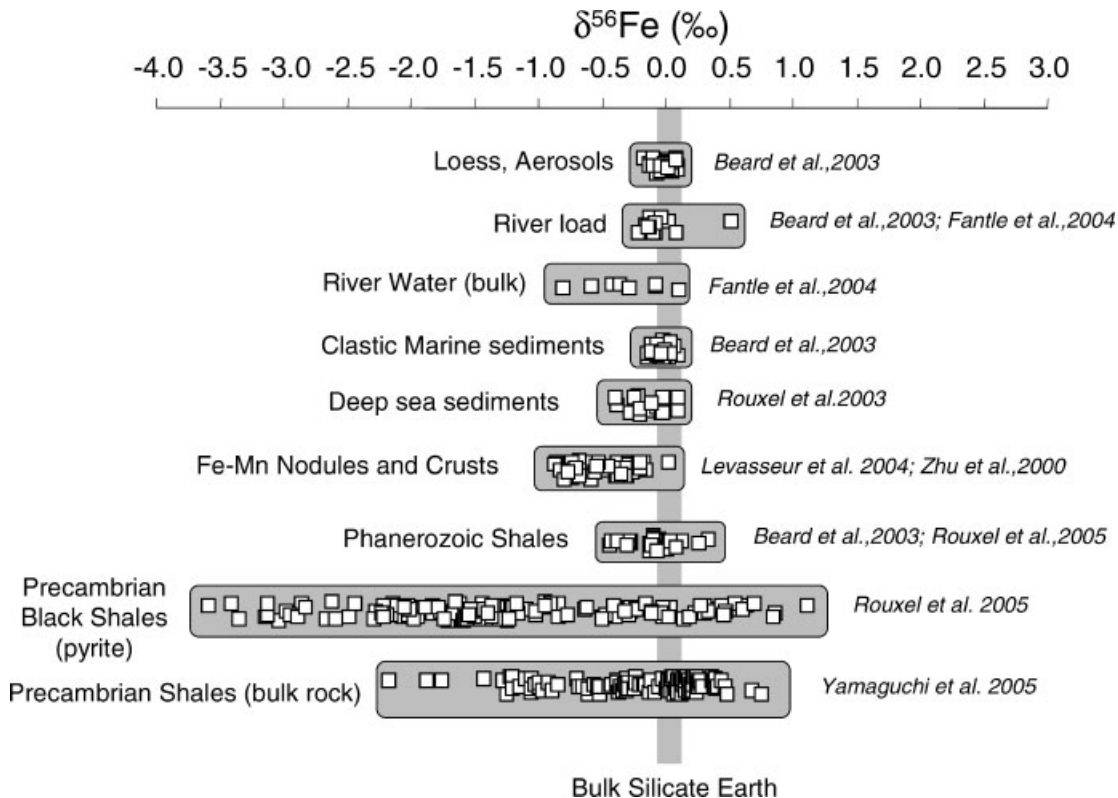

FIGURE 14. Iron isotope variations in modern and ancient sedimentary rocks and rivers.

& Raiswell, 2004). Iron isotope compositions of pyrite and bulk rocks from phanerozoic organic-rich sediments studied so far display a range between ∼0 and −1‰ (Beard et al., 2003b; Matthews et al., 2004; Rouxel, Bekker, & Edwards, 2005; Fig. 14). In contrast, larger Fe isotope variations, with δ^{56}Fe values between 1 and −3.5‰ are observed in Archean and Paleoproterozoic pyrite (Rouxel, Bekker, & Edwards, 2005) and bulk rock (Yamaguchi et al., 2005) from organic-rich sediments. The significances of such variations are presented in Section VI.D.2.

2. Isotope Fractionation during Continental Run-Off

In theory, continental run-off may lead to Fe isotope variability in rivers that is dependant on the weathering regime (chemical vs. physical erosion). Despite its importance, the isotopic composition of the riverine-dissolved Fe flux remains largely unexplored (Fig. 14). Preliminary Fe isotope data from the Amazon River suggest significant Fe isotope variability with δ^{56}Fe values as low as −2‰ (Berquist & Boyle, 2002). In contrast, the suspended loads of rivers define a restricted range of less than 0.3‰ around igneous rock composition (Beard et al., 2003b). Total Fe carried by rivers, including both dissolved and suspended fractions, has variable δ^{56}Fe values ranging between ∼0 and −1‰, suggesting that dissolved riverine Fe is isotopically light relative to igneous rocks (Fantle & DePaolo, 2004). The Fe isotopic composition varies along depth profiles in soils and this may provide information on the mechanism of Fe mobilization under different weathering regimes (von Blanckenburg, 2000; Wiederhold & von Blanckenburg, 2002; Fantle & DePaolo, 2004; Emmanuel et al., 2005). The Fe isotopic composition of lake sediments, which may be used as a paleogeographic proxy in local basins, can also be modified by redox cycling in the water column (Malinovsky et al., 2005).

Dissolved Fe concentrations in estuaries are strongly controlled by non-conservative (removal) behavior during mixing of river water and seawater (Sholkovitz, 1976; Boyle, Edmond, & Sholkovitz, 1977). Because the removal of Fe involves complex transformations between dissolved, colloidal, and particulate phases, it is possible that the Fe isotope composition of dissolved Fe is modified in estuaries. Consequently, the Fe isotope composition of the dissolved riverine Fe flux to the ocean remains poorly constrained but is likely characterized by lower δ^{56}Fe values relative to the bulk continental crust.

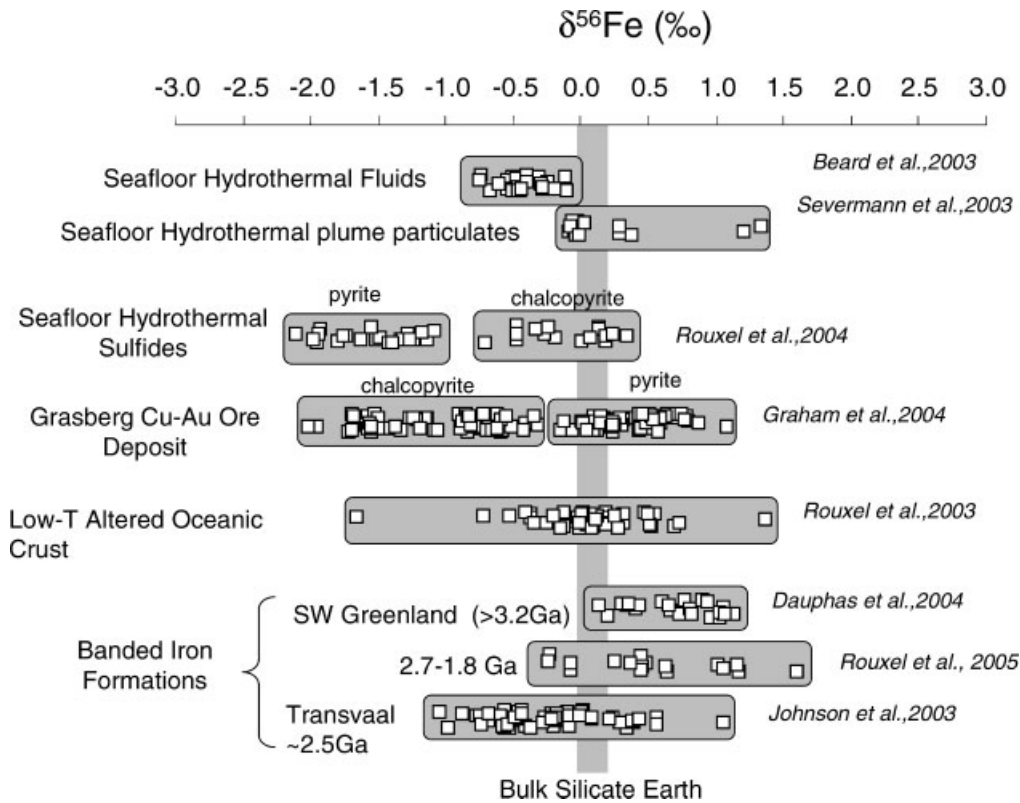## 3. Isotope Fractionation in Seafloor Hydrothermal Systems

Seafloor hydrothermal activity at mid-ocean ridges and ridge-flanks is one of the fundamental processes controlling the exchange of heat and chemical species between seawater and ocean rocks (Edmond et al., 1979; Stein & Stein, 1994; Elderfield & Schultz, 1996; Wheat & Mottl, 2004). Low temperature interaction of seawater with the upper oceanic crust is also an important process controlling global fluxes of elements and it provides an important sink for seawater alkalis, magnesium, and carbon (Staudigel et al., 1996; Alt & Teagle, 1999; Wheat &

Mottl, 2000). Traditionally, the behavior of Fe and other metals in modern seafloor hydrothermal systems has been investigated by integrating results from laboratory studies, theoretical models, mineralogy, and fluid and mineral chemistry (Seewald & Seyfried, 1990; Humphris, 1995; Tivey, 1995; von Damm, 1995). Recent studies of the isotopic composition of Fe in seafloor hydrothermal fluids (Sharma, Polizzotto, & Anbar, 2001; Beard et al., 2003b; Severmann et al., 2004b), hydrothermal chimneys (Rouxel, Fouquet, & Ludden, 2004), and altered basalts (Rouxel et al., 2003) revealed that Fe isotopes are fractionated during high and low temperature hydrothermal processes and might be useful geochemical tracers in these environments (Fig. 15).

The uppermost 400 m of basaltic oceanic crust is characterized by high permeability and basalts in this zone react with oxygenated deep-sea water to form secondary minerals, including Fe oxyhydroxides, smectite, and celadonite (Honnorez, 1981; Alt, 1995). Using samples from Ocean Drilling Program (ODP) Site 801 in Jurassic pacific oceanic crust, Rouxel et al. (2003) observed significant Fe-isotope fractionation in secondary Fe-bearing minerals formed during seafloor weathering. In particular, highly altered basalts that are depleted in Fe (up to 80%) display an increase in δ^{56}Fe values relative to fresh values (up to 1.3 ‰), which suggests preferential leaching of light Fe isotopes during alteration. The apparent fractionation factor between dissolved Fe^{2+} and Fe remaining in the mineral is between 0.5 and 1.3‰ and is consistent with a kinetic isotope fractionation during Fe leaching from the minerals. However, such effects are unlikely to affect the bulk of the remaining material unless diffusion domain sizes are comparable to the scale of diffusion over the timescale investigated. Alternatively, the formation of secondary clay minerals (celadonite) during basalt alteration may preferentially incorporate heavy Fe isotopes, resulting in the loss of light Fe isotopes in the fluids. Laboratory experiments are now required to determine Fe isotope fractionation factors between secondary Fe-phases produced during weathering.

Hot hydrothermal fluids (>300°C) from mid-ocean ridges define a narrow range in Fe isotopic composition that is shifted to lower δ^{56}Fe values by −0.2 to −0.5‰ relative to igneous rocks (Sharma, Polizzotto, & Anbar, 2001; Beard et al., 2003b; Severmann et al., 2004b). These hydrothermal fluids include both vapor and liquid (brine) phases from the Atlantic and Pacific oceanic ridges and this suggests that phase separation and geological setting do not produce significant Fe isotope variability. In contrast, Fe-oxyhydroxide particles in the near-vent hydrothermal plumes (buoyant stage) have variable δ^{56}Fe values (0.1–1.1‰) relative to the original vent fluid, consistent with fractionation during partial oxidation of Fe(II)aq to Fe(III)aq (Severmann et al., 2004b).

The effect of subsurface processes in producing Fe isotope variability has been evaluated at the Lucky Strike hydrothermal field on the Mid-Atlantic Ridge (Rouxel, Fouquet, & Ludden, 2004). The results indicate that high-temperature hydrothermal precipitates (>300°C), composed principally of chalcopyrite ($CuFeS_2$), have δ^{56}Fe values close to hydrothermal fluids whereas medium temperature hydrothermal precipitates (>100°C), composed principally of pyrite are systematically lighter (δ^{56}Fe values between −1 and −2‰). These results

FIGURE 15. Iron isotope variations in seafloor hydrothermal systems and altered oceanic crust. Iron isotope compositions of ore deposits and precambrian iron formations are shown for comparison.

suggest that reservoir effects due to sulfide precipitation during subsurface cooling of the hydrothermal fluid may be able to produce significant Fe isotope variability in hydrothermal deposits. However, the effects of equilibrium or kinetic isotope fractionation between sulfide pairs (pyrite-chalcopyrite) and temperature of precipitation need to be further evaluated. It is important to note that Fe isotope variations in chalcopyrite and pyrite from the Grasberg Cu–Au porphyry and its associated skarn deposits (Irian Jaya, West New Guinea) display opposite patterns (Graham et al., 2004). The δ^{56}Fe values for pyrite and chalcopyrite range from −2.0 to 1.1‰ and do not overlap, suggesting that pyrite preferentially incorporated heavy Fe isotopes.

Low-temperature hydrothermal deposits, composed mainly of silica (quartz) and Fe oxyhydroxides have variable δ^{56}Fe values ranging from −1.6 to 0.3‰ (Rouxel et al., 2003). These variations have been interpreted to result from the combined effects of mineral-fluid isotope fractionation during Fe-oxyhydroxide precipitation and reservoir effects during partial oxidation of hydrothermal Fe^{2+}. In contrast, Fe-oxyhydroxide-rich sediments precipitated from the hydrothermal plume have δ^{56}Fe values that are indistinguishable from the δ^{56}Fe values of the high-temperature hydrothermal fluids (Severmann et al., 2004b). These results suggest that the original composition of the vent fluid is preserved when all Fe(II)aq is fully oxidized in seawater.

D. Ancient Sedimentary Rocks

1. The Early Archean, the Origin of Life, and Iron Oxidation

Until 4 Ga, an intense rain of asteroids and comets bombarded the Earth (Chyba, 1990; Dauphas & Marty, 2002b). Unfortunately, almost not rocks or minerals from this time period (the Hadean) are available for study. Fossil and geochemical evidence for biological activity can be traced back to 3.4 Ga (Schopf, 1993; Furnes et al., 2004). The sediments that are older than that have been extensively metamorphosed and the record that they provide of past terrestrial environments is not straightforward to interpret. The place that has been the focus of most attention in this regard to is Southern West Greenland.

Mojzsis et al. (1996) analyzed the carbon isotopic composition of graphite enclosed in apatite crystals in what was thought to be a sedimentary rock, on Akilia Island. They found a biogenic signature and concluded that photosynthetic life had already developed by >3.85 Ga. There has been much controversy regarding the age of these rocks but they might be of similar age or older than those from another locality from Greenland, Isua, which is dated at >3.7 Ga and where biogenic carbon isotope signature has been found (Rosing, 1999). In addition to the age, several aspects of the study published in 1996

have been questioned subsequently. These include the age of the apatite crystals, the presence of graphite in the apatite crystals, the significance of some the graphite that had been analyzed, and the very nature of the host rock. In a recent study, Fedo and Whitehouse (2002) argued based on fieldwork and trace element analyzes that the rocks from Akilia were not sedimentary but were instead igneous rocks that had been metasomatized by quartz addition. Subsequent tectonic activity, notably boudinage, would explain the layering that is visible in the outcrop. As discussed earlier, the Fe isotopic composition of igneous rocks worldwide is to a large extent homogeneous. In contrast, BIFs measured at other localities show very variable Fe isotopic compositions. For instance, the BIFs from the Kaapvaal craton have isotopic compositions from -1 to $+0.5$ ‰/amu, with a strong mineralogical control on the composition (Johnson et al., 2003b). In order to better understand the origin of the quartz-pyroxene layered rocks from Akilia, Dauphas et al. (2004c) analyzed their Fe isotopic compositions. The rocks have variable Fe isotopic compositions, being enriched in the heavy isotopes of Fe by as much as $0.5-0.6$ ‰/amu relative to IRMM-014 (Fig. 16). Akilia samples have similar isotopic compositions to BIFs of unambiguous sedimentary origin from Isua. This signature is clearly distinct from that of igneous rocks, which suggests that these rocks are true BIFs and are not metasomatized igneous rocks.

The fact that the BIFs from Isua, Akilia, and Innersuartuut are systematically enriched in the heavy isotopes of Fe provides additional information on how the rocks may have formed (Dauphas et al., 2004c). There is general agreement that during the Archaean, and presumably during the Hadean as well, the partial pressure of oxygen in the atmosphere was very low ($<10^{-5}$ present atmospheric level, Pavlov & Kasting, 2002; Farquhar & Wing, 2003). Under these conditions, the residence time of iron in the oceans would have been much longer than what it is at present because ferrous iron would not have been oxidized into ferric iron, which has very low solubility in seawater. Ferrous iron emanating from hydrothermal vents could have been transported over wide distances before being oxidized and precipitating as Fe oxyhydroxides. The key to understanding the formation of BIFs is to identify the mechanism that could have caused the oxidation of ferrous iron in an ocean that was globally anoxic. There are three mechanisms that could have caused this oxidation:

(i) Oxygenic photosynthetic organisms could have released O_2 which could have then oxidized Fe(II) into Fe(III).

(ii) Some bacteria can use Fe(II) instead of H_2O as an electron donor during anoxygenic photosynthesis and can thus oxidize directly Fe(II) into Fe(III).

(iii) If the atmosphere had low oxygen content, then it was also devoid of ozone, and energetic UV photons could have penetrated into Earth's atmosphere all the way to the surface of oceans, where they could have oxidized directly Fe(II) into Fe(III), a process called photo-oxidation.

The first two processes require the involvement of life, while photo-oxidation is a purely abiotic process. To date, no experiments have been performed to characterize the isotopic fractionation of Fe during photo-oxidation. The other two
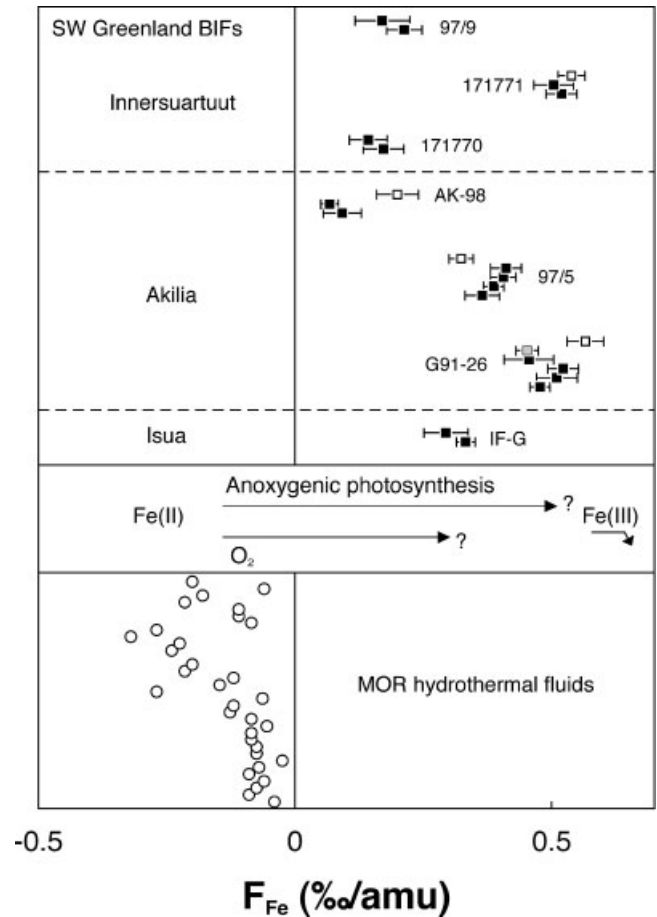
FIGURE 16. Iron isotopic compositions of banded iron formations from SW Greenland (Innersuartuut, Akilia, and Isua, Dauphas et al., 2004c). These formations, which are among the oldest sediments on Earth, show large enrichments in the heavy isotopes of Fe. A likely interpretation is that the original ferrous iron dissolved in the oceans had an isotopic composition similar to modern mid-ocean ridge hydrothermal fluids. This ferrous iron was subsequently oxidized into ferric iron by anoxygenic photosynthesis (FeII is the electron donor) or by free O_2 released by oxygenic photosynthesis (H_2O is the electron donor). These two processes are known to fractionate the precipitate relative to the fluid and the magnitude of this effect is comparable to the enrichment that is measured in the ancient sediments from SW Greenland.

processes (i and ii) have been characterized for their effects on Fe isotopes (Bullen et al., 2001; Welch et al., 2003; Croal et al., 2004) and they can be tested to check their consistencies with the observed enrichment in heavy Fe of the BIFs from Greenland (Dauphas et al., 2004c). BIF formation could have involved multiple stages that could all have contributed to the net isotopic shift between Fe(II) dissolved in the oceans and Fe(III) trapped in the sediment. For more details on these various aspects, see Figure 17 caption. During anoxygenic photosynthesis and O_2-mediated oxidation, net shifts of 0.75 and 0.4 ‰/amu have been documented, under specific experimental conditions (Bullen et al., 2001; Croal et al., 2004). Assuming that Fe(II) in the oceans at that time had the same isotopic composition as Fe(II) released in hydrothermal systems at present (-0.15 ‰/amu, Sharma,
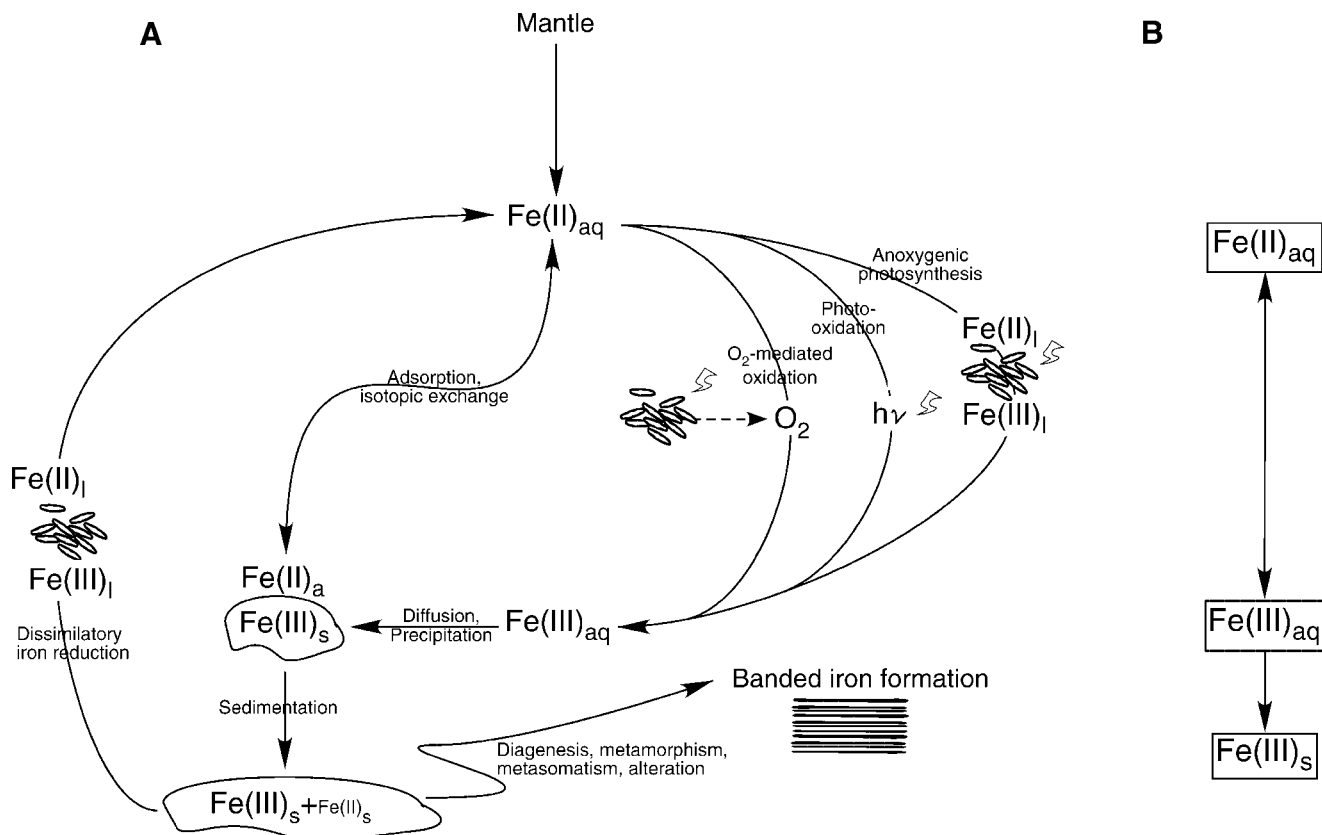
FIGURE 17. Possible processes involved in the formation of Archaean banded iron formations (**A**). Ferrous iron, which must ultimately have a mantle origin, was transported over large distances because the oxygen partial pressure in the atmosphere at that time was much lower than what it is at present. This $FeII_{aq}$ could have been oxidized into $FeIII_{aq}$ by three processes. (i) Some bacteria use ferrous iron as an electron donor in anoxygenic photosynthesis and produce ferric iron. (ii) During oxygenic photosynthesis, organisms use water as an electron donor and release O_2, which can then oxidize $FeII_{aq}$ into $FeIII_{aq}$. (iii) If the oxygen partial pressure in the Archaean atmosphere was much lower than what it is at present, energetic UV photons could have traveled all the way across the terrestrial atmosphere to reach the upper part of the oceans, where they could have photo-oxidized $FeII_{aq}$ into $FeIII_{aq}$. The ferric iron in solution formed by any of these three processes could diffuse to a nearby nucleation site where it could precipitate as hydrous ferric oxide. The particulate ferric iron could also serve as a site for adsorption of ferrous iron in solution. Part of the pool of precipitated ferric iron could be returned to aqueous ferrous iron by the action of organisms that do dissimilatory iron reduction, which is a form of respiration that uses FeIII in place of O_2. The precipitates could accumulate at the bottom of the ocean where they could subsequently endure diagenesis, metamorphism, metasomatism, and alteration, before being retrieved by geologists for isotopic analyzes. This complex network of chemical and physical pathways can be simplified as a two-step process, whereby ferrous iron in solution is oxidized into ferric iron in solution which then precipitates (**B**, Anbar, 2004; Beard & Johnson, 2004; Johnson et al., 2004). Interestingly, as far as isotopic ratios are concerned this description is amenable to quantification (see text, Eq. 33).

Polizzotto, & Anbar, 2001; Beard et al., 2003b; Severmann et al., 2004b), then the resulting effect would have been around 0.25–0.6 ‰/amu. Many additional parameters, including the rate of precipitation (Skulan, Beard, & Johnson, 2002), can modulate these values and larger or smaller shifts are conceivable. The bottom line is that the enrichment in heavy iron of the sediments is quantitatively consistent with the expected variations associated with biologic activity (oxygenic or anoxygenic photosynthesis). The two-stage model described in Section VI.A.5 could also be used to explore quantitatively Fe isotopic fractionation during BIF formation. However, to

adequately describe reality, a model capturing all the processes shown in Figure 17 may be required.

If any, ferrous iron adsorbed on the precipitate will be enriched in the heavy isotopes of Fe relative to ferrous Fe in solution (Icopini et al., 2004; Crosby et al., 2005; Teutsch et al., 2005). Further work remains to be done to check whether photo-oxidation (Braterman, Cairns-Smith, & Sloper, 1983), the only abiotic process that could have explained the formation of BIFs, can also explain the positive values that have been measured. If not, then Fe isotopes will prove to be useful tracers not only of sedimentary protoliths but also of biologic activity. It is worth

mentioning that because Fe is a major element in these rocks, it is much less sensitive to late contamination by biogenic input than carbon, which is often present at trace levels in metamorphosed sediments.

2. The Great Oxidation Event

The rise of atmospheric oxygen level, which started by ca. 2.3 Ga (Holland, 1984; Farquhar, Bao, & Thiemens, 2000; Bekker et al., 2004) was one of the most dramatic changes in the history of the Earth and the evolution of life. Major perturbations in biogeochemical and climatic record occurred during this period and include (i) negative and positive carbon isotope excursions in carbonates sandwiched between two glacial diamictites, (ii) Earth's earliest global glaciations; and (iii) oxidation of the Earth's atmosphere as suggested by increasing seawater sulfate content inferred from the $\delta^{34}S$ record and appearance of sulfate evaporites, disappearance of mass independent S isotope fractionation, appearance of red beds, oxidized paleosols, hematitic oölites and pisolites, Mn-oxide deposits, and Ce anomaly in chemical sedimentary deposits (Holland, 1984; Karhu & Holland, 1996; Canfield, 1998; Farquhar, Bao, & Thiemens, 2000; Bekker et al., 2004, 2005). How the oxidation state of the ocean and Fe oceanic cycling responded to the rise of oxygen in the atmosphere is still poorly known. Since Fe, along with C and S, are coupled with (and maintain) the redox state of the surface environment, concentrations, and isotopic compositions of Fe in seawater were likely affected by the change in the redox state of the atmosphere. Because of the high reactivity of Fe towards oxygen, the rise of atmospheric oxygen should have led to a dramatic change in oceanic Fe cycling by ca. 2.3 Ga. However, the abundance of banded iron formations (BIFs) during the Archean and Paleoproterozoic suggests that the deep ocean was widely anoxic until ca. 1.8 Ga, allowing high concentrations of Fe(II) to accumulate in the deep waters. The ocean redox state after 1.8 Ga is also a matter of controversy since the disappearance of major BIFs is thought to indicate that the deep ocean became either oxic or euxinic (Holland, 1984; Canfield, 1998; Isley & Abbott, 1999; Shen, Knoll, & Walter, 2003; Arnold et al., 2004b).

Recent studies of Fe isotope composition of marine sediments over geological time have provided new insights into the past Fe cycle and the evolution of ocean chemistry (Rouxel, Bekker, & Edwards, 2005; Yamaguchi et al., 2005; Fig. 18). In particular, Rouxel, Bekker, and Edwards (2005) investigated the record of Fe isotope composition in sedimentary pyrite in organic-rich marine sediments (black shales) ranging in age from Precambrian to Late Cretaceous, specifically focusing on Late Archean to early Paleoproterozoic time. Because of the large sulfate reservoir in modern seawater, the apparent limited variability of $\delta^{56}Fe$ values in phanerozoic pyrite (Fig. 18) suggests that most of reactive Fe is scavenged by biogenic H_2S to form Fe sulfide minerals, minimizing Fe isotope fractionation regardless of the isotope effect during Fe reduction and sulfide precipitation (the Fe isotopic composition of the precipitate must be equal to the initial Fe isotopic composition of the fluid when all Fe is precipitated). In contrast, when high concentrations of Fe(II) accumulate under anoxic conditions and low sulfide concentration, large Fe isotope fractionations may occur due to

partial Fe(II) oxidation, Fe(III) reduction, and distillation processes during Fe-mineral precipitation. Based on these hypotheses, Rouxel, Bekker, and Edwards (2005) proposed that Fe isotope variations in sedimentary pyrite are particularly sensitive to the concentration of dissolved Fe(II) and can be used to place important constraints on the source and sinks of the Fe(II) reservoir.

The general pattern of Fe isotope record (Fig. 18) allowed division of the Earth's history into three stages, which are strikingly similar to the stages defined by the $\delta^{34}S$, $\Delta^{33}S$, and $\delta^{13}C$ records as well as other indicators of the redox state of the atmosphere and ocean (Canfield, 1998; Farquhar, Bao, & Thiemens, 2000; Bekker et al., 2005). Stage 1 (>2.8 to 2.3 Ga) is characterized by highly variable and negative $\delta^{56}Fe$ values of pyrite (down to −3.5‰) that are interpreted to reflect reservoir effects during partial oxidation of hydrothermally derived Fe(II) and precipitation of isotopically heavy Fe oxides. Stage 2 (2.3 to ∼1.6 Ga) is characterized by $\delta^{56}Fe$ values ranging from −0.3 to 1.2‰ that might be related to the increased effect of sulfide precipitation in a redox-stratified ocean. Stage 3, from 1.6 Ga to the Phanerozoic, is characterized by sedimentary pyrite having a limited range of $\delta^{56}Fe$ variations (between ∼0‰ and −1‰) reflecting the establishment of an Fe-poor oxygenated ocean.

Since dissimilatory Fe(III) reduction (DIR) has been suggested to be important on the early Earth (Vargas et al., 1998) and is known to produce significant Fe isotope fractionation that may be preserved in organic-rich sediments (Matthews et al., 2004; Johnson et al., 2005), it has been hypothesized that the extreme Fe isotope fractionations during Stage 1 were produced by this metabolic activity (Yamaguchi et al., 2005). Because $\delta^{56}Fe$ analysis of bulk organic- and magnetite-rich Archean shales display strongly negative values, generally between −2.3 and −1 ‰, Yamaguchi et al. (2005) proposed that these rocks formed in the presence of Fe(II)aq that had very low $\delta^{56}Fe$ values, probably between −3 and −1 ‰. Although these results are consistent with the $\delta^{56}Fe$ record in pyrite (Rouxel, Bekker, & Edwards, 2005), Yamaguchi et al. (2005) proposed that DIR is the best explanation for producing such low $\delta^{56}Fe$ values. However, the lack of evidence for the complementary high $\delta^{56}Fe$ component that would be produced by DIR in the sedimentary sequence argues against DIR. Because Fe in archean and paleoproterozoic oceans is expected to undergo multiple bio-geochemical cycles, the interplay between abiotic *versus* biotic processes is complex and would complicate further the use of Fe isotopes as biosignatures in ancient sediments. Furthermore, the overprint of diagenetic effects in the Fe isotope record need to be thoroughly evaluated to better establish relationships between Fe isotope variations, changes of oceanic Fe cycle, and evolution of redox state of the ocean.

VII. CONCLUSION

With recent developments in mass spectrometry, iron has joined the realm of elements that can be measured routinely in laboratories around the world for their isotopic compositions. Much work has already been done to document isotopic variations in
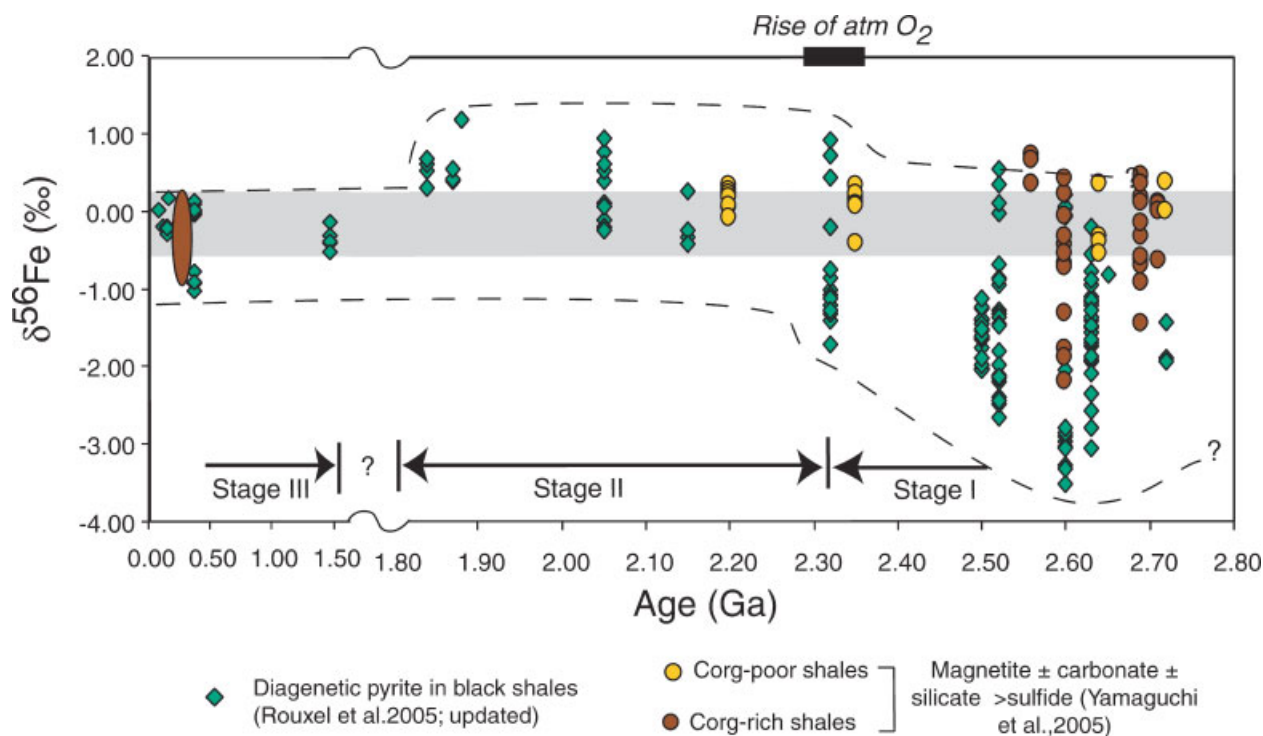
FIGURE 18. Plot of δ^{56}Fe values versus sample age for pyrite in black shales (Rouxel, Bekker, & Edwards, 2005 and unpublished results) and bulk shales (Yamaguchi et al., 2005). Organic-rich and organic-poor shales are composed primarily of Fe oxides, Fe-rich carbonates, and silicate with minor amount of sulfides. On the basis of the δ^{56}Fe values, the Fe ocean cycle can be roughly divided into three stages: (i) stage I is from 2.8 to 2.3 Ga, (ii) stage II is from 2.3 to 1.8 Ga, and (iii) stage III is less than 1.7 Ga (Rouxel, Bekker, & Edwards, 2005). Note the scale change between 1.5 and 1.8 Ga. The gray area corresponds to δ^{56}Fe values of Fe derived from igneous rocks (at 0.1‰) and hydrothermal sources (about −0.5‰). Dashed lines represent the contour lines of observed maximum and minimum Fe isotope compositions of sedimentary sulfides used to define stages I–III. The rise of atmospheric oxygen (atm O_2) is defined by multiple sulfur isotope analyses of pyrite in the same samples as analyzed for Fe isotopes (Bekker et al., 2004). [Color figure can be viewed in the online issue, which is available at www.interscience.wiley.com.]

natural systems and controlled laboratory experiments. Important avenues of research can be followed, which rely on the measurement of iron isotope variations in natural systems to unravel processes and sources. Variations are observed in igneous systems like differentiated planetesimals and the terrestrial mantle and more work is required on the experimental side to understand how iron isotopes partition between minerals and melts at high temperature. The geodynamic cycle of iron interfaces at many points with the biological cycle and Fe isotopic compositions may be used to shed some light on these past interactions between the geosphere and the biosphere. On the extraterrestrial side, sample return missions may allow us to apply the concepts developed on Earth to trace the mobilization and transport of iron in aqueous systems in past martian environments.

REFERENCES

Albarède F, Beard B. 2004. Analytical methods for non-traditional isotopes. In: Johnson CM, Beard BL, Albarede F, editors. Geochemistry of Non-traditional stable isotopes. Reviews in mineralogy and geochemistry. Washington, DC: Mineralogical Society of America; Geochemical Society. pp 113–152.

Alexander CMO'D, Wang J. 2001. Iron isotopes in chondrules: Implications for the role of evaporation during chondrule formation. Meteoritics Planet Sci 36:419–428.

Alexander CMO'D, Taylor S, Delaney JS, Ma P, Herzog GF. 2002. Mass-dependent fractionation of Mg, Si, and Fe isotopes in five stony cosmic spherules. Geochim Cosmochim Acta 66:173–183.

Alexander CMO'D, Hewins RH. 2004. Mass fractionation of Fe and Ni isotopes in metal in Hammadah Al Hamrah. Annual Meteoritical Society Meeting 2004, 67, #5080.

Alt JC. 1995. Subseafloor processes in mid-ocean ridge hydrothermal systems'. In: Humphris SE, Zierenberg RA, Mullineaux LS, Thomson RE, editors. Seafloor hydrothermal systems: Physical, chemical, biological, and geological interactions. Washington, DC: American Geophysical Union. pp 85–114.

Alt JC, Teagle DAH. 1999. The uptake of carbon during alteration of ocean crust. Geochim Cosmochim Acta 63:1527–1535.

Amari S, Lewis RS, Anders E. 1994. Interstellar grains in meteorites: I. Isolation of SiC, graphite, and diamond; size distribution of SiC and graphite. Geochim Cosmochim Acta 58:459–470.

Amelin Y, Krot AN, Hutcheon ID, Ulyanov AA. 2002. Lead isotopic ages of chondrules and calcium-aluminum-rich inclusions. Science 297:1678–1683.

Anbar AD, Roe JE, Barling J, Nealson KH. 2000. Nonbiological fractionation of iron isotopes. Science 288:126–128.

Anbar AD. 2004. Iron stable isotopes: Beyond biosignatures. Earth Planet Sci Lett 217:223–236.

Anbar AD, Jarzecki AA, Spiro TG. 2005. Theoretical investigation of iron isotope fractionation between $Fe(H_2O)_6^{3+}$ and $Fe(H_2O)_6^{2+}$: Implications for iron stable isotope geochemistry. Geochim Cosmochim Acta 69:825–837.

Anders E, Zinner E. 1993. Interstellar grains in primitive meteorites: Diamond, silicon carbide, and graphite. Meteoritics 28:490–514.

Anderson TF, Raiswell R. 2004. Sources and mechanisms for the enrichment of highly reactive iron in euxinic black sea sediments. Am J Sci 304:203–233.

Arnold GL, Weyer S, Anbar AD. 2004a. Fe isotope variations in natural materials measured using high mass resolution multiple collector ICPMS. Anal Chem 76:322–327.

Arnold GL, Anbar AD, Barling J, Lyons TW. 2004b. Molybdenum isotope evidence for widespread anoxia in mid-proterozoic oceans. Science 304:87–90.

Bazylinski DA, Schlezinger DR, Howes BH, Frankel RB, Epstein SS. 2000. Occurence and distribution of diverse populations of magnetic protists in a chemically stratified coastal salt pond. Chem Geol 169:319–328.

Beard BL, Johnson CM. 1999. High precision iron isotope measurements of terrestrial and lunar materials. Geochim Cosmochim Acta 63:1653–1660.

Beard BL, Johnson CM, Cox L, Sun H, Nealson KH, Aguilar C. 1999. Iron isotope biosignatures. Science 285:1889–1892.

Beard BL, Johnson CM, Skulan JL, Nealson KH, Cox L, Sun H. 2003a. Application of Fe isotopes to tracing the geochemical and biological cycling of Fe. Chem Geol 195:87–117.

Beard BL, Johnson CM, von Damm KL, Poulson RL. 2003b. Iron isotope constraints on Fe cycling and mass balance in oxygenated Earth oceans. Geology 31:629–632.

Beard BL, Johnson CM. 2004. Fe isotope variations in the modern and ancient earth and other planetary bodies. Rev Mineral Geochem 55:319–357.

Bearman RJ, Jolly DL. 1981. Mass dependence of the self-diffusion coefficient in 2 equimolar binary-liquid Lennard-Jones systems determined through molecular-dynamics simulation. Molec Phys 44:665–675.

Beck P, Chaussidon M, Barrat J-A, Gillet P, Bohn M. 2005. An ion microprobe study of lithium isotopes behavior in Nakhlites. Meteoritics Planet Sci 40:A18.

Bekker A, Holland HD, Wang PL, Rumble D III, Stein HJ, Hannah JL, Coetzee LL, Beukes NJ. 2004. Dating the rise of atmospheric oxygen. Nature 427:117–120.

Bekker A, Kaufman AJ, Karhu JA, Eriksson KA. 2005. Evidence for Paleoproterozoic cap carbonates in North America. Precambrian Res 137:167–206.

Belshaw NS, Freedman PA, O'Nions RK, Franks M, Guo Y. 1998. A new variable dispersion double-focusing plasma mass spectrometer with performance illustrated for Pb isotopes. Int J Mass Spectrom 181:51–58.

Belshaw NS, Zhu XK, Guo Y, O'Nions RK. 2000. High precision measurement of iron isotopes by plasma source mass spectrometry. Int J Mass Spectrom 197:191–195.

Benz M, Brune A, Schink B. 1998. Anaerobic and aerobic oxidation of ferrous iron at neutral pH by chemoheterotrophic nitrate-reducing bacteria. Arch Microbiol 169:159–165.

Berner RA. 1968. Rate of concretion growth. Geochim Cosmochim Acta 32:477–483.

Berner RA. 1984. Sedimentary pyrite formation: An udpate. Geochim Cosmochim Acta 48:605–615.

Berquist B, Boyle E. 2002. Iron isotopic composition of the Amazon River. Eos (Transactions, American Geophysical Union) 83:F767.

Birck J-L. 2004. An overview of isotopic anomalies in extraterrestrial materials and their nucleosynthetic heritage. Rev Mineral Geochem 55:25–64.

Boyd PW, Watson AJ, Law CS, Abraham ER, Troll T, Murdon R, and 24 co-authors. 2000. A mesoscale phytoplankton bloom in the polar Southern Ocean stimulated by iron fertilization. Nature 407:695–702.

Boyle EA, Edmond JM, Sholkovitz ER. 1977. The mechanism of iron removal in estuaries. Geochim Cosmochim Acta 41:1313–1324.

Brantley SL, Liermann L, Bullen TD. 2001. Fractionation of Fe isotopes by soil microbes and organic acids. Geology 29:535–538.

Brantley SL, Liermann LJ, Guynn RL, Anbar A, Icopini GA, Barling J. 2004. Fe isotopic fractionation during mineral dissolution with and without bacteria. Geochim Cosmochim Acta 68:3189–3204.

Braterman PS, Cairns-Smith AG, Sloper RW. 1983. Photo-oxidation of hydrated Fe^{2+}—Significance for banded iron formations. Nature 303:163–164.

Bullen TD, McMahon PM. 1998. Using stable Fe isotopes to assess microbially mediated Fe3+ reduction in a jet-fuel contaminated aquifer. Mineral Mag 62A:255–256.

Bullen TD, White AF, Childs CW, Vivit DV, Schulz MS. 2001. Demonstration of significant abiotic iron isotope fractionation. Geology 29:699–702.

Bullen TD, White AF, Childs CW. 2003. Comment on isotopic fraction between Fe(III) and Fe(II) in aqueous solutions by Clark Johnson et al. [Earth Planet. Sci. Lett. 195 (2002) 141–153]. Earth Planet Sci Lett 206:229–232.

Busigny V, Dauphas N. 2005. Iron isotopes in Utah hematite concretions: A terrestrial analogue for martian blueberries. Meteoritics Planet Sci 40:A27.

Butler IB, Archer C, Vance D, Oldroyd A, Rickard D. 2005. Fe isotope fractionation on FeS formation in ambient aqueous solution. Earth Planet Sci Lett 236:430–442.

Campbell AJ, Humayun M, Meibom A, Krot AN, Keil K. 2001. Origin of zoned metal grains in the QUE94411 chondrite. Geochim Cosmochim Acta 65:163–180.

Canfield DE. 1989. Reactive iron in marine sediments. Geochim Cosmochim Acta 53:619–632.

Canfield DE. 1998. A new model for Proterozoic ocean chemistry. Science 396:450–453.

Chan MA, Beitler B, Parry WT, Ormö J, Komatsu G. 2004. A possible terrestrial analogue for haematite concretions on Mars. Nature 429:731–734.

Chen JH, Papanastassiou DA, Wasserburg GJ, Ngo HH. 2004. Endemic Mo isotopic anomalies in iron and carbonaceous meteorites. Lunar Planet Sci XXXV:1431.

Chyba CF. 1990. Impact delivery and erosion of planetary oceans in the early inner solar system. Nature 343:129–133.

Clayton RN, Mayeda TK. 1977. Correlated oxygen and magnesium isotope anomalies in Allende inclusions. I. Oxygen. Geophys Res Lett 4:295–298.

Clayton RN. 1993. Oxygen isotopes in meteorites. Annu Rev Earth Planet Sci 21:115–149.

Clayton DD, Meyer BS, The L-S, El Eid MF. 2002. Iron implantation in presolar supernova grains. Astrophys J 578:L83–L86.

Cohen BA, Levasseur S, Zanda B, Hewins RH, Halliday AN. 2005. Isotopic mass fractionation of iron in chondrules, evaporation or reduction? Lunar Planet Sci XXXVI:1690.

Crank J. 1984. Free and moving boundary problems. Oxford: Oxford University Press.

Croal LR, Johnson CM, Beard BL, Newman DK. 2004. Iron isotope fractionation by Fe(II)-oxidizing photoautotrophic bacteria. Geochim Cosmochim Acta 68:1227–1242.

Crosby HA, Johnson CM, Roden EE, Beard BL. 2005. Coupled Fe(II)-Fe(III) electron and atom exchange as a mechanism for Fe isotope fractionation during dissimilatory iron oxide reduction. Environ Sci Technol 39:6698–6704.

Dauphas N, Marty B, Reisberg L. 2002a. Molybdenum evidence for inherited planetary scale isotope heterogeneity of the protosolar nebula. Astrophys J 565:640–644.

Dauphas N, Marty B. 2002b. Inference on the nature and the mass of Earth's late veneer from noble metals and gases. J Geophys Res 107(E12):5129. doi: 10.1029/2001JE001617.

Dauphas N, Janney PE, Mendybaev RA, Wadhwa M, Richter FM, Davis AM, van Zuilen M, Hines R, Foley CN. 2004a. Chromatographic separation and multicollection-ICPMS analysis of iron. Investigating mass-dependent and -independent isotope effects. Anal Chem 76:5855–5863.

Dauphas N, Davis AM, Marty B, Reisberg L. 2004b. The cosmic molybdenum-ruthenium isotope correlation. Earth Planet Sci Lett 226:465–475.

Dauphas N, van Zuilen M, Wadhwa M, Davis AM, Marty B, Janney PE. 2004c. Clues from Fe isotope variations on the origin of early archean BIFs from Greenland. Science 306:2077–2080.

Davis AM, Clayton RN, Mayeda TK, Brownlee DE. 1991. Large mass fractionation of iron isotopes in cosmic spherules collected from deep-sea sediments. Lunar Planet Sci XXII:281–282.

Davis AM, Brownlee DE. 1993. Iron and nickel isotopic mass fractionation in deep-sea spherules. Lunar Planet Sci XXIV:373–374.

Davis AM, Gallino R, Lugaro M, Tripa CE, Savina MR, Pellin MJ, Lewis RS. 2002. Presolar grains and the nucleosynthesis of iron isotopes. Lunar Planet Sci XXXIII:2018.

Davis AM, Richter F. 2004;. Condensation and evaporation of solar system materials. In Treatise on Geochemistry. Amsterdam: Elsevier. pp 407–430.

de Barr HJW, de Jong JTM. 2001;. Distributions, sources and sinks of iron in seawater. Review Chapter 5. In: Turner D, Hunter KA, editors. Biogeochemistry of iron in seawater. IUPAC Book Series on Analytical and Physical Chemistry of Environmental Systems. John Wiley & Sons, Ltd., Chichester. pp 123–253.

Dideriksen K, Baker J, Stipp S. 2005. Iron isotopes in natural carbonate minerals determined by MC-ICP-MS with a ^{58}Fe-^{54}Fe double spike. Geochim Cosmochim Acta (in press).

Douglas DJ, French JB. 1992. Collisional focusing effects in radio frequency quadripoles. J Am Soc Mass Spectrom 3:398–408.

Edmond JM, Measures C, McDuff RE, Chan LH, Collier R, Grant B, Gordon LI, Corliss JB. 1979. Ridge crest hydrothermal activity and the balances of the major and minor elements in the ocean: the Galapagos data. Earth Planet Sci Lett 46:1–18.

Edwards KJ, Bond PL, Gihring TM, Banfield JF. 2000. An archaeal iron-oxidizing extreme acidophile important in acid mine drainage. Science 287:1796–1799.

Elderfield H, Schultz A. 1996. Mid-ocean ridge hydrothermal fluxes and the chemical composition of the ocean. Annu Rev Earth Planet Sci 24:191–224.

Emerson D, Moyer C. 1997. Isolation and characterization of novel iron-oxidizing bacteria that grow at circumneutral pH. Appl Environ Microbiol 61:2681–2687.

Emmanuel S, Erel Y, Mathews A, Teutsch N. 2005. A preliminary mixing model for Fe isotopes in soils. Chem Geol 222:23–34.

Fantle MS, DePaolo DJ. 2004. Iron isotopic fractionation during continental weathering. Earth Planet Sci Lett 228:547–562.

Farquhar J, Bao H, Thiemens M. 2000. Atmospheric influence of Earth's earliest sulfur cycle. Science 289:756–758.

Farquhar J, Wing BA. 2003. Multiple sulfur isotopes and the evolution of the atmosphere. Earth Planet Sci Lett 213:1–13.

Fedo CM, Whitehouse MJ. 2002. Metasomatic origin of quartz-pyroxene rock, Akilia, Greenland, and implications for Earth's earliest life. Science 296:1448–1452.

Frank FC. 1950. Radially symmetric phase growth controlled by diffusion. Proc Roy Soc London A201:586–599.

Frankel RB, Blakemore RP, Wolfe RS. 1979. Magnetite in freshwater magnetotactic bacteria. Science 203:1355–1356.

Furnes H, Banerjee NR, Muehlenbachs K, Staudigel H, de Wit M. 2004. Early life recorded in Archean pillow lavas. Science 304:578–581.

Galy A, Yoffe O, Janney PE, Williams RW, Cloquet C, Alard O, Halicz L, Wadhwa M, Hutcheon ID, Ramon E, Carignan J. 2003. Magnesium isotope heterogeneity of the isotopic standard SRM980 and new reference materials for magnesium-isotope-ratio measurements. J Anal At Spectrom 18:1352–1356.

Graham S, Pearson N, Jackson S, Griffin W, O'Reilly SY. 2004. Tracing Cu and Fe from source to porphyry: In situ determination of Cu and Fe isotope ratios in sulfides from the Grasberg Cu–Au deposit. Chem Geol 207:147–169.

Günther D, Heinrich CA. 1999a. Comparison of the ablation behaviour of 266 nm Nd:YAG and 193 nm ArF excimer lasers for LA-ICP-MS analysis. J Anal At Spectrom 14:1369–1374.

Günther D, Heinrich CA. 1999b. Enhanced sensitivity in laser ablation-ICP mass spectrometry using helium-argon mixtures as aerosol carrier. J Anal At Spectrom 14:1363–1368.

Halliday AN, Lee D-C, Christensen JN, Walder AJ, Freedman PA, Jones CE, Hall CM, Yi W, Teagle D. 1995. Recent developments in inductively coupled plasma magnetic sector multiple collector mass spectrometry. Int J Mass Spectrom Ion Process 146(147):21–33.

Hashimoto A. 1990. Evaporation kinetics of forsterite and implications for the early solar nebula. Nature 347:53–55.

Herzog GF, Xue S, Hall GS, Nyquist LE, Shih C-Y, Wiesmann H, Brownlee DE. 1999. Isotopic and elemental composition of iron, nickel, and chromium in type I deep-sea spherules: Implications for origin and composition of the parent micrometeoroids. Geochim Cosmochim Acta 63:1443–1457.

Hirata T, Ohno T. 2001. In situ isotopic ratio analysis of iron using laser ablation-multiple collector-inductively coupled plasma mass spectrometry (LA-MC-ICP-MC). J Anal At Spectrom 16:487–491.

Hirata T, Hayano Y, Ohno T. 2003. Improvements in precision of isotopic ratio measurements using laser ablation-multiple collector-ICP-mass spectrometry: Reduction of changes in measured isotopic ratios. J Anal At Spectrom 18:1283–1288.

Holland HD. 1984. The chemical evolution of the atmosphere and oceans. New York: Princeton University Press.

Honnorez J. 1981. The aging of the oceanic crust at low temperature. In: Emiliani C, editor. Oceanic lithosphere. Londres: J. Wiley. pp 525–587.

Humayun M, Clayton RN. 1995. Potassium isotope cosmochemistry: Genetic implications of volatile element depletion. Geochim Cosmochim Acta 59:2132–2148.

Humayun M, Cassen P Processes determining the volatile abundances of the meteorites and terrestrial planets 2000. In: Canup RM, Righter K,

editors. Origin of the earth and moon, Tucson: University of Arizona Press. pp 3–23.

Humphris SE, Herzig PM, Miller DJ, Alt JC, Becker K, Brown D and 19 co-authors. 1995. The internal structure of an active sea-floor massive sulphide deposit. Nature 377:713–716.

Huss GR, Lewis RS. 1995. Presolar diamond, SiC, and graphite in primitive chondrites: Abundances as a function of meteorite class and petrologic type. Geochim Cosmochim Acta 59:115–160.

Hutchins DA, DiTullio GR, Bruland KW. 1993. Iron and regenerated production: Evidence for biological iron recycling in two marine environments. Limnol Oceanogr 38:1242–1255.

Hutchins DA, Bruland KW. 1998. Iron-limited diatom growth and Si:N uptake ratios in a coastal upwelling regime. Nature 393:561–564.

Hutchins DA, Witter AE, Butler A, Luther GW III. 1999. Competition among marine phytoplankton for different chelated iron species. Nature 400:858–861.

Icopini GA, Anbar AD, Ruebush SS, Tien M, Brantley SL. 2004. Iron isotope fractionation during microbial reduction of iron: The importance of adsorption. Geology 32:205–208.

Isley AE, Abbott DH. 1999. Plume-related mafic volcanism and the deposition of banded iron formation. J Geophys Res 104:15461–15477.

Jarzecki AA, Anbar AD, Spiro TG. 2004. DFT analysis of $Fe(H_2O)_6^{3+}$ and $Fe(H_2O)_6^{2+}$ structure and vibrations; implications for isotope fractionation. J Phys Chem A 108:2726–2732.

Johnson KS, Gordon RM, Coale KH. 1997. What controls dissolved iron concentrations in the world ocean? Marine Chemistry 57:137–161.

Johnson KS, Chavez FP, Friederich GE. 1999. Continental-shelf sediment as a primary source of iron for coastal phytoplankton. Nature 398:697–700.

Johnson CM, Beard BL. 1999. Correction of instrumentally produced mass fractionation during isotopic analysis of Fe by thermal ionization mass spectrometry. Int J Mass Spectrom 193:87–99.

Johnson CM, Skulan JL, Beard BL, Sun H, Nealson KH, Braterman PS. 2002. Isotopic fractionation between Fe(III) and Fe(II) in aqueous solutions. Earth Planet Sci Lett 195:141–153.

Johnson CM, Beard BL, Braterman PS, Welch SA. 2003a. Reply to comment on Isotopic fractionation between Fe(III) and Fe(II) in aqueous solutions by Thomas D. Bullen, Arthur F. White and Cyril W. Childs. Earth Planet Sci Lett 206:233–236.

Johnson CM, Beard BL, Beukes NJ, Klein C, O'Leary JM. 2003b. Ancient geochemical cycling in the Earth as inferred from Fe isotope studies of banded iron formations from the Transvaal Craton. Contrib Mineral Petrol 144:523–547.

Johnson CM, Beard BL, Roden EE, Newman DK, Nealson KH. 2004. Isotopic constraints on biogeochemical cycling of Fe. Rev Mineral Geochem 55:359–408.

Johnson CM, Roden EE, Welch SA, Beard BL. 2005. Experimental constraints on Fe isotope fractionation during magnetite and Fe carbonate formation coupled to dissimilatory hydrous ferric oxide reduction. Geochim Cosmochim Acta 69:963–993.

Karhu JA, Holland HD. 1996. Carbon isotopes and the rise of atmospheric oxygen. Geology 24:867–870.

Kashiv Y, Cai Z, Lai B, Sutton SR, Lewis RS, Davis AM, Clayton RN, Pellin MJ. 2001. Synchrotron X-ray fluorescence: A new approach for determining trace element concentrations in individual presolar SiC grains. Lunar Planet Sci XXXII:2192.

Kavner A, Bonet F, Shahar A, Simon J, Young E. 2005. The isotopic effects of electron transfer: An explanation for Fe isotope fractionation in nature. Geochim Cosmochim Acta 69:2971–2979.

Kehm K, Hauri EH, Alexander CMO'D, Carlson RW. 2003. High precision iron isotope measurements of meteoritic material by cold plasma ICP-MS. Geochim Cosmochim Acta 67:2879–2891.

Kosler J, Pedersen RB, Kruber C, Sylvester PJ. 2005. Analysis of Fe isotopes in sulfides and iron meteorites by laser ablation high-mass resolution

multi-collector ICP mass spectrometry. J Anal Atom Spectrom 20:192–199.

Levasseur S, Frank M, Hein JR, Halliday AN. 2004. The global variation in the iron isotope composition of marine hydrogenetic ferromanganese deposits: Implications for seawater chemistry? Earth Planet Sci Lett 224:91–105.

Lodders K. 2003. Solar system abundances and condensation temperatures of the elements. Astrophys J 591:1220–1247.

Lovley DR, Stolz JF, Nord GL, Phillips EJP. 1987. Anaerobic production of magnetite by a dissimilatory iron-reducing microorganism. Nature 330:252–254.

Lundstrom CC, Chaussidon M, Hsui AT, Kelemen P, Zimmerman M. 2005. Observations of Li isotopic variations in the Trinity ophiolite: Evidence for isotopic fractionation by diffusion during mantle melting. Geochim Cosmochim Acta 69:735–751.

Macrellis HM, Trick CG, Rue EL, Smith G, Bruland KW. 2001. Collection and detection of natural iron-binding ligands from seawater. Mar Chem 76:175–187.

Malinovsky D, Stenberg A, Rodushkin I, Andren H, Ingri J, Ohlander B, Baxter DC. 2003. Performance of high resolution MC-ICPMS for Fe isotope ratio measurements in sedimentary geological materials J Anal Atom Spectrom 18:687–695.

Malinovsky DN, Rodyushkin IV, Shcherbakova EP, Ponter C, Öhlander B, Ingri J. 2005. Fractionation of Fe isotopes as a result of redox processes in a basin. Geochemistry Int 43:878–885.

Mandernack KW, Bazylinski DA, Shanks WC, Bullen TD. 1999. Oxygen and iron isotope studies of magnetite produced by magnetotactic bacteria. Science 285:1892–1896.

Maréchal CN, Télouk P, Albarède F. 1999. Precise analysis of copper and zinc isotopic compositions by plasma-source mass spectrometry. Chem Geol 156:251–273.

Marhas KK, Hoppe P, Besmehn A. 2004. A NanoSIMS study of iron-isotopic compositions in presolar silicon carbide grains. Lunar Planet Sci XXXV:1834.

Martin JH. 1990. Glacial-interglacial CO_2 change: The iron hypothesis. Paleoceanography 5:1–13.

Matthews A, Zhu XK, O'Nions K. 2001. Kinetic iron stable isotope fractionation between iron (-II) and (-III) complexes in solution. Earth Planet Sci Lett 192:81–92.

Matthews A, Morgans-Bell HS, Emmanuel S, Jenkyns HC, Erel Y, Halicz L. 2004. Controls on iron-isotope fractionation in organic-rich sediments (Kimmeridge Clay, Upper Jurassic, Southern England). Geochim Cosmochim Acta 68:3107–3123.

Meibom A, Petaev MI, Krot AN, Wood JA, Keil K. 1999. Primitive FeNi metal grains in CH carbonaceous chondrites formed by condensation from a gas of solar composition. J Geophys Res 104:22053–22059.

Mojzsis SJ, Arrhenius G, McKeegan KD, Harrison TM, Nutman AP, Friend CRL. 1996. Evidence for life on Earth before 3800 million years ago. Nature 384:55–59.

Mullane E, Russell SS, Gounelle M, Mason T, Din V, Weiss D, Coles B. 2003. Precise and accurate determination of iron isotopes by multi-collector inductively coupled plasma mass spectrometry. In plasma source mass spectrometry: Applications and emerging technologies. London: The Royal Society of Chemistry. pp 351–361.

Neilands JB. 1982. Microbial envelope proteins related to iron. Ann Rev Microbiol 36:285–309.

Newsom HE, Drake MJ. 1979. The origin of metal clasts in the Bencubbin meteoritic breccia. Geochim Cosmochim Acta 43:689–707.

Nicolussi GK, Pellin MJ, Lewis RS, Davis AM, Amari S, Clayton RN. 1998. Molybdenum isotopic composition of individual presolar silicon carbide grains from the Murchison meteorite. Geochim Cosmochim Acta 62:1093–1104.

Ohno T, Shinohara A, Kohge I, Chiba M, Hirata T. 2004. Isotopic analysis of Fe in human red blood cells by multiple collector-ICP-mass spectrometry. Anal Sci 20:617–621.

Pagel BEJ. 1997. Nucleosynthesis and chemical evolution of galaxies. Cambridge: Cambridge University Press.

Papanastassiou DA, Chen JH, Wasserburg GJ. 2004. More on Ru endemic isotope anomalies in meteorites. Lunar Planet Sci XXXV:1828.

Parry WT, Chan MA, Beitler B. 2004. Chemical bleaching indicates episodes of fluid flow in deformation bands in sandstone. AAPG Bull 88:175–191.

Pavlov AA, Kasting JF. 2002. Mass-independent fractionation of sulfur isotopes in archean sediments: Strong evidence for an anoxic Archean atmosphere. Astrobiology 2:27–41.

Poitrasson F, Freydier R. 2005. Heavy iron isotope composition of granites determined by high resolution MC-ICP-MS. Chem Geol 222:132–147.

Poitrasson F, Halliday AN, Lee D-C, Levasseur S, Teutsch N. 2004. Iron isotope differences between Earth, Moon, Mars and Vesta as possible records of contrasted accretion mechanisms. Earth Planet Sci Lett 223:253–266.

Poitrasson F, Levasseur S, Teutsch N. 2005. Significance of iron isotope mineral fractionation in pallasites and iron meteorites for the core-mantle differentiation of terrestrial planets. Earth Planet Sci Lett (in press).

Polyakov VB. 1997. Equilibrium fractionation of the iron isotopes: Estimation from Mossbauer spectroscopy data. Geochim Cosmochim Acta 61:4213–4217.

Polyakov VB, Mineev SD. 2000. The use of Mossbauer spectroscopy in stable isotope geochemistry. Geochim Cosmochim Acta 64:849–865.

Powell PE, Cline GR, Reid CPP, Szaniszlo PJ. 1980. Occurrence of hydroxamate siderophore iron chelators in soils. Nature 287:833–834.

Richter FM, Liang Y, Davis AM. 1999. Isotope fractionation by diffusion in molten oxides. Geochim Cosmochim Acta 63:2853–2861.

Richter FM, Davis AM, Ebel DS, Hashimoto A. 2002. Elemental and isotopic fractionation of type B calcium-,aluminum-rich inclusions: Experiments, theoretical considerations, and constraints on their thermal evolution. Geochim Cosmochim Acta 66:521–540.

Richter FM, Davis AM, DePaolo DJ, Watson EB. 2003. Isotope fractionation by chemical diffusion between molten basalt and rhyolite. Geochim Cosmochim Acta 67:3905–3923.

Richter FM. 2004. Timescales determining the degree of kinetic isotope fractionation by evaporation and condensation. Geochim Cosmochim Acta 68:4971–4992.

Roden E. 2004. Analysis of long-term bacterial vs. chemical Fe(III) oxide reduction kinetics. Geochim Cosmochim Acta 68:3205–3216.

Rodushkin I, Stenberg A, Andrén H, Malinovsky D, Baxter DC. 2004. Isotopic fractionation during diffusion of transition metal ions in solution. Anal Chem 76:2148–2151.

Roe JE, Anbar AD, Barling J. 2003. Nonbiological fractionation of Fe isotopes: Evidence of an equilibrium isotope effect. Chem Geol 195:69–85.

Rosing MT. 1999. ^{13}C-depleted carbon microparticles in >3700-Ma sea-floor sedimentary rocks from west Greenland. Science 283:674–676.

Roskosz M, Luais B, Toplis MJ. 2005a. Experimental determination of iron isotope fractionation during high temperature segregation of metal from silicate liquids: evaporation or diffusion? Lunar Planet Sci XXXVI:1959.

Roskosz M, Luais B, Watson HC, Toplis MJ, Alexander CMO'D, Mysen BO. 2005b. High temperature fractionation of iron isotopes during metal segregation from a magma: An experimental insight. Submitted.

Rouxel O, Ludden J, Carignan J, Marin L, Fouquet Y. 2002. Natural variations of Se isotopic composition determined by hydride generation multiple collector coupled mass spectrometer. Geochim Cosmochim Acta 66:3191–3199.

Rouxel O, Dobbek N, Ludden J, Fouquet Y. 2003. Iron isotope fractionation during oceanic crust alteration. Chem Geol 202:155–182.

Rouxel O, Fouquet Y, Ludden JN. 2004. Subsurface processes at the lucky strike hydrothermal field, mid-atlantic ridge: Evidence from sulfur, selenium and iron isotopes. Geochim Cosmochim Acta 68:2295–2311.

Rouxel O, Bekker A, Edwards K. 2005. Iron Isotope Constraints on the Archean and Paleoproterozoic Ocean Redox State. Science 307:1088–1091.

Sakaguchi T, Arakaki A, Matsunaga T. 2002. Desulfovibrio magneticus sp. nov., a novel sulfate-reducing bacterium that produces intracellular single-domain-sized magnetite particles. Int J Syst Evol Microbiol 52:215–221.

Savina MR, Pellin MJ, Tripa CE, Veryovkin IV, Calaway WF, Davis AM. 2003. Analyzing individual presolar grains with CHARISMA. Geochim Cosmochim Acta 67:3215–3225.

Savina MR, Davis AM, Tripa CE, Pellin MJ, Gallino R, Lewis RS, Amari S. 2004. Extinct technetium in silicon carbide stardust grains: Implications for stellar nucleosynthesis. Science 202:649–652.

Schauble EA, Rossman GR, Taylor HP. 2001. Theoretical estimates of equilibrium Fe-isotope fractionations from vibrational spectroscopy. Geochim Cosmochim Acta 65:2487–2497.

Schauble EA. 2004. Applying stable isotope fractionation theory to new systems. Rev Mineral Geochem 55:65–111.

Schoenberg R, von Blanckenburg F. 2005. An assessment of the accuracy of stable Fe isotope ratio measurements of samples with organic and inorganic matrices by high-resolution multicollector ICP-MS. Int J Mass Spectrom 243:257–272.

Schopf JW. 1993. Microfossils of the Early Archean Apex chert: New evidence of the antiquity of life. Science 260:640–646.

Schuler D, Baeuerlein E. 1996. Iron-limited growth and kinetics of iron uptake in Magnetospirulum gryphiswaldense. Arch Microbiol 166:301–307.

Seewald JS, Seyfried WE. 1990. The effect of temperature on metal mobility in subseafloor hydrothermal systems: Constraints from basalt alteration experiments. Earth Planet Sci Lett 101:388–403.

Severmann S, McManus J, Johnson CM, Beard BL. 2004a. Iron isotope geochemistry in California Margin sediments and pore waters Eos Trans. AGU 2004a, Ocean Science Meeting Supplement 84, Abstract#OS1L-019. Paper presented at the American Geophysical Union Meeting, Portland.

Severmann S, Johnson CM, Beard BL, German CR, Edmonds HN, Chiba H, Green DRH. 2004b. The effect of plume processes on the Fe isotope composition of hydrothermally derived Fe in the deep ocean as inferred from the Rainbow vent site, Mid-Atlantic Ridge, 36°14′ N. Earth Planet Sci Lett 225:63–76.

Sharma M, Polizzotto M, Anbar AD. 2001. Iron isotopes in hot springs along the Juan de Fuca Ridge. Earth Planet Sci Lett 194:39–51.

Shen Y, Knoll AH, Walter MR. 2003. Evidence for low sulphate and anoxia in a mid-Proterozoic marin basin. Nature 423:632–635.

Sholkovitz ER. 1976. Flocculation of dissolved organic and inorganic matter during the mixing of river water and seawater. Geochim Cosmochim Acta 40:831–845.

Simmons SL, Sievert SM, Frankel RB, Bazylinski DA, Edwards KJ. 2004. Spatio-temporal distribution of marine magnetotactic bacteria in a monomictic coastal salt pond. Submitted.

Skulan JL, Beard BL, Johnson CM. 2002. Kinetic and equilibrium Fe isotope fractionation between aqueous Fe(III) and hematite. Geochim Cosmochim Acta 66:2995–3015.

Spring S, Amann R, Ludwig W, Schleifer K, Petersen N. 1993. Dominating role of an unusual magnetotactic bacteria. System Appl Microbiol 15:116–122.

Staudigel H, Plank T, White B, Schmincke H-U. 1996. Geochemical fluxes during seafloor alteration of the basaltic upper oceanic crust: DSDP

Sites 417 and 418, Subduction: Top to Bottom. Geophysical Monograph 96:19–38. Washington, DC: American Geophysical Union.

Stein CA, Stein S. 1994. Constraints on hydrothermal heat flux through the oceanic lithosphere from global heat flow. J Geophys Res 99:3081–3095.

Steinhoefel G, Horn I, Schoenberg R, Von Blanckenburg F. 2005. In situ-Fe isotope determination using femtosecond LA-MC-ICP-MS. Geochim Cosmochim Acta 69S1:A374.

Stenberg A, Malinovsky D, Rodushkin I, Andren H, Ponter C, Ohlander B, Baxter DC. 2003. Separation of Fe from whole blood matrix for precise isotopic ratio measurements by MC-ICP-MS: A comparison of different approaches. J Anal At Spectrom 18:23–28.

Stenberg A, Malinovsky D, Öhlander B, Andrén H, Forsling W, Engström L-M, Wahlin A, Engström E, Rodushkin I, Baxter C. 2005. Measurement of iron and zinc isotopes in human whole blood: Preliminary application to the study of HFE genotypes. J Trace Elem Med Bio 19:55–60.

Stolz JF, Chang SBR, Kirschvink JL. 1986. Magnetotactic bacteria and single-domain magnetite in hemipelagic sediments. Nature 321:849–851.

Strelow FEW. 1980. Improved separation of iron from copper and other elements by anion-exchange chromatography on a 4% cross-linked resin with high concentrations of hydrochloric acid. Talanta 27:727–732.

Taylor PDP, Maeck R, De Bièvre P. 1992. Determination of the absolute isotopic composition and atomic weight of a reference sample of natural iron. Int J Mass Spectrom Ion Processes 121:111–125.

Taylor S, Alexander CMO'D, Delaney J, Ma P, Herzog GF, Engrand C. 2005. Isotopic fractionation of iron, potassium, and oxygen in stony cosmic spherules: Implications for heating histories and sources. Geochim Cosmochim Acta 69:2647–2662.

Teutsch N, von Gunten U, Porcelli D, Cirpka OA, Halliday AN. 2005. Adsorption as a cause for iron isotope fractionation in reduced groundwater. Geochim Cosmochim Acta 69:4175–4185.

Tivey MK. 1995. Modeling chimney growth and associated fluid flow at seafloor hydrothermal vent sites. In: Humphris SE, Zierenberg RA, Mullineaux LS, Thomson RE, editors. Seafloor hydrothermal systems: Physical, chemical, biological, and geological interactions. Washington, DC: American Geophysical Union. pp 158–177.

Tripa CE, Pellin MJ, Savina MR, Davis AM, Lewis RS, Clayton RN. 2002. Fe isotopic compositions of presolar SiC mainstream grains. Lunar Planet Sci XXXIII:1975.

Truran JW, Heger A. 2004;. Origin of the elements. In: Treatise on geochemistry, meteorites, comets, and planets, Vol. 1. Amsterdam: Elsevier. pp 1–15.

Tsuchiyama A, Kawamura K, Nakao T, Uyeda C. 1994. Isotopic effects on diffusion in MgO melt simulated by the molecular dynamics (MD) method and implications for isotopic mass fractionation in magmatic systems. Geochim Cosmochim Acta 58:3013–3021.

Tsuchiyama A, Tachibana S, Takahashi T. 1999. Evaporation of forsterite in the primordial solar nebula: Rates and accompanied isotopic fractionation. Geochim Cosmochim Acta 63:2451–2466.

Turner PJ, Mills DJ, Schroder E, Lapitajs G, Jung G, Lacone LA, Haydar DA, Montaser A. 1998;. Instrumentation for low- and high-resolution ICP-MS. In: Montaser A, editor. Inductively coupled plasma mass spectrometry. New York: Wiley-VCH. pp 421–501.

Vargas M, Kashefi K, Blunt-Harris EL, Lovley DR. 1998. Microbiological evidence for Fe(III) reduction on early Earth. Nature 395:65–67.

Völkening J, Papanastassiou DA. 1989. Iron isotope anomalies. Astrophys J 347:L43–L46.

Von Blanckenburg F. 2000. Iron isotope fractionation in soils. Geochim Cosmochim Acta 5:1057.

von Damm KL. 1995. Controls on the chemistry and temporal variability of seafloor hydrothermal fluids. In: Humphris SE, Zierenberg RA, Mullineaux LS, Thomson RE, editors. Seafloor hydrothermal systems: Physical, chemical, biological, and geological interactions. Washington, DC: American Geophysical Union. pp 222–247.

Walczyk T, von Blanckenburg F. 2002. Natural iron isotope variations in human blood. Science 295:2065–2066.

Walczyk T, von Blanckenburg F. 2005. Deciphering the iron isotope message of the human body. Int J Mass Spectrom 242:117–134.

Walder AJ, Freedman PA. 1992. Isotope ratio measurements using a double focusing magnetic sector mass analyser with an inductively coupled plasma ion source. J Anal At Spectrom 7:571–575.

Wang J, Davis AM, Clayton RN, Mayeda TK. 1994. Kinetic isotopic fractionation during the evaporation of the iron oxide from liquid state. Lunar Planet Sci XXV:1459–1460.

Wang J, Davis AM, Clayton RN, Hashimoto A. 1999. Evaporation of single crystal forsterite: Evaporation kinetics, magnesium isotope fractionation, and implications of mass-dependent isotopic fractionation of a diffusion-controlled reservoir. Geochim Cosmochim Acta 63:953–966.

Wasserburg GJ, Lee T, Papanastassiou DA. 1977. Correlated O and Mg isotopic anomalies in Allende inclusions. II-Magnesium. Geophys Res Lett 4:299–302.

Watson AJ, Bakker DCE, Ridgwell AJ, Boyd PW, Law CS. 2000. Effect of iron supply on Southern Ocean CO2 uptake and implications for glacial atmospheric CO2. Nature 407:730–733.

Welch SA, Beard BL, Johnson CM, Braterman PS. 2003. Kinetic and equilibrium Fe isotope fractionation between aqueous Fe(II) and Fe(III). Geochim Cosmochim Acta 67:4231–4250.

Wells ML, Price NM, Bruland KW. 1995. Iron chemistry in seawater and its relationship to phytoplankton: A workshop report. Mar Chemistry 48:157–182.

Weyer S, Schwieters JB. 2003. High precision Fe isotope measurements with high mass resolution MC-ICPMS. Int J Mass Spectrom 226:355–368.

Wheat CG, Mottl MJ. 2000. Composition of pore and spring waters from baby bare: Global implications of geochemical fluxes from a ridge flank hydrothermal system. Geochim Cosmochim Acta 64:629–642.

Wheat CG, Mottl MJ. 2004. Geochemical fluxes through Mid-Ocean Ridge flanks. In: Davis EE, Elderfield H, editors. Hydrogeology of the Oceanic Lithosphere. Cambridge: Cambridge University Press.

Widdel F, Schnell S, Heising S, Ehrenreich A, Assmus B, Schink B. 1993. Ferrous iron oxidation by anoxygenic phototrophic bacteria. Nature 362:834–836.

Wiederhold JG, von Blanckenburg F. 2002. Iron isotope variations in a complete natural soil catena with lateral mobilization and reprecipitation. Geochim Cosmochim Acta 66:A834.

Wiesli RA, Beard BL, Taylor LA, Johnson CM. 2003. Space weathering processes on airless bodies: Fe isotope fractionation in the lunar regolith. Earth Planet Sci Lett 216:457–465.

Wiesli RA, Beard BL, Johnson CM. 2004. Experimental determination of Fe isotope fractionation between aqueous Fe(II), siderite and green rust in abiotic systems. Chem Geol 211:343–362.

Wijsman JWM, Middelburg JJ, Herman PMJ, Bottcher ME, Heip CHR. 2001. Sulfur and iron speciation in surface sediments along the northwestern margin of the Black Sea. Mar Chemistry 74:261–278.

Williams HM, McCammon CA, Peslier AH, Halliday AN, Teutsch N, Levasseur S, Burg J-P. 2004a. Iron isotope fractionation and the oxygen fugacity of the mantle. Science 304:1656–1659.

Williams HM, Halliday AN, Teutsch N, Levasseur S. 2004b. Iron isotope fractionation in iron meteorites: New insights into metal-sulfide segregation and core crystallization. Eos Trans AGU 85:P33A–1000.

Williams HM, Peslier AH, McCammon C, Halliday AN, Levasseur S, Teutsch N, Burg J-P. 2005. Systematic iron isotope variations in mantle rocks and minerals: The effects of partial melting and oxygen fugacity. Earth Planet Sci Lett 235:435–452.

Woosley SE, Heger A, Weaver TA. 2002. The evolution and explosion of massive stars. Rev Mod Phys 74:1015–1071.

Wombacher F, Rehkämper M, Mezger K, Münker C. 2003. Stable isotope compositions of cadmium in geological materials and meteorites determined by multiple-collector ICPMS. Geochim Cosmochim Acta 61:4639–4654.

Wombacher F, Rehkämper M, Mezger K. 2004. Determination of the mass-dependence of cadmium isotope fractionation during evaporation. Geochim Cosmochim Acta 68:2349–2357.

Wu J, Boyle E, Sunda W, Wen L-S. 2001. Soluble and colloidal iron in the Oligotrophic North Atlantic and North Pacific. Science 293:847–849.

Yamaguchi KE, Johnson CM, Beard BL, Ohmoto H. 2005. Biogeochemical cycling of iron in the Archean–Paleoproterozoic Earth: Constraints from iron isotope variations in sedimentary rocks from the Kaapvaal and Pilbara Cratons. Chem Geol 218:135–169.

Young ED, Galy A, Nagahara H. 2002. Kinetic and equilibrium mass-dependent isotope fractionation laws in nature and their geochemical and cosmochemical significance. Geochim Cosmochim Acta 66:1095–1104.

Zanda B. 2004. Chondrules. Earth Planet. Sci Lett 224:1–17.

Zhu XK, O'Nions RK, Guo Y, Reynolds BC. 2000. Secular variation of iron isotopes in North Atlantic deep water. Science 287:2000–2002.

Zhu XK, Guo Y, O'Nions RK, Young ED, Ash RD. 2001. Isotopic homogeneity of iron in the early solar nebula. Nature 412:311–313.

Zhu XK, Guo Y, Williams RJP, O'Nions RK, Matthews A, Belshaw NS, Canters GW, de Waal EC, Weser U, Burgess BK, Salvato B. 2002. Mass fractionation processes of transition metal isotopes. Earth Planet Sci Lett 200:47–62.

ERRATUM TO:

MASS SPECTROMETRY AND NATURAL VARIATIONS OF IRON ISOTOPES

Nicolas Dauphas[1]* and Olivier Rouxel[2]

[1]*Origins Laboratory, Department of the Geophysical Sciences, Enrico Fermi Institute, and Chicago Center for Cosmochemistry, The University of Chicago, 5734 South Ellis Avenue, Chicago, Illinois 60637*
[2]*Woods Hole Oceanographic Institution, Marine Chemistry and Geochemistry Department, MS#8, Woods Hole, Massachusetts 02543*

The above article was published in N. Dauphas and O. Rouxel, *Mass Spectrometry Reviews* 2006, 25:515–550.

In Table 2, (Compilation of Fe isotopic compositions for geostandards and carbonaceous chondrites), some entries were omitted and others were incorrect. This is the corrected table. We regret any inconvenience this may have caused.

*Correspondence to: Nicolas Dauphas, Origins Laboratory, Department of the Geophysical Sciences and Enrico Fermi Institute, The University of Chicago, 5734 South Ellis Avenue, Chicago IL 60637. E-mail: dauphas@uchicago.edu

Sample	Description	Reference	#	[Fe] wt%	δ^{56}Fe ‰	± 2σ	δ^{57}Fe ‰	± 2σ	F_{Fe} ‰/amu	± 2σ
AC-E	Granite, Ailsa Craig island, Scotland (IWG-GIT)	Dauphas et al. (in prep)	5	*1.77*	*0.289*	*0.024*	*0.353*	*0.044*	*0.145*	*0.012*
AGV-1	Andesite, Oregon, USA (USGS)	Beard et al. (2003a)	2		0.130	0.102	0.140	0.152	0.065	0.051
		Poitrasson et al. (2004)	3				0.139	0.064	0.046	0.021
		Average AGV-1		*4.73*	*0.130*	*0.102*	*0.139*	*0.059*	*0.049*	*0.020*
AGV-2	Andesite, Oregon, USA (USGS)	Dauphas et al. (2004c)	1	*4.68*	*0.112*	*0.081*	*0.165*	*0.275*	*0.056*	*0.041*
BCR-1	Basalt, Oregon, USA (USGS)	Beard et al. (2003a)	3		0.090	0.128	0.120	0.146	0.045	0.064
		Fantle & DePaolo (2004)	1		0.240	0.128			0.120	0.064
		Poitrasson et al. (2004)	6				0.109	0.055	0.036	0.018
		Rouxel et al. (2003)	4				0.080	0.100	0.027	0.033
		Butler et al. (2005)	18		0.117	0.017	0.206	0.026	0.059	0.009
		Average BCR-1		*9.37*	*0.119*	*0.017*	*0.181*	*0.023*	*0.054*	*0.007*
BCR-2	Basalt, Oregon, USA (USGS)	Dauphas et al. (2004c, in prep)	2		0.039	0.055	0.116	0.131	0.019	0.028
		Weyer et al. (2005)	3		0.079	0.043			0.040	0.022
		Average BCR-2		*9.66*	*0.064*	*0.034*	*0.116*	*0.131*	*0.032*	*0.017*
BE-N	Basalt, Essey-la-Cote, France (IWG-GIT)	Rouxel et al. (2003)	2	*8.99*			*0.180*	*0.060*	*0.060*	*0.020*
BHVO-1	Basalt, Hawaii, USA (USGS)	Poitrasson et al. (2004)	5				0.164	0.032	0.055	0.011
		Rouxel et al. (2003)	3				0.220	0.130	0.073	0.043
		Rouxel et al. (2005)	20		0.106	0.108	0.149	0.133	0.053	0.054
		Weyer et al. (2005)	3		0.117	0.028			0.059	0.014
		Average BHVO-1		*8.55*	*0.116*	*0.027*	*0.166*	*0.030*	*0.057*	*0.008*
BIR-1	Basalt, Reykjavik, Iceland (USGS)	Poitrasson et al. (2004)	46				0.102	0.015	0.034	0.005
		Rouxel et al. (2003)	1				0.060		0.020	
		Williams (2005)	6				0.090	0.130	0.030	0.043
		Weyer et al. (2005)	9		0.054	0.017			0.027	0.009
		Average BIR-1		*7.90*	*0.054*	*0.017*	*0.102*	*0.015*	*0.032*	*0.004*
BR	Basalt, Essey-la-Cote, France (CRPG)	Rouxel et al. (2003)	12	*9.02*			*0.120*	*0.190*	*0.040*	*0.063*
DR-N	Diorite, Neuntelsein, France (ANRT)	Poitrasson et al. (2004)	3	*6.78*			*0.054*	*0.053*	*0.018*	*0.018*
DTS-1	Dunite, Washington, USA (USGS)	Poitrasson et al. (2004)	3				0.159	0.044	0.053	0.015
		Rouxel et al. (2005)	3		0.056	0.101	0.082	0.154	0.028	0.051
		Average DTS-1		*6.08*	*0.056*	*0.101*	*0.153*	*0.042*	*0.051*	*0.014*
DTS-2	Dunite, Washington, USA (USGS)	Dauphas et al. (2004c)	1	*5.43*	*0.022*	*0.041*	*-0.058*	*0.072*	*0.011*	*0.021*
G-2	Granite, Rhode Island, USA (USGS)	Beard et al. (2003a)	1	*1.86*	*0.070*	*0.172*	*0.130*	*0.161*	*0.035*	*0.086*
GA	Granite, Vosges Mountains, France (CRPG)	Poitrasson & Freydier (2005)	9	*1.98*			*0.137*	*0.027*	*0.046*	*0.009*
GSP-1	Granodiorite, Colorado, USA (USGS)	Beard et al. (2003a)	1	*3.00*	*0.110*	*0.128*	*0.080*	*0.152*	*0.055*	*0.064*
GSR-1	Granite, Binzhou, China (IGGE)	Poitrasson & Freydier (2005)	9	*1.50*			*0.243*	*0.049*	*0.081*	*0.016*
IF-G	Iron formation, Isua, Greenland (IWG-GIT)	Dauphas et al. (2004c, in prep)	14		0.630	0.021	0.942	0.047	0.315	0.010
		Rouxel et al. (2005)	4		0.639	0.058	0.957	0.087	0.320	0.029
		Average IF-G		*39.10*	*0.631*	*0.019*	*0.945*	*0.041*	*0.316*	*0.010*
JB-2	Basalt, Oshima volcano, Japan (GSJ)	Weyer et al. (2005)	3	*10.04*	*0.056*	*0.030*			*0.028*	*0.015*
JP-1	Dunite, Horoman, Japan (GSJ)	Poitrasson et al. (2004)	8				0.006	0.034	0.002	0.011
		Weyer et al. (2005)	3		0.003	0.046			0.002	0.023
		Average JP-1		*5.85*	*0.003*	*0.046*	*0.006*	*0.034*	*0.002*	*0.010*
MAG-1	Marine mud, Gulf of Maine, USA (USGS)	Beard et al. (2003b)	1	*4.76*	*0.050*	*0.172*	*0.150*	*0.213*	*0.025*	*0.086*
KAL-1	Komatiite, Alexo, Canada (CRPG)	Weyer et al. (2005)	9		*0.072*	*0.013*			*0.036*	*0.007*
OU-2 (WS-E)	Dolerite, Belford, UK (IAG)	Poitrasson et al. (2004)	3	*9.30*			*0.132*	*0.071*	*0.044*	*0.024*
PCC-1	Peridotite, California, USA (USGS)	Beard et al. (2003a)	3		0.030	0.156	0.020	0.184	0.015	0.078
		Poitrasson et al. (2004)	6				0.034	0.038	0.011	0.013
		Weyer et al. (2005)	3		0.043	0.023			0.022	0.012
		Average PCC-1		*5.78*	*0.043*	*0.023*	*0.033*	*0.037*	*0.017*	*0.008*
SDC-1	Micaschist, Washington DC, USA (USGS)	Beard et al. (2003b)	1	*4.42*	*0.120*	*0.242*	*0.170*	*0.172*	*0.060*	*0.121*
SGR-1	Shale, Wyoming, USA (USGS)	Beard et al. (2003b)	1	*2.12*	*-0.270*	*0.316*	*-0.390*	*0.519*	*-0.135*	*0.158*
PM-S	Microgabbro, Pitscurrie, UK (GIT-IWG)	Poitrasson et al. (2004)	9	*7.06*			*0.168*	*0.044*	*0.056*	*0.015*
RGM-1	Rhyolite, California, USA (USGS)	Beard et al. (2003a)	1	*1.30*	*0.180*	*0.242*	*0.290*	*0.172*	*0.090*	*0.121*
SRM-1649A	Urban dust, Washington DC, USA (NIST)	Beard et al. (2003b)	2	*2.98*	*0.000*	*0.141*	*0.010*	*0.172*	*0.000*	*0.071*
SRM-2709	Soil, San Joaquin Valley, USA (NIST)	Beard et al. (2003b)	2	*3.50*	*0.040*	*0.128*	*0.070*	*0.184*	*0.020*	*0.064*
STM-1	Syenite, Oregon, USA (USGS)	Beard et al. (2003a)	1	*3.65*	*0.040*	*0.471*	*0.060*	*0.539*	*0.020*	*0.235*
WITS-1	Komatiite, Barberton, South Adrica	Poitrasson et al. (2004)	5	*8.34*			*0.057*	*0.024*	*0.019*	*0.008*
Orgueil	CI1	Dauphas et al. (2004c)	1	18.30	0.015	0.074	0.108	0.192	0.008	0.037
Orgueil	CI1	Poitrasson et al. (2004)	5	18.30			-0.043	0.066	-0.014	0.022
Orgueil	CI1	Kehm et al. (2003)	1	18.30	0.050	0.156			0.025	0.078
Orgueil	CI1	Zhu et al. (2001)	1	18.30	0.380	0.060	0.600	0.060	0.200	0.020
		Average CI1			*0.021*	*0.067*	*-0.027*	*0.062*	*-0.007*	*0.018*
Murchison	CM2	Poitrasson et al. (2005)	3	20.90			-0.037	0.108	-0.012	0.036
Murchison	CM2	Dauphas et al. (2004c)	1	20.90	0.015	0.096	0.049	0.186	0.008	0.048
Murchison	CM2	Kehm et al. (2003)	1	20.90	-0.030	0.156			-0.015	0.078
Murchison	CM2	Zhu et al. (2001)	1	20.90	0.000	0.060	-0.010	0.060	-0.003	0.020
		Average CM2			*0.001*	*0.048*	*-0.012*	*0.050*	*-0.004*	*0.016*
Lance	CO3	Dauphas et al. (in prep)	1	24.80	0.030	0.157	0.191	0.135	0.015	0.079
Ornans	CO3	Dauphas et al. (in prep)	1	24.70	-0.094	0.082	-0.224	0.212	-0.047	0.041
		Average CO3			*-0.067*	*0.073*	*0.071*	*0.114*	*-0.034*	*0.036*
Allende	CV3	Poitrasson et al. (2005)	4	23.70			-0.105	0.066	-0.035	0.022
Allende	CV3	Dauphas et al. (2004c)	1	23.70	0.040	0.110	0.103	0.083	0.020	0.055
Allende	CV3	Kehm et al. (2003)	1	23.70	0.030	0.102			0.015	0.051
Allende	CV3	Zhu et al. (2001)	1	23.70	-0.040	0.060	-0.050	0.060	-0.017	0.020
Leoville	CV3	Kehm et al. (2003)	1	23.87	-0.040	0.156			-0.020	0.078
Vigarano	CV3	Dauphas et al. (in prep)	1	23.10	0.034	0.110	-0.060	0.587	0.017	0.055
		Average CV3			*-0.006*	*0.042*	*-0.035*	*0.039*	*-0.017*	*0.013*
		Average carbonaceous chondrites			*-0.008*	*0.027*	*-0.021*	*0.027*	*-0.012*	*0.009*

All the measurements reported relative to igneous rocks have been renormalized to IRMM-014 using the relationship given by Beard et al. (2003a), $\delta^{56}\text{Fe}_{IRMM-014} = \delta^{56}\text{Fe}_{Igneous} + 0.09 \pm 0.10$ (2σ) and $\delta^{57}\text{Fe}_{IRMM-014} = \delta^{57}\text{Fe}_{Igneous} + 0.11 \pm 0.14$ (2σ), where δ^{56}Fe is for the $^{56}\text{Fe}/^{54}\text{Fe}$ ratio and δ^{57}Fe is for the $^{57}\text{Fe}/^{54}\text{Fe}$ ratio. When δ^{56}Fe was available, F_{Fe} was calculated as $\delta^{56}\text{Fe}/2$. When only δ^{57}Fe was available, F_{Fe} was calculated as $\delta^{57}\text{Fe}/3$. The averages are weighted by $1/\sigma^2$ and their uncertainties are calculated accordingly. Uncertainties are reported as 2σ.